Universität Rostock

Traditio et Innovatio

Preparation, Production, and Modification of Regenerated Cellulose Film

Dissertation

to obtain the academic degree

„doctor rerum naturalium“(Dr. rer. nat.)

submitted at the

Faculty of Mathematics and Natural Sciences

University of Rostock

by

M.Sc. Nguyen Le Tuan Minh

born on August 22nd, 1994, in Hai Duong, Vietnam.

Rostock, September 2025

https://doi.org/10.18453/rosdok_id00005692

Referees:

1st Referee: **Dr. Dirk Holmann**
University of Rostock
Institute of Chemistry
Department of Analytical and Technical Chemistry
Albert-Einstein-Str. 3a
18059 Rostock, Germany

2nd Referee: **Assoc. Prof. Tran Dinh Phong**
University of Science and Technology Hanoi
Department of Chemical and Environment Technology
A21 building, 18 Hoang Quoc Viet, Nghia Do Ward
11355 Hanoi, Vietnam

Dissertation submission: 10 September 2025
PhD Defense: 13 January 2026

The current study was conducted from May 2022 to August 2025 under the guidance of Prof. Dr. Udo Kragl and Dr. Dirk Hollmann at the Institute of Chemistry, University of Rostock.

ACKNOWLEDGEMENT

I want to begin by sincerely thanking Dr. Dirk Hollmann, my immediate supervisor. His patience, insightful advice, and steadfast encouragement played a crucial role in helping me complete this dissertation and in my development as a researcher. Working under his guidance for three years in Rostock, Germany, has been both an honour and a valuable learning experience.

I want to express my gratitude to Prof. Dr. Udo Kragl for the opportunity to join his research group. The suggestions and insightful discussions throughout my PhD have been invaluable to me.

Special thanks to my colleagues at GeViCat, Hanoi University of Science and Technology, who have consistently supported me, particularly Prof. Le Minh Thang and Dr. Nguyen Ngoc Mai.

I would like to thank the RoHan project for the sponsorship during my PhD journey in Germany.

Beyond the academic sphere, I would like to express my heartfelt gratitude to my family and loved ones. Their unwavering support and understanding have helped me overcome the challenges of pursuing a Ph.D. program. We faced many hardships together, including my unexpected serious health problems in this journey and the recent passing of my beloved grandmother. Their resilience and love have been a source of strength and inspiration.

This dissertation is dedicated to everyone who has supported me throughout this journey. Without your encouragement and support, both professionally and personally, reaching this milestone would not have been possible.

TABLE OF CONTENTS

LIST OF SYMBOLS AND ABBREVIATIONS

$[N_{1,1,1,1}]OH$	Tetramethyl hydroxide
$[N_{1,1,1,a}]OH$	Trimethyl adamantyl ammonium hydroxide
$[N_{2,2,2,2}]OH$	Tetraethylammonium hydroxide
$[N_{3,3,3,3}]OH$	Tetrapropylammonium hydroxide
$[N_{4,4,4,4}]OAc$	Tetrabutylammonium acetate
$[N_{4,4,4,4}]OH$	Tetrabutylammonium hydroxide
$[P_{4,4,4,4}]OH$	Tetrabutylphosphonium hydroxide
AFM	Atomic force microscopy
AGU	Anhydroglucose unit
BmimCl	1-butyl-3-methylimidazolium chloride
CHNS	Carbon, hydrogen, nitrogen, and sulfur
CS	Chitosan
DDA	Degree of deacetylation
DES	Deep eutectic solvents
DMAc	N, N-dimethylacetamide
DMSO	Dimethyl sulfoxide
DP	Degree of polymerisation
FT-IR	Fourier transform infrared spectroscopy
GlcNac	N-acetyl-D-glucosamine
Gly	Glycerol
HMW-CS	High-molecular-weight chitosan
ICP	Inductively Coupled Plasma
IL/ILs	Ionic liquid/ionic liquids
KC	Kraft cellulose
LMW-CS	Low-molecular-weight chitosan
MCC	Microcrystalline cellulose
MDCell	Mai-Dirk-Cellulose
MMW-CS	Medium-molecular-weight chitosan
Mw	Molecular weight

NBHK	northern bleached hardwood kraft
NBSK	northern bleached softwood kraft
NMMO	N-methylmorpholine N-oxide
NMR	Nuclear magnetic resonance
Nw	Number of water per onium hydroxide ion
OHS	Onium hydroxide solution
P	Primary wall
PC	Propylene carbonate
PEG	Polyethylene glycol
PE-LD	Polyethene low-density
PET	Polyethylene terephthalate
PHA	polyhydroxyalkanoates
PLA	polylactic acid
PP	Polypropylene
RC	Regenerated cellulose
RCS	Regenerated chitosan
RKC	Regenerated Kraft cellulose
RKC/RCS	Regenerated Kraft cellulose/regenerated chitosan
S	Secondary wall
SEC	Size exclusion chromatography
SEM	Scanning electron microscopy
UN SDGs	United Nations Sustainable Development Goals
w/v%	Weight per volume percentages
wt.%	Weight percentages
WVTR	Water vapour transmission rate
XRD	X-ray diffraction

ABSTRACT

The circular economy has become an essential strategy for reducing resource depletion and minimising the environmental impact of production. Over the past few decades, more policies worldwide have been introduced to promote sustainable development and emphasise the importance of the circular economy. Plastic is especially strongly regulated. Therefore, this research focuses on modifying the MDCell (Mai-Dirk-Cellulose) process to produce plastic-free, regenerated cellulose packaging films. The MDCell process, developed in our group, is an innovative and environmentally friendly method that enables the production of regenerated cellulose film at room temperature within a short period using tetrabutyl ammonium hydroxide ($[N_{4,4,4,4}]OH$). The regenerated cellulose film exhibited good mechanical properties and displayed rapid biodegradability in both soil and seawater environments. This film has excellent potential to replace fossil-fuel-based plastics.

Lithium chloride was identified as a novel plasticiser for regenerated cellulose film. The treated film's elongation exceeded that of the original by more than seven times. Compared to traditional plasticisers such as glycerol and polyethylene glycol, lithium chloride also demonstrated superior performance.

Additionally, $[N_{4,4,4,4}]OH$ is a solvent capable of dissolving large amounts of chitosan under the same conditions as cellulose. It can also be recycled after use. By regenerating this solvent, it can be reused for other applications. Furthermore, cellulose and chitosan can be combined to produce homogeneous solutions. This enables the development of regenerated cellulose/chitosan blended film using the modified MDCell process. The ratios of the components influence the mechanical, physical, and biodegradability properties of the blended film. By tailoring the cellulose-chitosan mixture, application-specific products can be manufactured.

ZUSAMMENFASSUNG

Die Kreislaufwirtschaft ist zu einer wichtigen Strategie geworden, um die Ressourcenknappheit zu reduzieren und die Umweltauswirkungen der Produktion zu minimieren. In den letzten Jahrzehnten wurden weltweit verstärkt Maßnahmen zur Förderung nachhaltiger Entwicklung eingeführt und die Bedeutung der Kreislaufwirtschaft hervorgehoben. Insbesondere der ölbasierte Kunststoff wird momentan stark reguliert. Daher fokussiert sich dieses Forschungsprojekt auf der Modifizierung des MDCell-Verfahrens für die Herstellung von regenerierte plastikfreier Zellulosefolie. Dieses innovative und umweltfreundliche Verfahren ermöglicht die Herstellung von regenerierter Zellulosefolie bei Raumtemperatur innerhalb kurzer Zeit unter Verwendung von Tetrabutylammoniumhydroxid ($[N_{4,4,4,4}]OH$). Die regenerierte Zellulosefolie weist gute mechanische Eigenschaften auf und ist sowohl im Boden als auch im Meerwasser schnell biologisch abbaubar. Diese Folie hat damit großes Potenzial, fossile Kunststoffe zu ersetzen.

Lithiumchlorid wurde als neuartiger Weichmacher für regenerierte Zellulosefolie identifiziert. Die Dehnung der behandelten Folie übertraf die der Originalfolie um mehr als das Siebenfache. Im Vergleich zu herkömmlichen Weichmachern wie Glycerin und Polyethylenglykol zeigte Lithiumchlorid zudem eine überlegene Leistung.

Interessanterweise ist $[N_{4,4,4,4}]OH$ ein sehr gutes Lösungsmittel, um Chitosan in großen Mengen lösen. Das Lösemittel kann nach Gebrauch recycelt und für andere Anwendungen wiederverwendet werden. Cellulose und Chitosan können zudem zu homogenen Lösungen kombiniert werden. Dies ermöglicht die Entwicklung von regenerierten Cellulose-Chitosan-Mischfolien im modifizierten MDCell-Verfahren. Die Verhältnisse der Komponenten beeinflussen die mechanischen, physikalischen und biologischen Abbaubarkeitseigenschaften. Durch Anpassung der Cellulose-Chitosan-Mischung können gezielt anwendungspezifische Produkte hergestellt werden

1 INTRODUCTION

1.1 Circular economy and green chemistry

Modern society is increasingly embracing the concept of a circular economy to address the urgent need for sustainable development and reduce waste. In contrast to the traditional linear model, the circular economy aims to decouple the economy from the consumption of finite resources. This approach focuses on the loop of material use, which encourages recycling, reuse, and designing products for longevity.[1-3] Thus, waste from manufacturing can be minimised. The concept of a circular economy has gained significant momentum in the past few decades as a solution to the limitations of linear production. Figure 1 illustrates the linear and circular economy models.

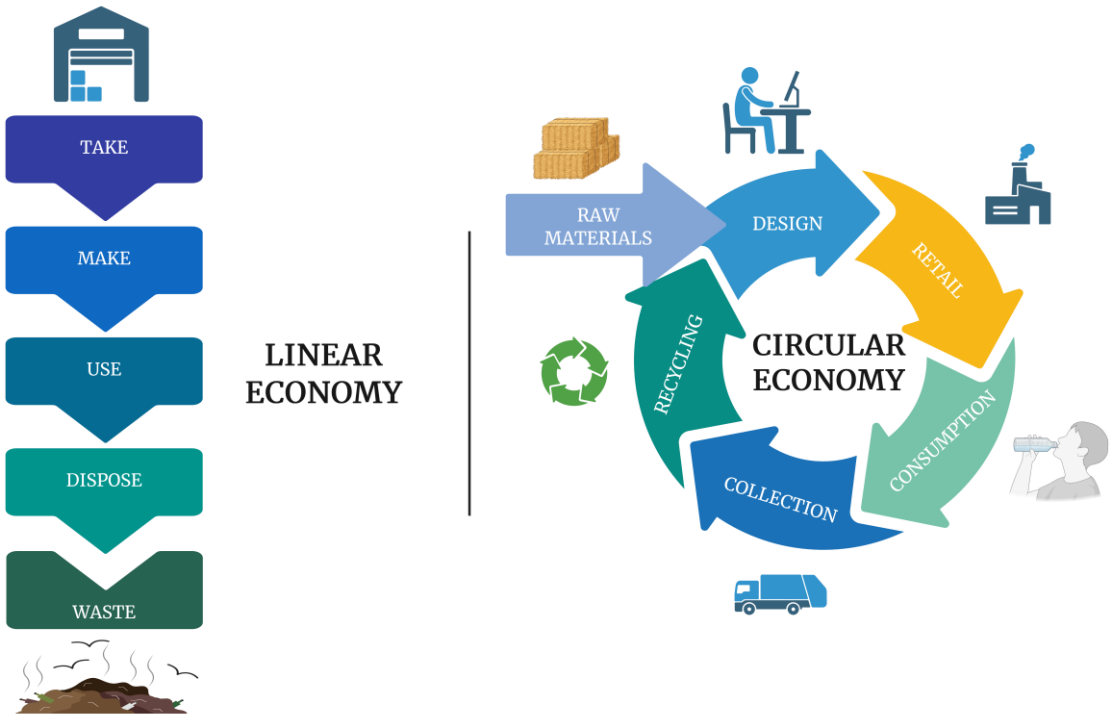

Figure 1. Linear and circular economy model

In 2015, the United Nations Sustainable Development Goals (UN SDGs) were proposed as a framework of 17 goals that need to be achieved by 2030 to protect our planet and reduce poverty (Figure 2).[4] It emphasises that shifts towards sustainable development are necessary to reach these goals. The circular economy helps to reduce waste and pollution, improve environmental protection, and create new economic opportunities.

Figure 2. The United Nations Sustainable Development Goals [4]

To support the circular economy concept, chemistry plays a crucial role in redesigning chemical processes and products, allowing waste and materials to be looped back into the manufacturing process.[3, 5] Chemistry also plays a crucial role in developing new materials and molecules that are safer, more durable, and recyclable, alongside innovative recycling and recovery technologies. Therefore, shifting from a traditional linear process to a circular one in chemistry is a key step toward sustainable development.

Green chemistry is a branch of chemistry. This field focuses on designing chemical products and processes that minimise or eliminate the use and generation of hazardous compounds. Safer chemicals and methodologies have been developed by fundamentally rethinking traditional methods to reduce risks to humans and the environment. In 1998, Paul Anastas and John C. Warner published 12 principles that guide chemistry practices.[6] These principles have become fundamental for educating chemists and developing new chemical products, syntheses and techniques. This is how science and chemistry contribute to sustainable development.

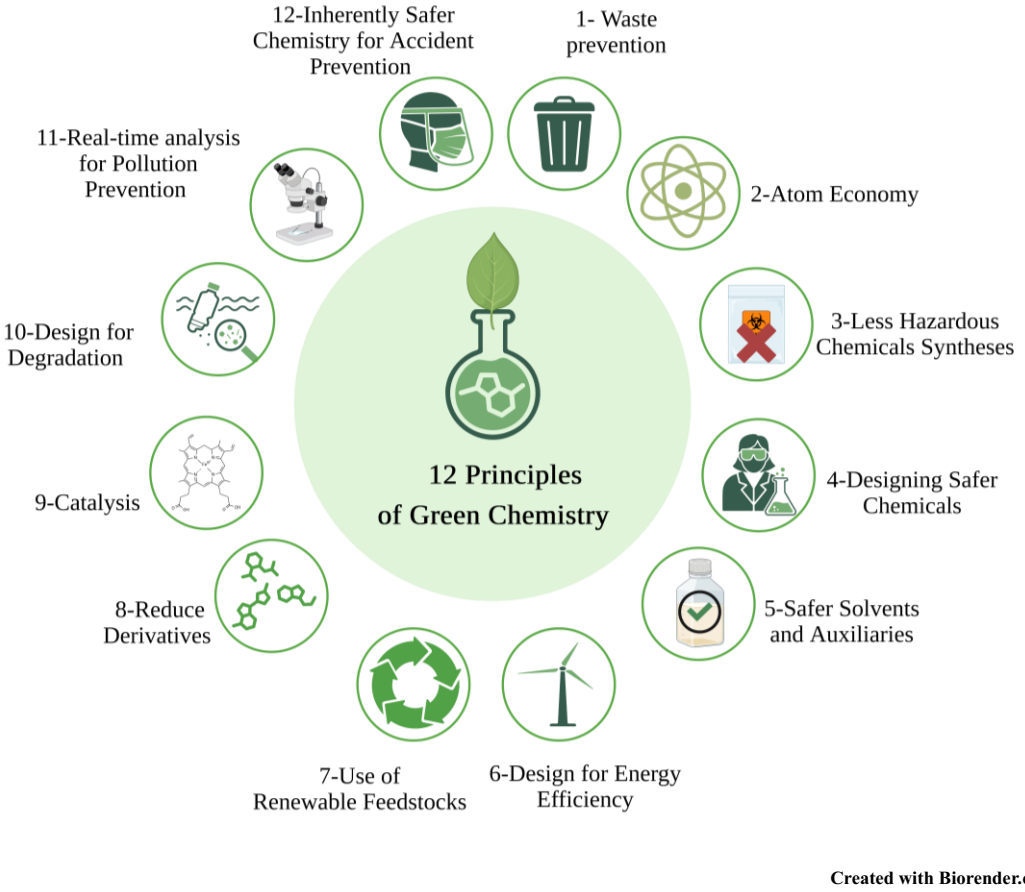

Figure 3. The 12 principles of Green Chemistry proposed by Paul Anastas and John C. Warner

These 12 principles of green chemistry encourage chemists to consider safety, efficiency, and environmental impact when designing chemicals and processes. Following these guidelines is key to achieving sustainability in chemistry and circular economies. By ensuring that products are non-toxic, easy to recycle, or biodegradable, a closed loop of materials becomes more feasible. Additionally, 14 of the 17 goals in the framework of the UN SDGs have been identified as requiring the application of green chemistry.[1] This emphasises the central role of green chemistry in sustainable development.

1.2 Biopolymer: the sustainable material

One critical area of coverage for both circular economy and green chemistry principles is the development of environmentally friendly polymer materials. Synthetic polymers are primarily produced from petroleum and have numerous applications in modern

society. However, the production of fossil fuels is energy-intensive and contributes significantly to greenhouse gas emissions.[7] They are also considered non-biodegradable materials; therefore, they persist for centuries in waste landfills and oceans.[8, 9] Plastic pollution has become a major problem since this material became popular worldwide in the last century. This is why scientists have been seeking a replacement material, and biopolymers have become an option that fits the circular economy and green chemistry.

Biopolymers have emerged as one of the most promising solutions for making polymer production more sustainable. Biopolymers include polymers produced or derived from living organisms or synthesised from renewable resources.[10] They can be considered almost inexhaustible resources on Earth. Most current polymeric products are synthesised from fossil fuel resources. They are often called “bioplastic” to distinguish them from conventional plastics. These materials have gained significant attention as ideal replacements for petro-plastics because they can reduce the environmental footprint of polymer production.

Biopolymers can be classified in different ways; however, based on their origin, they can be divided into three major categories: natural, synthetic, and microbial polymers.[10, 11] Natural polymers are the most abundant in the world and are easily found in living organisms. They have a wide distribution on both land and water. Thus, it can reduce the over-dependence on petroleum in the manufacture of polymers. In addition to their abundance, they possess diverse and interesting properties and applications. Biopolymers have been widely applied in packaging, biofuels (such as ethanol and hydrogen), medical fields (including tissue engineering and drug delivery), commodities (e.g., clothing), and agriculture. In terms of performance, modern biopolymers have been proven to have good durability, which can be comparable to petroleum polymers.[12] Additionally, this material is normally biodegradable, and it can greatly reduce the burden of plastic waste if it is disposed of properly. Several types of bioplastics are already available on the market, such as polylactic acid (PLA) and polyhydroxyalkanoates (PHA). Although challenges remain, the use of environmentally friendly polymers is one of the strategies for achieving a circular economy.

1.3 Cellulose and Chitosan: biopolymers

Among the most extensively studied biopolymers, cellulose and chitosan stand out due to their abundance, biodegradability, and broad range of applications. Cellulose is the most abundant natural polymer on Earth and is extracted mainly from plant biomass (wood, cotton, and fibrous plants). Chitosan is produced from chitin, the second most abundant natural polysaccharide after cellulose. The use of cellulose and chitosan proves that bio-based polymers can replace synthetic plastics in a circular and environmentally friendly manner.

1.3.1 Cellulose

Cellulose was successfully isolated from plants by the French chemist Anselme Peyene in 1838.[13] Scientists have been trying to exploit the full potential of this molecule, and research on cellulose is still ongoing. In addition to plant sources, cellulose can be extracted from other living organisms such as bacteria and algae. The cellulose produced by typical bacteria, known as bacterial cellulose, is reported to have higher purity than plant cellulose due to the complex components and structure of plants.

Cellulose is a linear natural polymer composed of repeating D-glucopyranose monomers linked by β-1,4-glycosidic bonds, and its structure is illustrated Figure 4. The basic unit of cellulose is an anhydroglucose unit (AGU). The size of cellulose molecules refers to the average number of AGUs in the cellulose chain length, and this number is called the degree of polymerisation (DP). The DP value of cellulose materials varies depending on the cellulose source and the extraction method. [14, 15] Each AGU in the cellulose chain is rotated 180˚ axially to its neighbours, and a pair of AGUs creates a cellobiose unit. Typically, AGU has three active hydroxyl groups at the C_2, C_3, and C_6 positions, except for the two terminal units of the cellulose chains. These two units have distinct chemical properties because of the position of the hydroxyl group in each unit. An ending AGU is called a reducing end group when the anomeric carbon of this AGU freely reduces to an aldehyde. In contrast, the anomeric carbon of AGU is involved in glycosidic bonding and cannot act as a reducing agent, which is known as a non-reducing end group.

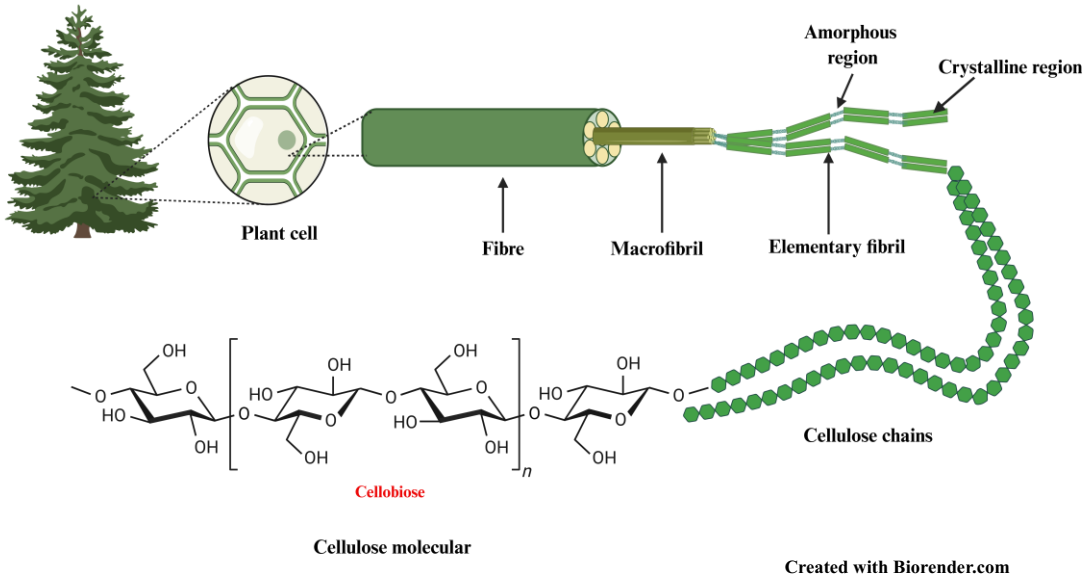

Figure 4. Cellulose hierarchical structure

The three active hydroxyl groups in the equatorial position and the oxygen atom in the pyranose ring promote the interaction between the inter- and intra-chain via hydrogen bonding. [16, 17] The numerous hydrogen bonding interactions combined with van der Waals forces lead to the parallel aggregation of multiple cellulose chains, forming larger cellulose structures.[18] These interactions are responses to the very high-order structure of the polymer network, which provides cellulose with chemical and physical stability. Figure 4 describes the cellulose hierarchical structure, which is essentially composed of different levels of fibrillar bundles, with a fundamental building block called the "elementary fibril". Elementary fibrils comprise glucan chains with a typical cross-section of 2–20 nm diameter. The elementary fibrils aggregate to form microfibrils (4-35nm) and then cellulose fibres (20-50µm).[19, 20]

Cellulose fibres exhibit a complex layered structure, transitioning from the primary wall to the lumen (Figure 5A).[21, 22] The primary wall (P), the outermost layer, is composed of matrix cellulose, hemicelluloses, and pectins. It is characterised by a less organised arrangement of cellulose microfibrils and is relatively thin. The secondary wall (S) comprises three distinct layers: S1, S2, and S3, each with a unique fibre orientation. The S1 layer features cellulose microfibrils arranged in a crossed fibre structure with either S or Z-helix variations.[23] This thin layer constitutes approximately 10% of the total fibre

thickness. The S2 layer is the thickest and contains the highest cellulose mass within the fibre. The cellulose microfibrils in this region typically adopt a Z-helix orientation. The innermost layer, S3, is adjacent to the lumen and is exceptionally thin, and is sometimes absent in the fibre. Figure 5B shows the SEM image of the cross-sectional area of the Norway Spurne fibre provided by Dupont and Anne Laurence.[24] It indicates the distinct layers in the fibre and their thickness. The layer thickness varies depending on the type of cellulose fibre.

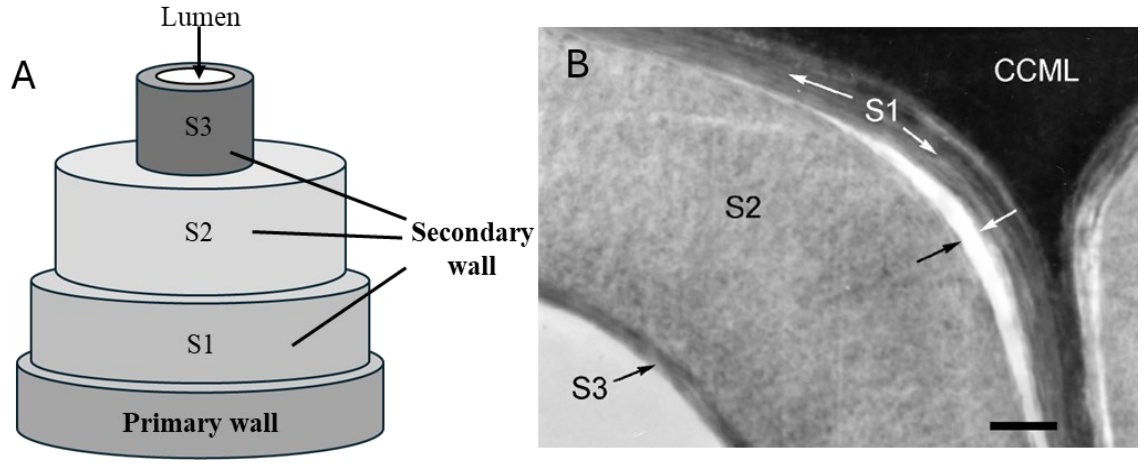

Figure 5. A) Schematic of cellulose fibre morphology with primary wall and secondary wall with S1, S2 and S3 layer, and lumen. B) SEM image of cross-section of the secondary wall of Norway Spure fibre [24]

Cellulose is a polymorphic material with different crystalline structures. The crystalline structure of a cellulose chain aligned parallel is called cellulose I, which is divided into two polymorphs, Iα and Iβ.[25] Cellulose Iα is dominant in plants, such as wood and cotton, whereas Iβ is predominant in bacterial cellulose.[13] The Cellulose II allomorph has an antiparallel structure, making it more thermodynamically stable than cellulose I and other forms of cellulose. This is a crucial property of cellulose II. This polymorph can only be obtained by regenerating cellulose I that has been dissolved in strong alkaline media.[26] The third polymorph lattice structure of cellulose is known as cellulose III. By treating cellulose I or II polymorphs in liquid ammonia or specific diamine solutions at low temperatures, cellulose III_I and III_{II} are obtained.[27] The crystalline form of cellulose III is transformed into cellulose IV when the crystal form of cellulose is heated to 250°C in glycerol.[28, 29] The transformation of cellulose polymorphs is shown in Figure 6 .

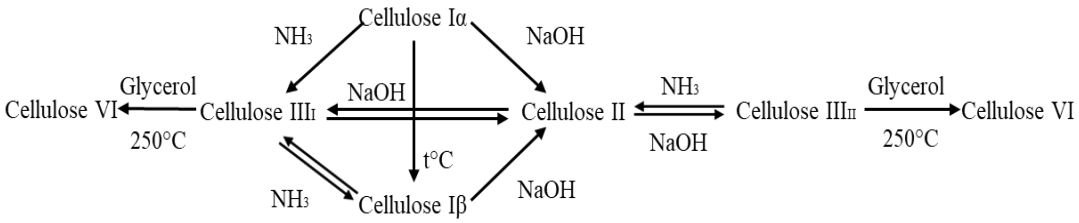

Figure 7. Cellulose polymorphs transformation

Figure 7 illustrates the arrangements of inter- and intramolecular hydrogen bonding in cellulose I and II, respectively. Cellulose I has two intramolecular hydrogen bonds that correlate with its parallel structure and contribute to the axial stiffness of the native cellulose. In comparison with cellulose I, the hydroxymethyl group is already rotated, making the glycosidic hydrogen bond at the C_2-OH position impossible.[30, 31] The intermolecular hydrogen bond of cellulose II is between C_2-OH and C_6-OH, whereas that of cellulose I is between C_3-OH and C_6-OH. The antiparallel structure of Cellulose II allows hydrogen bonds to form between layers, making this polymorph very stable.[30] The complexity of the hydrogen bond network of cellulose is one of the reasons why this material is insoluble in water and common organic solvents.

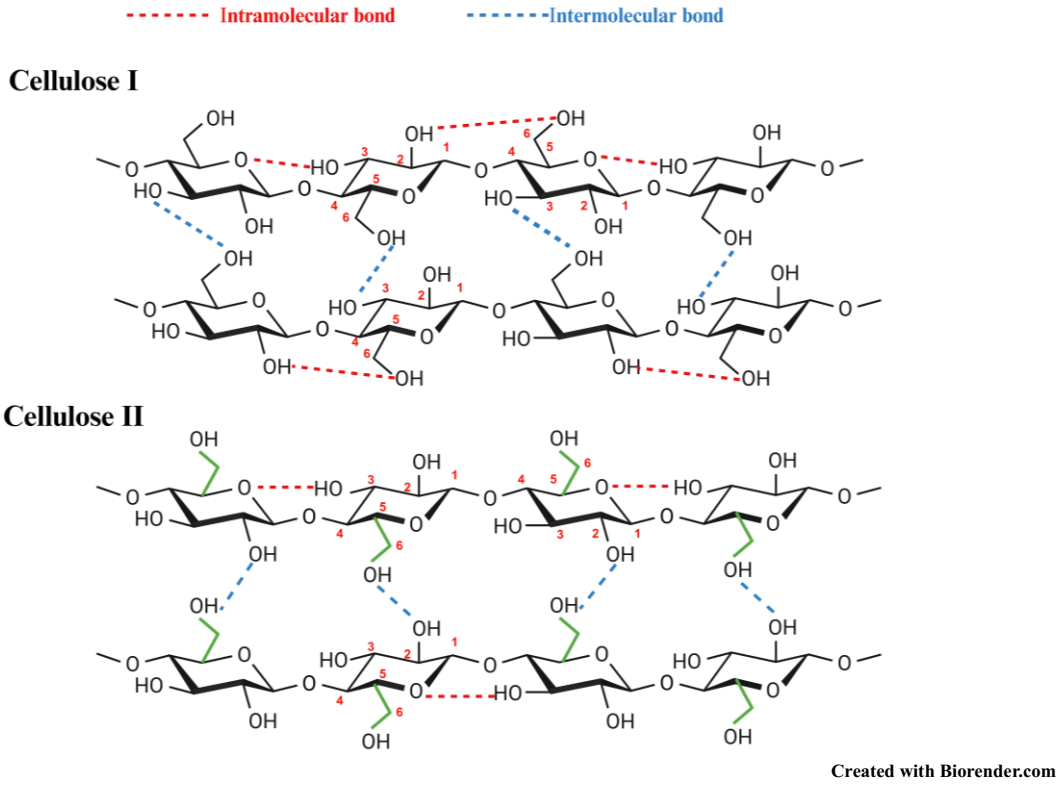

Figure 6. The hydrogen bond network of cellulose I and Cellulose II polymorph

Cellulose and its derivatives are extensively used across various industries, including food, packaging, medical, textile, pharmaceutical, and cosmetic sectors. In materials science, cellulose fibres and nanocellulose are used to reinforce composite materials due to their lightweight, strength, and durability. Moreover, the growing use of cellulose-based materials in the packaging industry is increasing. Cellulose films serve as alternatives to petroleum-based plastics because of their excellent mechanical properties and biodegradability. In the textile industry, cellulose forms the basis of natural fibres (cotton and linen) and regenerated fibres (viscose and lyocell), which have been utilised in manufacturing processes for some time. Overall, cellulose materials have a wide range of applications, from ancient papermaking to modern nanomaterials, emphasising their crucial role in advanced sustainable technology and addressing societal needs.

1.3.2 Chitosan

The chitosan journey began with the discovery of chitin by Professor Henri Braconnot, a French chemist and pharmacist who extracted it from fungi in 1811. In 1859, another French Professor, Charles Rouget, discovered chitosan after treating chitin with hot potassium hydroxide. However, the name "chitosan" was only used after it was introduced by Hoppe-Seyler in 1894. This substance was discovered nearly 200 years ago, but research and application did not begin until after 1970.[32] The chemical structures of chitin and chitosan are illustrated in Figure 8.

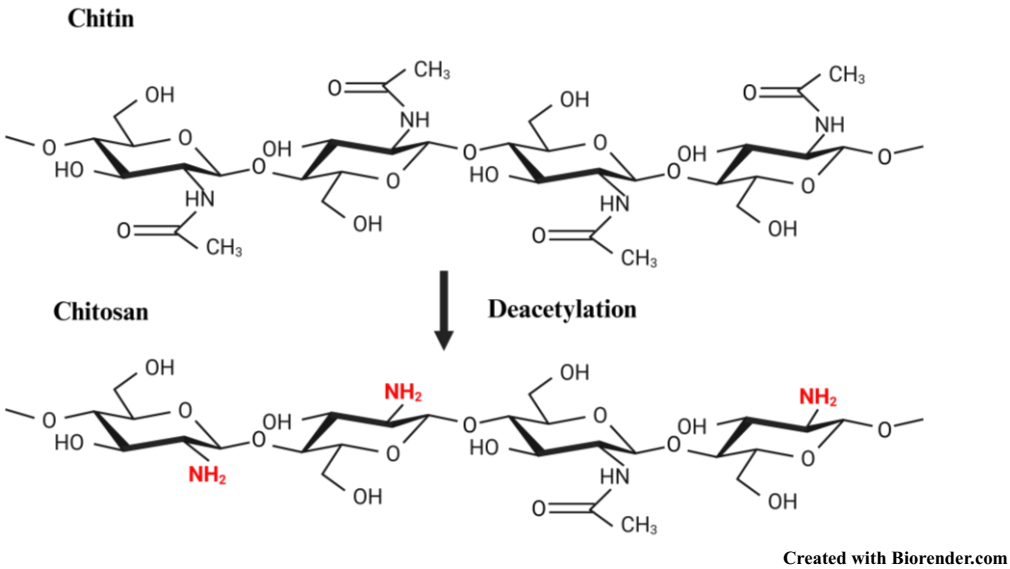

Figure 8. Chemical structure of chitin and chitosan

Chitin is a linear polymer consisting of N-acetyl-D-glucosamine (GlcNac) linked through β-1,4-glycosidic bonds and is primarily found in the exoskeleton or endoskeleton of crustacean species (shrimp, crab, or lobster) or insects. It is also present in the cell walls of fungi, yeasts, and algae. Compared to chitin, chitosan rarely exists naturally and is only found in certain microorganisms, such as Mucoraceae.[33] Generally, chitosan is produced mainly from chitin through deacetylation. The acetylamino group (-NH-$COCH_3$) in N-acetyl-D-glucosamine is replaced by an amino group (-NH_2), converting it to D-glucosamine. This conversion process never reaches 100%, and the degree of deacetylation (DDA) is used to determine the percentage of acetyl groups converted to amino groups during the deacetylation process. Chitin is referred to as chitosan when the DDA exceeds 50%. Thus, the chemical structure of chitosan is established by D-glucosamine and N-acetyl-D-glucosamine; however, the number of N-acetyl-D-glucosamine units is always smaller than that of D-glucosamine units.

Chitin has three allomorphs: α, β, and γ, which are antiparallel, parallel, and a mixture of both anti- and parallel structures, respectively.[34] α-Chitin is the most dominant crystalline structure of chitin in nature. Chitosan is derived from chitin, but the polymorph of this material has not been well defined as chitin.[35] Similar to cellulose, chitin and chitosan both have extensive hydrogen bonding within their polymer chain, as shown in Figure 9.The polymer chains of α-chitin are aligned in an antiparallel fashion. Each chitin chain adopts two strong intra-chain hydrogen bonds between C_3-OH and the adjacent in-ring oxygen, as well as between C=O of acetyl amine and C_6-OH.[36] Two intermolecular interactions are formed: NH···C=O and C_6-OH···HO-C_6 between two polymer chains. Additionally, the hydrogen bonds of chitin are formed not only between chains but also between sheets, which makes the polymer structure very tightly packed and rigid. [34, 37] Compared to chitin, the explanation of the hydrogen bond network of chitosan varies between researchers.[38-40]According to Mohammad et al.[40], the hydrogen bond network of chitosan, which is illustrated in Figure 9. The inter- and intra-molecular hydrogen bonds of chitosan mainly occur between amine groups (NH_2) and hydroxyl groups. Additionally, the remaining acetylamino groups can interact with

amine groups to form intermolecular hydrogen bonds. This indicates that the hydrogen bond network of chitosan is more complex due to its chemical structure.

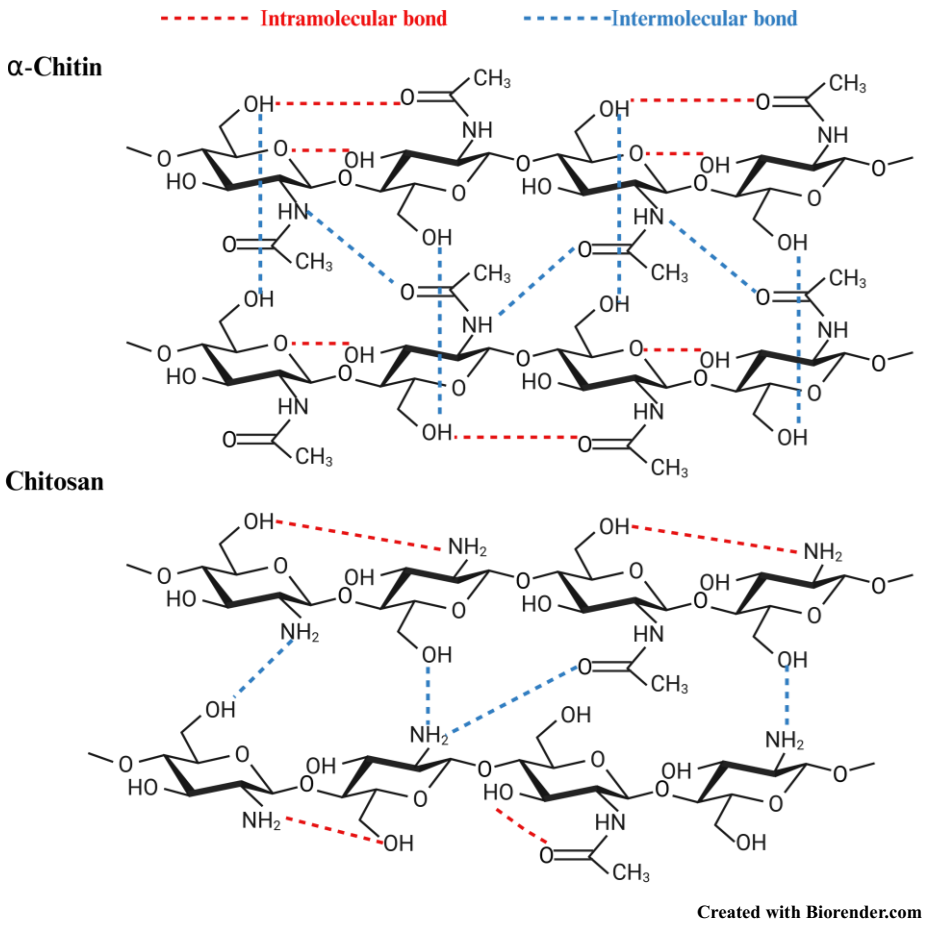

Figure 9. Hydrogen bond network of α-chitin and chitosan

Chitosan is a versatile biopolymer whose physicochemical properties depend on various factors. The parameters that can influence its characteristics include molecular weight (Mw), degree of deacetylation (DDA), raw material, and manufacturing process used.[41-44] Compared to fossil fuel-based materials, chitosan has many advantages, including biocompatibility, biodegradability, non-toxicity, and eco-friendliness. Based on its favourable properties, chitosan has been applied in biotechnology, pharmaceuticals, biomedicine, water treatment, food, and chemical industries.

In the biomedical sector, chitosan is used in wound dressing and drug delivery technology, where it accelerates healing and safely transports medications within the body.[45, 46] Furthermore, the active amine groups in the backbone can chelate with various metal ions at an appropriate pH. This chelating ability has been utilised in wastewater

treatment, where chitosan serves as an effective absorbing agent for removing metal ions.[47] Moreover, chitosan exhibits excellent film-forming ability and antimicrobial properties, making it a promising material for designing packaging materials in the food industry. The film made from pure chitosan film or blended with other polymers has proven to extend shelf life and improve food safety.[48, 49]

1.3.3 Cellulose-chitosan functional biopolymer

The combination of cellulose and chitosan creates a material that combines the strengths of both biopolymers and remains a popular topic today. Cellulose provides a rigid structural backbone with high mechanical strength and stability in water and common organic solvents. In contrast, chitosan introduces a functional amine group that acts as an electron donor, imparting bioactive properties to the product, primarily antimicrobial activity. Therefore, cellulose-chitosan blends exhibit excellent mechanical, antimicrobial, and biocompatibility qualities that are not found in the individual polymers when separated. By adjusting the ratio of the two components, specific functional properties can be customised. The result is a versatile biopolymer that balances durability and reactivity, making it useful for creating sustainable materials in line with circular economy principles.

Cellulose-chitosan functional polymers can be fabricated with diverse morphologies to optimise their performance. Table 1 shows the diversity of the applications, techniques, forms, and structures of blended materials. Depending on the specific application, products with different morphologies have been developed, including aerogels, foams, sponges, membranes, hydrogels, films, nanoparticles, and fibres. The ability to produce such a range of structures is enabled by the chemical compatibility of cellulose and chitosan, both of which are polysaccharides that can be blended or co-formed through solution casting, coating, and related techniques.

The unique combination of functionalities of cellulose-chitosan polymers broadens their application across various fields. In biomedical and healthcare applications, this biopolymer combination has been utilised in wound dressings and tissue scaffolds due to its biocompatibility and antimicrobial properties.[50, 51] Cellulose-chitosan films are

applied to suitable packaging materials. These films not only show good mechanical strength but also inhibit microbial growth to extend the shelf life of food.[52] Furthermore, it has also been reported to have been applied in textile technology, environmental technology or memory technology (Table 1). The versatility of the morphology and functionality of cellulose-chitosan allows researchers to tailor a wide range of applications.

Table 1. The overview of research on cellulose/chitosan in various applications, product morphology, and preparation processes.

Application	Products/morphology	Preparation process	References
Memory technology	Multifilament fibres	Homogeneous blending solution	Kunkun Zhu et al. [53]
Medical/control drug release	Fibres	Coating	Liu et al. [54]
Medical/ control drug release	Hydrogel beads	Coating	Song et al. [50]
Wastewater treatment/dye adsorption	Sponge	Heterogeneous mixture, freeze-drying	Li et al. [55]
Packaging	Films	Homogeneous solution, regenerated	Yang et al. [56]
Carbon fibres	Fibres	Co-dissolution	Zahra et al. [57]
Water treatment/dye adsorption	Aerogel	Homogeneous solution, crosslink, freeze-drying	Liu et al. [58]

1.4 Cellulose and chitosan solubilisation

As mentioned earlier, despite the many interesting properties of cellulose and chitosan, there remains great potential for further research on these materials. Unlike polymers derived from fossil fuels, cellulose, chitosan, and other natural polymers cannot be melted and shaped using conventional plastic processes because they decompose before they melt. This limits their application in manufacturing processes. Instead, they need

to be chemically modified or dissolved to facilitate processing and enhance their use. To retain the original properties of these polymers, it is essential to dissolve them without altering their chemical structures and to minimise degradation. Therefore, finding an appropriate solvent for both biopolymers is crucial.

1.4.1 Cellulose solvent

The complex hydrogen bond systems of cellulose make it stable in most common solvents. Various solvents have been developed for the dissolution process, which are categorised and depicted in Figure 10. Derivatizing and non-derivatizing solvents are the two main categories, distinguished by their interaction with cellulose molecules. The solubilisation of the derivatizing solvent occurs only by modifying the functional group of cellulose into a new functional group. Non-derivatising solvents can dissolve cellulose without changing its chemical structure by disrupting the intra- and intermolecular bonds of cellulose. Unmodified cellulose is recovered after the solvent is removed.

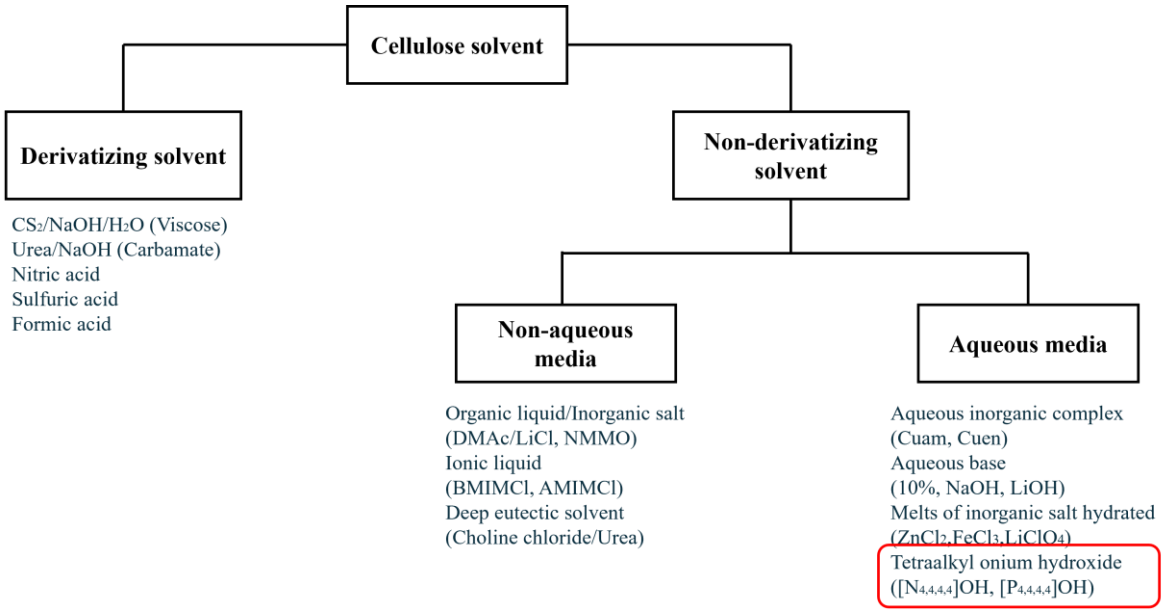

Figure 10. Classification of cellulose solvent

The most famous and vital process that uses a derivatizing solvent system is viscose. This process manufactures regenerated fibres by treating wood pulp in sodium solution and carbon disulfide (CS_2), which turns cellulose into soluble cellulose xanthate.[59] The viscous solution is then processed through an acid bath to remove the xanthate group and obtain the regenerated cellulose material. Carbamate is an alternative to the viscose

process, which replaces carbon disulfide with urea.[60] However, both these processes are highly toxic and pollute the environment, negatively impacting both the environment and humans.

Compared to derivatizing solvents, non-derivatizing solvents can dissolve cellulose without chemical modification, thereby simplifying the process and potentially lowering its environmental impact. The Lyocell process is the most well-known method and has been employed at an industrial scale. In this process, N-methyl morpholine N-oxide (NMMO) is used to dissolve cellulose at elevated temperatures, with a recycling rate of 99% after the manufacturing process. However, NMMO is unstable and easily decomposes at high temperatures.[61] Additionally, N,N-dimethylacetamide (DMAc)/lithium chloride (LiCl) is a classic cellulose solvent. The advantages of this solvent system are that it can dissolve various types of cellulose without decomposition.[24] Hence, it has been used to determine the properties of cellulose materials using various techniques, such as ^{13}C-NMR spectroscopy, size exclusion chromatography (SEC), viscometry, and light scattering.

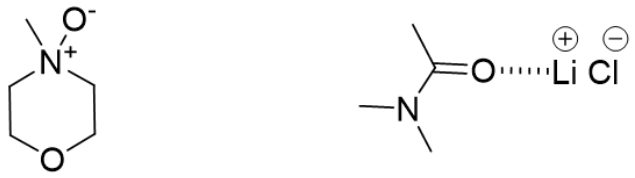

N-methyl-morpholine-N-oxide
NMMO

N, N-dimethylacetamide/Lithium Chloride

Figure 11. Chemical structure of non-derivatisation solvent

In 2002, Swatloski et al.[62] reported that cellulose can be solubilised in ionic liquids (ILs). Different imidazolium-based ILs were examined, and some could dissolve high-molecular-weight cellulose (DP~1000). In this study, 1-butyl-3-methylimidazolium chloride (BmimCl) can dissolve up to 25 wt. % cellulose pulp under microwave heating. Additionally, they exhibit superior properties such as thermal stability, negligible vapour pressure, high recovery, and reusability. ILs are also considered more environmentally friendly than traditional solvents. Hence, an increasing number of ILs has been developed. Both the cation and anion of the Ils were involved in interrupting the hydrogen bond, leading to solubilisation of cellulose. However, the role of anions is

more significant than that of cations in this process. Figure 12 illustrates several common cations, including imidazole, pyridine, ammonium, and phosphonium. These cations primarily combine with halides, carboxylates, and thiocyanates to form ILs that can dissolve cellulose.

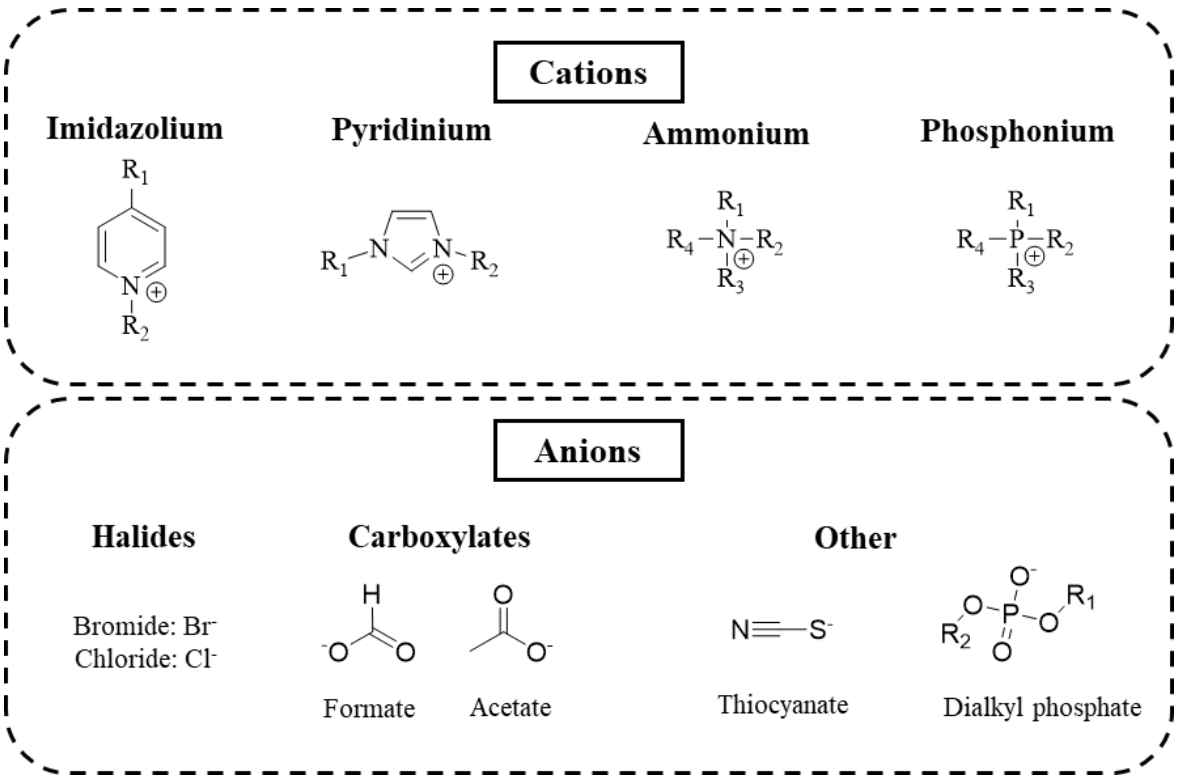

Figure 12. The most common cation and anion of ILs that able to dissolve cellulose

Deep eutectic solvents (DES) are mixtures of hydrogen bond donors and acceptors, which were introduced by Abbott et al.[4] in 2003. Typically, DES combinations involve urea or choline chloride alongside other agents, such as imidazole (IL), halide salts (such as $ZnCl_2$), glycerol, or organic acids (such as oxalic acid and malic acid). The benefits of DESs include their low cost, low toxicity, and straightforward preparation. However, DESs are inefficient at processing high DP cellulose, which limits their application in cellulose processing.

In the early 2010s, tetrabutylammonium and phosphonium hydroxide ($[N_{4,4,4,4}]OH$ and $[P_{4,4,4,4}]OH$) at 60% in water were proven to be solvents that can dissolve high amounts of cellulose at room temperature.[63] Additionally, this solvent is reported to be capable

of isolating cellulose from biomass.[64] Moreover, it is also easy to recover after the process. Thus, onium hydroxides have attracted increasing attention from researchers in the field of cellulose.

In an aqueous solvent system, cuprammonium hydroxide (Cuam) and cupriethylendiamine (Cuem) are the most well-known.[65] The regenerated cellulose generated from the Cuam solution has been applied in the textile industry for over a century. This solvent has contributed to the development of various types of regenerated fibres and its use as an analytical solvent for cellulose material. Aqueous alkalis, such as NaOH/water and NaOH/urea, are classical cellulose solvents. However, this solvent system can only dissolve cellulose under harsh conditions and struggles to dissolve cellulose with high DP.

Many cellulose dissolution solvents have been developed over time. However, the dissolution mechanism remains only partially understood because of the variety of solvent systems and cellulose polymorphs. In today's world, environmental concerns demand the development of green solvent systems to replace traditional solvents, which are often harmful to the environment. This ongoing challenge is driven by issues related to toxicity, volatility, high costs, and low recovery efficiency.

1.4.2 Chitosan solvent

Compared to cellulose dissolution solvents, the number of solvents available for chitosan dissolution is limited. This may be due to the complex hydrogen-bond network and chemical structure of chitosan. Chitosan is insoluble in water and most organic solvents. The most common solvents for chitosan are aqueous acids, with acetic acid being particularly popular among them. Recently, IL and DES have been also reported that also able to dissolve chitosan. [66-68]

The presence of free amino group (NH_2) in the polymer backbone of chitosan easily protonates to form a positively charged ammonium group (NH_3^+) in an acidic medium. This protonation disrupts the intermolecular hydrogen bonds and introduces electrostatic repulsion between the polymer chains, resulting in the solubilisation of chitosan. Weak acids like acetic or lactic acid are commonly used solvents because they

protonate enough to dissolve chitosan and keep a pH that minimises polymer degreadation.[69, 70] Chitosan solution can be forced to precipitate using an alkali solution, such as NaOH or NH_4OH. This phenomenon can be explained by the deprotonation of the ammonium group back to the neutral amino group.

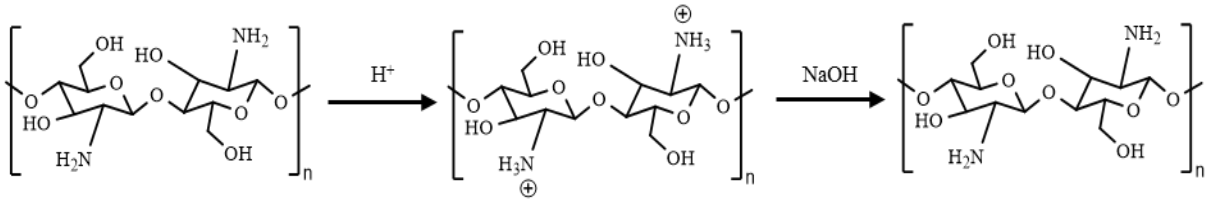

Figure 13. Dissolution mechanism of chitosan in acidic media and precipitated by NaOH

Another solvent is a combination of concentrated aqueous alkaline (NaOH, LiOH) with urea or thiourea, which allows chitosan to dissolve via the freeze-thaw process.[71-73] The mechanism of this solvent system is proposed to be similar to that of the non-derived solvent system of cellulose, which disrupts the hydrogen bond network, leading to dissolution.

IL and DES have also been recently researched as chitosan dissolution solvents due to their superior characteristics compared to classical solvents. Mok et al.[74] screened the dissolution ability of 640 ILs by using COSMO-RS. This study assumed that both cations and anions are involved in the chitosan dissolution process by disrupting the hydrogen bond system, but the role of anions is more critical. However, the impact of cations on the dissolution cannot be neglected.[75] Hence, this indicates several similarities in the dissolution mechanism between cellulose and chitosan when using IL.

1.4.3 Cellulose and chitosan alternatives solvent

The 12 principles of green chemistry drive us towards sustainable and environmentally responsible chemical processes. Finding alternative green solvents suitable for cellulose and chitosan is challenging. ILs are potential candidates with several advantages. However, toxicity, low biodegradability, and high cost are some of the disadvantages of IL.

Onium hydroxides are categorised as a small group of ILs. They are ionic compounds composed of quaternary ammonium or phosphonium paired with hydroxide anions

$[OH]^-$. It was known in the early 20th century and has been applied in various fields for a long time. In 1956, Strepikheev et al.[76] demonstrated that dimethylphenylbenzyl ammonium, triethyl benzyl ammonium, and triethylfury ammonium hydroxides could dissolve cellulose at a DP of 860. In the following decades, this type of solvent nearly disappeared from cellulose research.

In the last decade, there has been an increasing interest in the use of onium hydroxides as cellulose solvents. Beginning with the study of Abe and colleagues, it was indicated that tetrabutylammonium and phosphonium hydroxide ($[N_{4,4,4,4}]OH$ and $[P_{4,4,4,4}]OH$) solutions can dissolve up to 20 wt. % of microcrystalline cellulose (MCC) at room temperature by adjusting the onium concentration.[63] After that, Ema et al.[77] reported that the solubility power of $[N_{4,4,4,4}]OH$ differs between the providers; some of them are also not able to dissolve cellulose. This is because trace amounts of alkali ions are present in the product. By adding 18-crown-6 to the $[N_{4,4,4,4}]OH$ solution, the undesirable effect of trace alkali was eliminated. Then 10wt.% of cellulose can be solubilised in the treated $[N_{4,4,4,4}]OH$ solution. In 2016, Chao et al.[64] was able to extract cellulose from wheat straw using $[N_{4,4,4,4}]OH$ 50 wt. %. This study indicated that $[N_{4,4,4,4}]OH$ maintained high activity after several recycling cycles. The cellulose dissolution mechanism using $[P_{4,4,4,4}]OH$ is illustrated in Figure 14, which is proposed by Nguyen et al.[78]

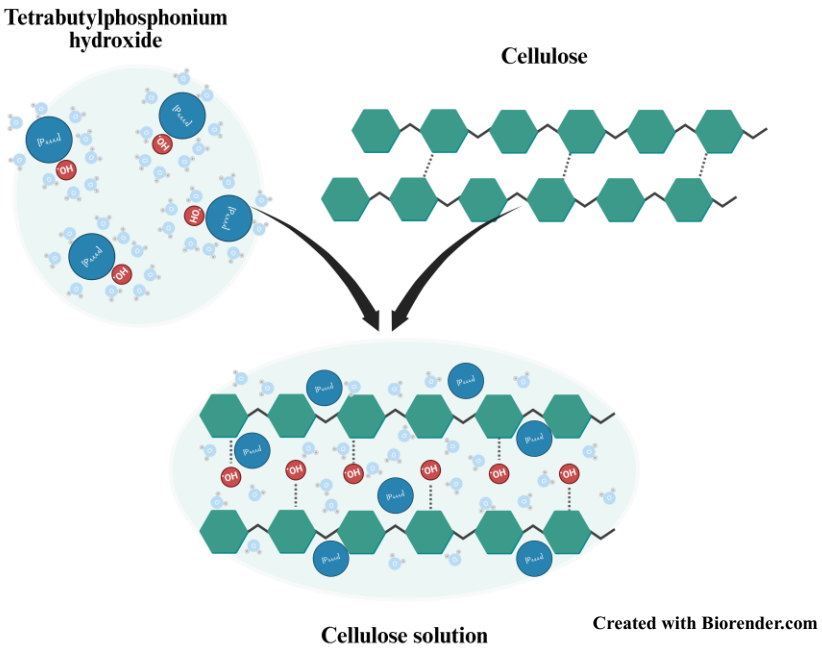

Figure 14. Cellulose dissolution mechanism using$[P_{4,4,4,4}]OH$

The use of onium hydroxides for chitosan dissolution has not been reported, unlike their use for cellulose dissolution. In 2016, Abe et al.[79] found that onium hydroxide solutions can dissolve chitin at room temperature. Tetraethylammonium hydroxide ($[N_{2,2,2,2}]OH$) and tetrapropylammonium hydroxide ($[N_{3,3,3,3}]OH$) were found to dissolve up to 0.2 wt. % of chitin after 2 weeks, and chitosan was obtained after the solution was precipitated. The recycling rate of $[N_{2,2,2,2}]OH$ in this process reached 87%. Furthermore, Ma et al.[80] dissolved chitin using $[N_{4,4,4,4}]OH$ in 2020. The amount of dissolved chitin increased from 4.0 mg/mL to 11.1 mg/mL with increasing concentration of onium hydroxide. Recently, Dinh et al.[81] used $[N_{4,4,4,4}]OH$ 40 wt.% for treating chitin at a 2.5 wt.% ratio using a microwave or heating at 100°C in 2 hours. Chitosan was obtained, and its DDA reached 71%; however, a reduction in the MW of chitosan compared to that of chitin was recorded.

Overall, onium hydroxides are promising solvents for cellulose and chitosan. They have been proven to be excellent solvents for cellulose; however, their application in chitosan dissolution remains unexplored.

1.5 Developing regenerated cellulose/chitosan material using the MDCell process

Identifying suitable solvents for cellulose and chitosan is the first step in processing these polymers. Converting them from solid to solution is essential because it allows for uniform mixing and precise control of their properties. In this PhD research, the MDCell process will be employed to investigate and produce regenerated cellulose and chitosan. The MDCell process was developed by our research group in 2020.[78] Specifically, microcrystalline cellulose was dissolved using $[P_{4,4,4,4}]OH$ 50 wt.%. Propylene carbonate (PC) was able to solidify the cellulose solution within 5 minutes rapidly. This is explained by the reaction between PC and $[OH]^-$, which releases propylene glycol and carbon dioxide, leading to the precipitation of cellulose. The process mechanism is illustrated in Figure 15.

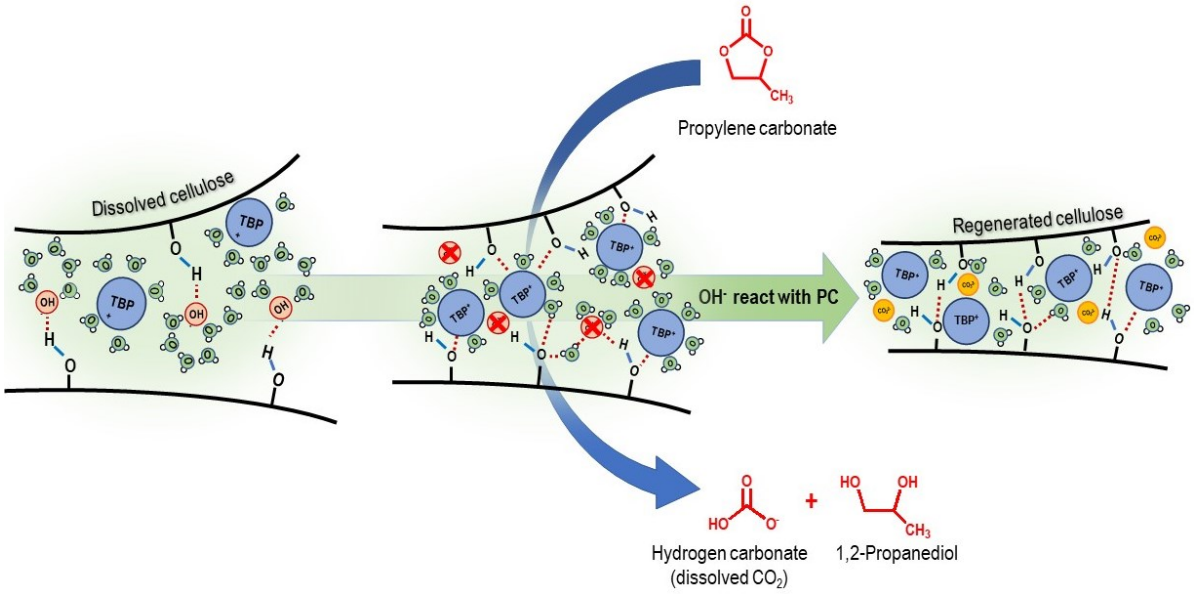

Figure 15. The mechanism for cellulose/[$P_{4,4,4,4}$]OH solution precipitated in PC [78]

In this study, cellulose membranes were produced using the casting method after solidification in a PC bath. The membrane appeared homogeneous and was utilised for wastewater treatment. Additionally, Dimethyl sulfoxide (DMSO) was employed as co-solvent for the cellulose/[$P_{4,4,4,4}$]OH solution to modify the viscosity. Membrane flexibility and transparency were improved after the addition of DMSO. The MDCell method is an eco-friendly and rapid method for processing cellulose materials. It also has potential for application in other polysaccharide materials. If this method proves effective for other polysaccharide materials, specially tuned polymer solutions could produce various blended polysaccharide products in a sustainable and environmentally friendly manner.

2 RESEARCH OBJECTIVES

The circular economy is vital for the modern world, which emphasises reducing reliance on finite resources and avoiding environmental damage. It advocates replacing fossil fuel-based materials with greener and more environmentally friendly options. This vision drives the development of polymers from biomass, offering an alternative to fossil fuel-derived polymers. Additionally, the process of producing these polymers must be rapid and safe for both humans and the environment.

The main goal of this study is to develop biopolymers based on the MDCell process. Cellulose is the primary material used to create blended biopolymers. First, different cationic structures of tetraalkyl onium hydroxides were used to examine their ability to dissolve cellulose at room temperature. The high viscosity of pure OHS could be ignored by using the swelling process in DMSO. By comparing cellulose dissolution with and without a swelling step, the influence of the cationic structure (alkyl chain length and centre atom) and water content was revealed. Additionally, the cellulose dissolution process in the onium hydroxide solution was recorded by microscopic observation, which helped deepen the understanding of the cellulose dissolution mechanism. A regenerated cellulose film was produced using the modified MDCell method. Various analytical measurements were performed to examine the properties of this cellulose film, which demonstrated good physical qualities, high transparency, and environmentally friendly characteristics.

Conversely, the regenerated cellulose film displayed brittleness and stiffness, which is typical of cellulosic materials. Therefore, it is essential to address the weaknesses in production. The flexibility of the film improved markedly when immersed in a lithium chloride solution. Compared to traditional plasticisers such as glycerol and polyethylene glycol, lithium chloride provides excellent enhancement for cellulose films at low concentrations.

Various materials have been tested to enhance the properties of cellulose films. Chitosan was found to be compatible with the MDCell procedures and had a strong ability to combine with cellulose. Owing to the limited information on dissolving chitosan in tetra-

alkyl onium hydroxide, a similar evaluation strategy used for cellulose was also applied to chitosan with some minor modifications. A homogeneous polymer solution of cellulose and chitosan was successfully created using tetrabutylammonium hydroxide as a solubilising agent. The ratio of each component in the blend can be adjusted before solidification in the PC. Regenerated cellulose/chitosan was produced using the MDCell process.

3 RESULTS AND DISCUSSION

3.1 Evaluation of cellulose dissolution in onium hydroxide solutions

Previous studies have demonstrated that onium hydroxide solutions can dissolve different types of cellulosic materials at room temperature.[63, 82, 83] Similar to ionic liquids, the anion $[OH]^-$ of onium hydroxide is the primary agent that disrupts the hydrogen bond network, leading to the dissolution of cellulose. Abe et al.[84] reported that the water content of aqueous onium hydroxide solution is also a crucial factor for cellulose dissolution. This study indicated that cellulose material could only dissolve in $[P_{4,4,4,4}]OH$ and $[N_{4,4,4,4}]OH$, which have water concentrations ranging from 60 to 30 wt.%. Inspired by that research, the cellulose dissolution ability of six tetraalkyl-onium hydroxides solution (OHS), including: tetramethyl hydroxide ($[N_{1,1,1,1}]OH$), trimethyladamantylammonium hydroxide ($[N_{1,1,1,a}]OH$), dipropyldimethylammonium hydroxide ($[N_{3,3,1,1}]OH$), tetrapropylammonium hydroxide ($[N_{3,3,3,3}]OH$), tetrabutylammonium hydroxide ($[N_{4,4,4,4}]OH$), and tetrabutylphosphonium hydroxide ($[P_{4,4,4,4}]OH$) in different onium concentrations, was evaluated in room temperature condition. The cationic structures of the six onium cations are illustrated in Figure 16.

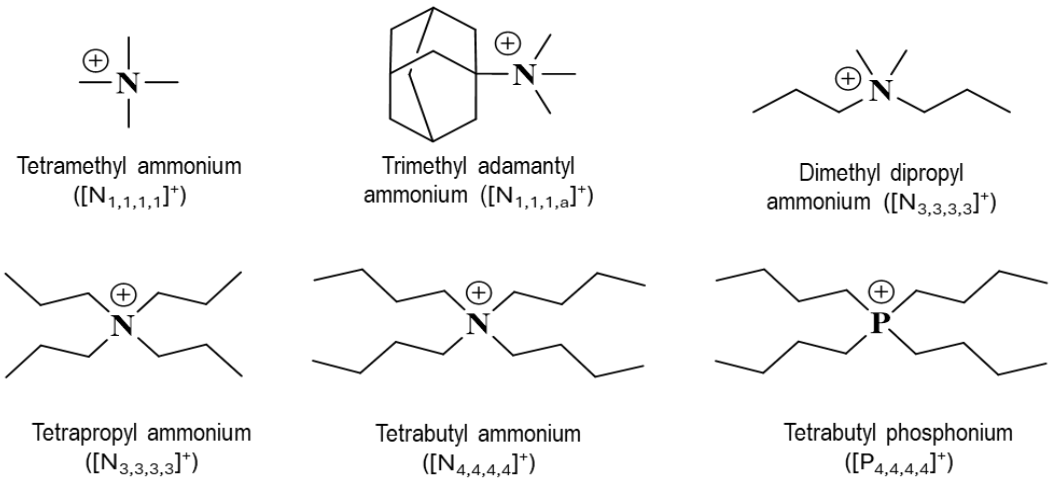

Figure 16. Cationic structure of six evaluation tetra-alkyl onium hydroxide

To evaluate the cellulose dissolution ability of the six selected OHS, microcrystalline cellulose (MCC) was used, owing to its low degree of polymerisation (normally DP < 350), which leads to fast dissolution and moderate viscosity of the cellulose solution.[85] The evaluation process is divided into two processes. The first process involved

screening the cellulose dissolution ability of OHS at different onium concentrations. Then, a quantitative measure of cellulose dissolution was applied to determine the optimum solvent for this process. The evaluation process is illustrated in Figure 17 (details described in Section II.b).

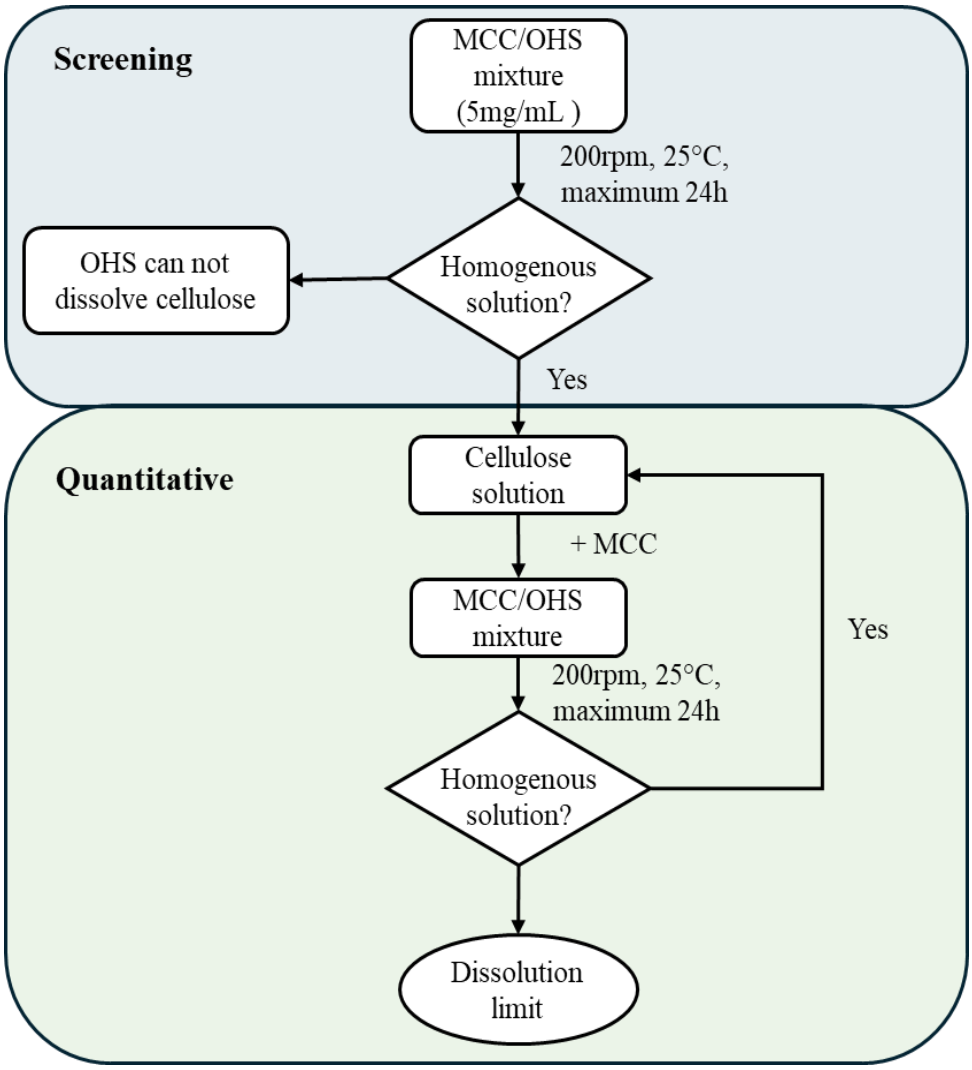

Figure 17. Schematic for screening and quantitative cellulose dissolution of onium hydroxide solution

During the evaluation process, three different states were used to assess the cellulose dissolution capacity OHS, as shown in Figure 18. The OHS is considered a non-dissolvable cellulose solution if the MCC particles settle at the bottom of the vial after the stirring process. OHS can dissolve cellulose, resulting in a transparent solution. This solution can have a clear or slightly yellow colour, according to the previous research of Nguyen et al. [78, 86]. During the quantitative process, after MCC was added, the mixture

became blurry and was considered partially dissolved. If the mixture became too viscous or remained blurry after stirring, the dissolution limit of pure OHS was determined. Additionally, MCC can be dissolved quite quickly in OHS, mostly within 2 hours.

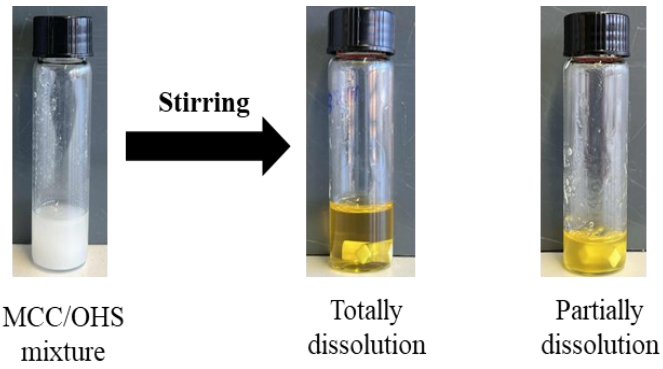

Figure 18. Images of MCC in OHS before mixing, after totally dissolve and partially dissolved

Table 2 shows the results of the screening process of cellulose dissolution of six types of onium hydroxides at different onium concentrations. This result aligns with previous research, which indicates that water content is a crucial factor in the dissolution of cellulose in OHS.[82, 84] Cellulose solubilisation increased due to the decrease in water content in every type of OHS. Only $[N_{1,1,1,1}]OH$ did not dissolve MCC under the tested conditions. The other five OHS were able to dissolve MCC. $[N_{1,1,1,a}]OH$ is the OHS with the narrowest concentration range capable of dissolving cellulose, which is limited to a 50 wt.% solution. Meanwhile, the $[P_{4,4,4,4}]OH$ solution has the broadest dissolution range, spanning from 40 to 60 wt.%.

Table 2. Cellulose dissolution ability in different onium concentration (5mg/mL) at 23°C

Cation	Onium content (wt%)			
	30	**40**	**50**	**60**
$[N_{1,1,1,1}]^+$	x	x	-	-
$[N_{1,1,1,a}]^+$	x	x	o	x
$[N_{3,3,1,1}]^+$	-	o	o	x
$[N_{3,3,3,3}]^+$	-	o	o	x
$[N_{4,4,4,4}]^+$	-	-	o	o
$[P_{4,4,4,4}]^+$	-	o	o	o

_: not measurement, x: not dissolved, o: dissolved

After the screening process was completed, the quantity of MCC dissolved in each onium hydroxide was measured. Figure 19 illustrates the cellulose dissolution limit of pure OHS at different concentrations. This result indicates that water has a significant impact on the dissolution of cellulose in OHS. For instance, at 40wt% [$P_{4,4,4,4}$], OH could dissolve only 50 mg/mL of MCC, whereas this number increased to 150 mg/mL at 50 and 60wt%. This number is also the maximum amount of MCC that other pure OHS can dissolve at room temperature. At 50wt%, [$N_{3,3,1,1}$]OH, [$N_{3,3,3,3}$]OH, [$N_{4,4,4,4}$]OH, and [$P_{4,4,4,4}$]OH were able to dissolve a high amount of cellulose in several minutes. However, these results highlight the weakness of pure OHS, specifically its high viscosity, which limits the amount of cellulose that can be dissolved. Nguyen et al. [86] indicated the viscosity of [$P_{4,4,4,4}$]OH increased proportionally with the onium concentration, as well as the cellulose solubilised concentration. According to this study, the viscosities of [$P_{4,4,4,4}$]OH at 40, 50, and 60 wt.% are 4.9, 11, and 17.2 mPa s, respectively. At 20 wt. % solubilised cellulose, the viscosity of the solution dissolved by [$P_{4,4,4,4}$]OH 50 wt.% was 9610 mPa s, while that by [$P_{4,4,4,4}$]OH 60 wt.% was 12638 mPa s. The high viscosity of the cellulose solution reduced mass transfer, making it difficult for the magnetic stirrer. Consequently, 150 mg/mL was the dissolution limit of pure OHS

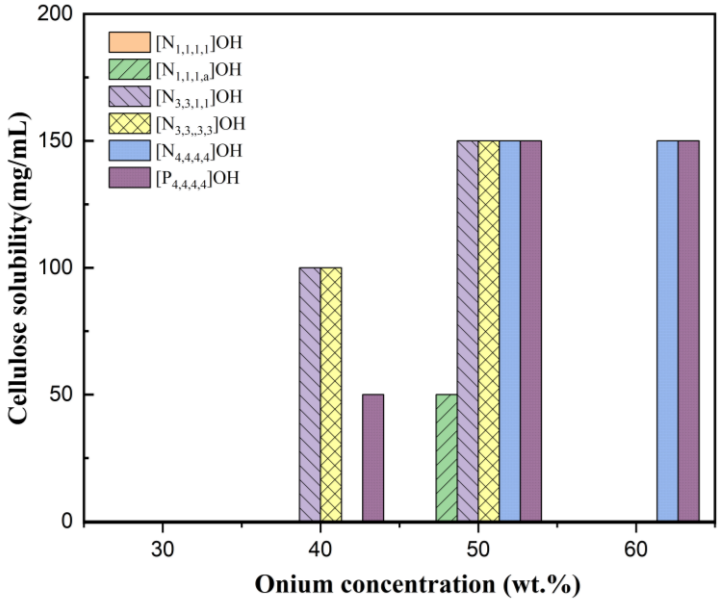

Figure 19. MCC dissolution limit of six types of onium hydroxide in different concentrations at room temperature

In addition to the onium concentration, Abe et al.[82] used another value to explain the dependence of cellulose dissolution on OHS, it is called "a number of water molecules per hydroxide ion (Nw)". This study indicated the Nw value for OHS that can dissolve cellulose is below 25. However, its value depends on the cationic structure of the onium hydroxide. Wei et al.[87] indicated that the most suitable range for cellulose dissolution in $[N_{4,4,4,4}]OH$ solution is between 50 and 60 wt. % concentration. This study assumes that if Nw is too high (onium concentration under 30 wt.%), the water mainly remains in the free state and does not bind with the alkyl chain of the cation to form hydrophobic interactions (via van der Waals forces), so the solution exhibits mainly hydrophilic properties. Adjusting the concentration of the OHS solution changes the amphiphilicity of the solution. When the onium concentration exceeds 70 wt.%, the solution primarily exhibits hydrophobic properties due to an increase in hydrophilic interactions. Both too high or too low Nw values negatively affect cellulose dissolution. Table 3 lists the Nw values for each onium hydroxide at different concentrations used in this study. (The red colour number in the table represents the cellulose solubilisation solvent.)

Table 3. The number of water (Nw) of onium hydroxides at different concentrations

Cation	Onium content (wt%)			
	30	40	50	60
	Number of water (Nw)			
$[N_{1,1,1,1}]^+$	11.8	7.6	5.1	3.4
$[N_{1,1,1,a}]^+$	27.4	17.6	11.7	7.8
$[N_{3,3,1,1}]^+$	19.1	12.3	8.2	5.54
$[N_{3,3,3,3}]^+$	26.4	17	11.3	7.5
$[N_{4,4,4,4}]^+$	33.6	21.6	14.4	9.6
$[P_{4,4,4,4}]^+$	35.8	23.0	14.3	10.2

The increase in the hydrophobic interaction between the alkyl chain and water with increasing onium hydroxide concentration led to phase separation of the OHS. Figure 20 display $[N_{4,4,4,4}]OH$ at 60 and 70 wt.%, with the 60 wt.% solution being homogeneous while the 70 wt.% solution exhibits two separate layers. It is noted that the OHS solution with Nw below 8 cannot dissolve any MCC under the tested conditions. Therefore, OHS

must have suitable amphiphilicity to dissolve cellulose. This can be achieved by adjusting the water content of OHS, depending on the cationic structure. According to our results, the suitable range of Nw for cellulose dissolution is approximately 8–25.

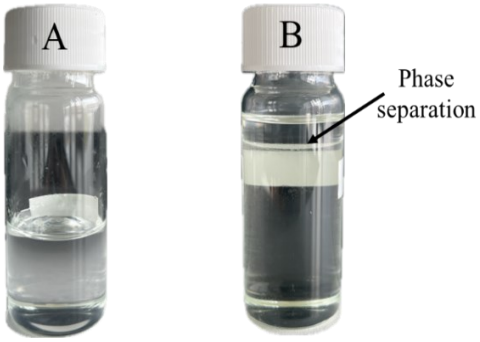

Figure 20. [$N_{4,4,4,4}$]OH solution at A) 60 wt.%, and B) 70 wt.%

The results also demonstrated that the cationic structure is a highly influential factor in the dissolution ability of OHS. It was observed that only the [$N_{1,1,1,1}$]OH solvent could not dissolve cellulose at any of the tested concentrations. A similar finding was reported for the dissolution of cellulose in [$N_{1,1,1,1}$]OH in a study by Abe et al.[82]. This study suggests that the steric effect could be the reason for the undissolved cellulose of short alkyl chain lengths of tetraalkyl onium hydroxide. For instance, [$N_{1,1,1,1}$]OH 30 wt% and [$N_{1,1,1,a}$] 50 wt. % both have a similar value of Nw (11.7 and 11.8, respectively); the difference is one methyl group replaced by an adamantyl group. The bulkiness of the adamantyl groups prevents $[OH]^-$ and water molecules from interacting with the central ammonium atom, leading to increased free $[OH]^-$ within the medium. As a result, [$N_{1,1,1,a}$]OH exhibited cellulose dissolution ability, whereas [$N_{1,1,1,1}$]OH cannot. Recently, the combination of [$N_{1,1,1,1}$]OH with NaOH was reported to dissolve up to 5 wt. % of MCC at 30°C, while [$N_{1,1,1,1}$]OH is also not able to dissolve cellulose under the same conditions.[88] Additionally, ILs with long alkyl chains are reported to have higher hydrophilicity compared to short alkyl chains, leading to better cellulose dissolution ability. [89-91] Our results also indicate that the amount of MCC dissolved by [$N_{3,3,1,1}$]OH, [$N_{3,3,3,3}$]OH, and [$N_{4,4,4,4}$]OH was higher than that by [$N_{1,1,1\ a}$]OH.

On the other hand, extending the alkyl chain length is not always beneficial for cellulose dissolution. Abe et al.[90] examined the cellulose dissolution of long alkyl chains of tetraalkyl phosphonium formate salt. This research found that the tetra-butyl

phosphonium cation ([$P_{4,4,4,4}$]) was the only salt that could dissolve cellulose, whereas longer alkyl chain phosphonium cations ([$P_{5,5,5,5}$], [$P_{6,6,6,6}$], and [$P_{8,8,8,8}$]) could not. Other studies have also observed a reduction in cellulose solubility with the increase in the length of the alkyl chain of imidazolium salts.[62, 92-94] These studies suggested that an excessively bulky cationic structure (containing extensive alkyl chains or bulky groups) increases the steric hindrance effect, which significantly decreases the interaction of anion groups with the hydroxide groups of cellulose. This leads to a lower efficiency of long alkyl chain onium salts in cellulose dissolution.

In general, onium hydroxide solutions exhibit good cellulose dissolution ability, and can dissolve cellulose at room temperature. The dissolving capacity of this type of solvent depends on its amphiphilic nature, which is influenced by various factors, including the cationic structure, water content, and central atoms. During evaluation, [$N_{3,3,3,3}$]OH, [$N_{3,3,1,1}$]OH, [$N_{4,4,4,4}$]OH, and [$P_{4,4,4,4}$]OH showed high cellulose dissolution, reaching up to 150mg/mL of MCC. However, it is essential to note that the high viscosity of OHS significantly affects its dissolution limit.

3.2 The impact of pre-swelling cellulose in DMSO on the dissolution limit

The weakness of pure onium solvent systems is their high viscosity, as discussed in the previous section. Therefore, the potential of OHS in cellulose dissolution has not been fully realised. Using a co-solvent is one solution that has proven effective in overcoming this weakness and improving the dissolution limit.[95-97] Different solvents have been examined, and dimethyl sulfoxide (DMSO) has appeared to be one of the most effective co-solvents.[97-100] The study of Medroho et al.[101] analysed the cellulose solubility in various mixtures of [$N_{4,4,4,4}$]OH and DMSO, finding that cellulose was able to dissolve in the mixture with a DMSO ratio content of 90 wt.%. Additionally, Kuzmina et al. [102] found that cellulose swells in DMSO before being dissolved by ILs, which not only accelerates the dissolution process but also does not significantly change the DP of cellulose. DMSO is an excellent solvent when combined with ILs for cellulose dissolution, but its combination with onium hydroxide remains very limited.

This section explores how swelling in DMSO affects the dissolution capability of onium hydroxides, and the examination procedure is illustrated in Figure 21. The impact of DMSO on the dissolution limit of OHS was also evaluated in two parts: screening and quantitative dissolution capacity. A similar ratio between MCC and pure OHS was used for the screening, even though MCC was prewetted in DMSO before OHS was added. The quantitative procedure was similar to the screening process, but a larger amount of MCC was used compared to the amount used in the screening step.

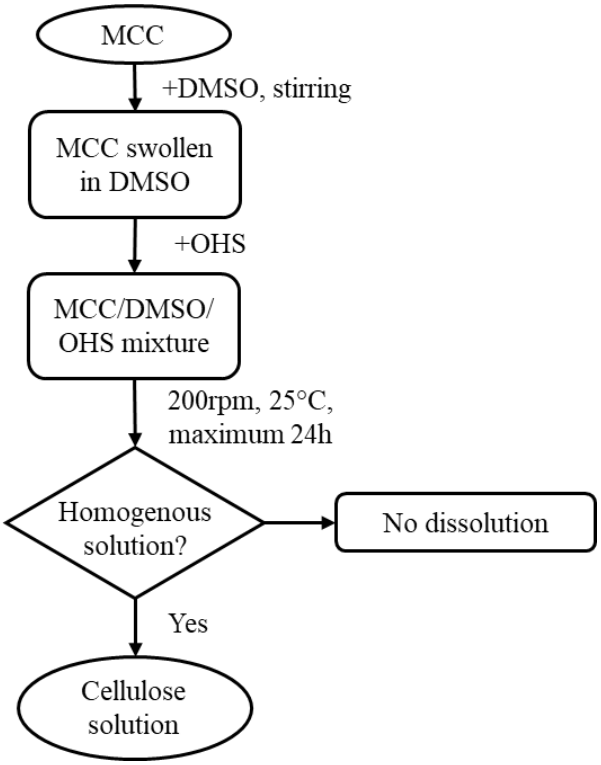

Figure 21. Schematic to investigate the impact of DMSO on the dissolution ability of OHS

Figure 22 shows the MCC at different states before and after swelling in DMSO and cellulose solution. At the beginning of the swelling process, the MCC powder settled at the bottom of the vial. After swelling in DMSO, the MCC particles absorbed DMSO into their inner structure and expanded, resulting in a slurry mixture.[103] The slurry of MCC with DMSO appeared blurry. After OHS was added, the mixture became clear and slightly yellow, indicating that the solvent could dissolve cellulose. If not, the vial remains blurry. Moreover, the cellulose only partially dissolved, and the mixture appeared similar to cellulose solution, as indicated in Figure 18.

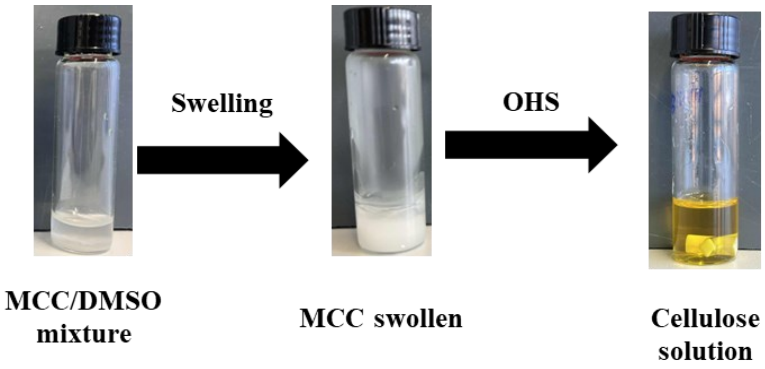

Figure 23. Images of MCC before and after swelling, then totally dissolved

Figure 23 illustrates the cellulose solubility of OHS after the MCC was swollen in DMSO. This indicates a significant increase in the amount of MCC that onium hydroxide can dissolve. Due to the high viscosity of the cellulose solution, 150 mg/ml was the threshold of pure OHS. $[N_{4,4,4,4}]OH$ was found to be the most effective cellulose dissolution solvent; 450 mg/mL was the highest concentration of MCC that dissolved by 60 wt.% solution. An increase in cellulose-dissolving ability was also observed for other OHS types except for the $[N_{1,1,1,1}]OH$ solution. The results indicated the influence of cationic structure more clearly, with the dissolution ability $[N_{4,4,4,4}]^+ > [N_{3,3,3,3}]^+ > [N_{3,3,1,1}]^+ > [N_{1,1,1,a}]^+$.

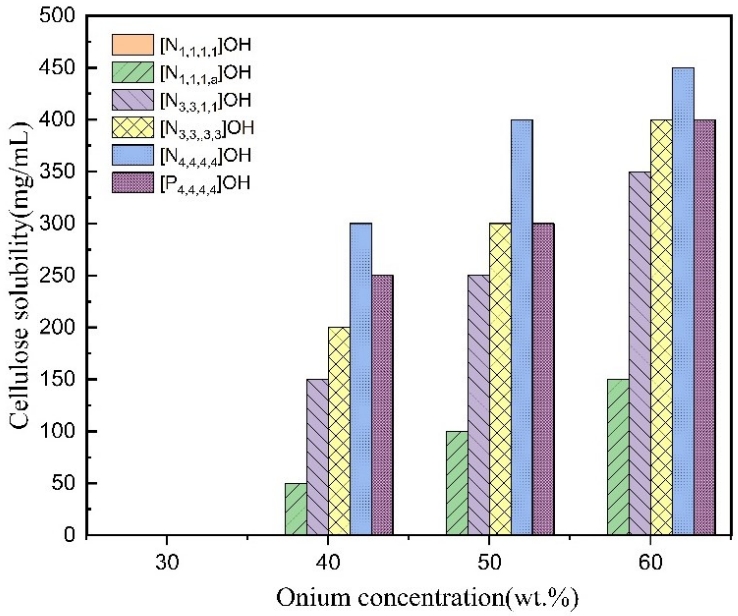

Figure 22.MCC dissolution limit of six types of onium hydroxide at various concentrations after MCC has swollen in DMSO

The influence of the onium central atom (ammonium and phosphonium) on the cellulose dissolution limit is evident, according to the results shown in Figure 23. $[N_{4,4,4,4}]OH$ solution in both 50 and 60 wt.% concentration dissolved more MCC compared to $[P_{4,4,4,4}]OH$ at the same onium concentrations. This result differs from the study by De Wever and colleagues.[104] In this study, $[P_{4,4,4,4}]OH$ 50 wt. % can dissolve 15 wt.% pretreated cellulose pulp, while it is 10 wt.% for $[N_{4,4,4,4}]OH$ at the same concentration. The hydrophobicity of the cation is beneficial for the dissolution of cellulose. [89-91] According to studies by Kohno and colleagues, quaternary phosphonium cations are more hydrophobic than quaternary ammonium cations when comparing cations with the same alkyl chain length, so $[P_{4,4,4,4}]OH$ is more hydrophobic than $[N_{4,4,4,4}]OH$ in the same solution concentration. [105, 106] However, our results show that $[N_{4,4,4,4}]OH$ exhibited better cellulose dissolution at all tested concentrations. It indicated that the increased hydrophilicity of OHS is not always beneficial for cellulose dissolution.

It is noted that pre-swelling in DMSO improved the cellulose dissolution capacity of all tested OHS, except $[N_{1,1,1,1}]OH$. For example, a 40 wt.% solution of $[N_{3,3,3,3}]OH$ can dissolve only 100 mg of MCC in 1 mL, but this amount increases to 200 mg when MCC is swollen in DMSO with the same volume used. This is because DMSO penetrates the cellulose structure, reducing the interaction between cellulose chains, which allows OHS to interact more effectively with the chains and dissolve cellulose more easily. Consequently, more cellulose can be dissolved in the solvent. In the previous section, 60 wt. % of pure $[N_{1,1,1,a}]OH$, $[N_{3,3,1,1}]OH$, and $[N_{3,3,3,3}]OH$ were unable to dissolve even tiny amounts of MCC. However, by pre-swelling cellulose in DMSO, the solution could dissolve a significantly larger amount of cellulose. The results also indicated that the concentration of the onium hydroxide correlates with its ability to dissolve cellulose. The authors suggested that DMSO helps reduce the negative impact caused by the high hydrophobicity of concentrated onium hydroxide solutions, which inhibits cellulose solubilisation. Recently, it was reported that water reduces the dissolution ability of cellulose in tetrabutylammonium/DMSO ($[N_{4,4,4,4}]OAc$/DMSO).[107] This study explained that increasing the water ratio decreases the basicity of the mixture. The basicity of the mixture is crucial for cellulose dissolution efficiency. Therefore, this

might explain why a solution with a low onium ratio could not dissolve cellulose, even though the cellulose was swollen in DMSO.

The cellulose solubilization of OHS was increased through swelling cellulose in DMSO, where a concentration of 450 mg/mL was achieved using $[N_{4,4,4,4}]OH$ at 60 wt.%. However, the obtained solution gelled faster than at lower cellulose concentrations with the same dissolution agent, $[N_{4,4,4,4}]OH$ 60 wt.%. Previous research has indicated that a higher cellulose concentration accelerates the gelation time.[108, 109] This is because a higher concentration promotes interactions between cellulose chains, bonding them together and resulting in a gel network. The concentration at which gelation occurs varies depending on the solvent and DP of cellulose. The differences between the standard cellulose solution and the gelled solution are shown in Figure 24. The gelled solution no longer exhibited fluid characteristics, even when the vial was inverted. Additionally, prolonged storage also results in the gelation of the cellulose solution. [110, 111]

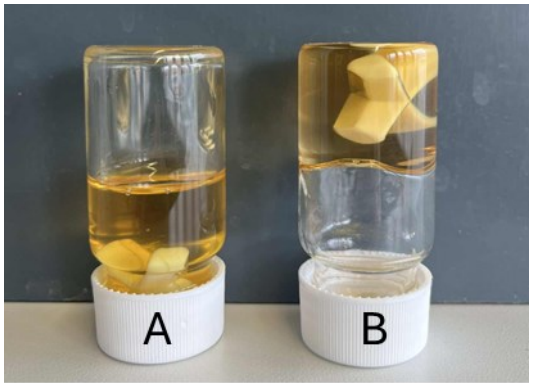

Figure 24. A) Normal cellulose solution, B) gelated cellulose solution

To better understand the cellulose dissolution mechanism in onium hydroxides, NMR spectroscopy was performed. Figure 25 illustrates ^{13}C-NMR spectra of MCC dissolved in $[N_{4,4,4,4}]OH$ at different concentrations of MCC (200 and 300 mg/mL) and DMSO-d_6/$[N_{4,4,4,4}]OH$ in the carbohydrate region (60 to 110 ppm).[112] According to previous research, the signals at 105, 79.5, 76.6, 75.4, 74.5, and 61.4 ppm correspond to C_1, C_4, C_5, C_3, C_2, and C_6 of the AGU of cellulose, as depicted in the ^{13}C-NMR.[113-115] The intensity of the cellulose signal is also proportional to the cellulose concentration, with

six-carbon signals only dectected in the NMR spectra with higher cellulose concentration.

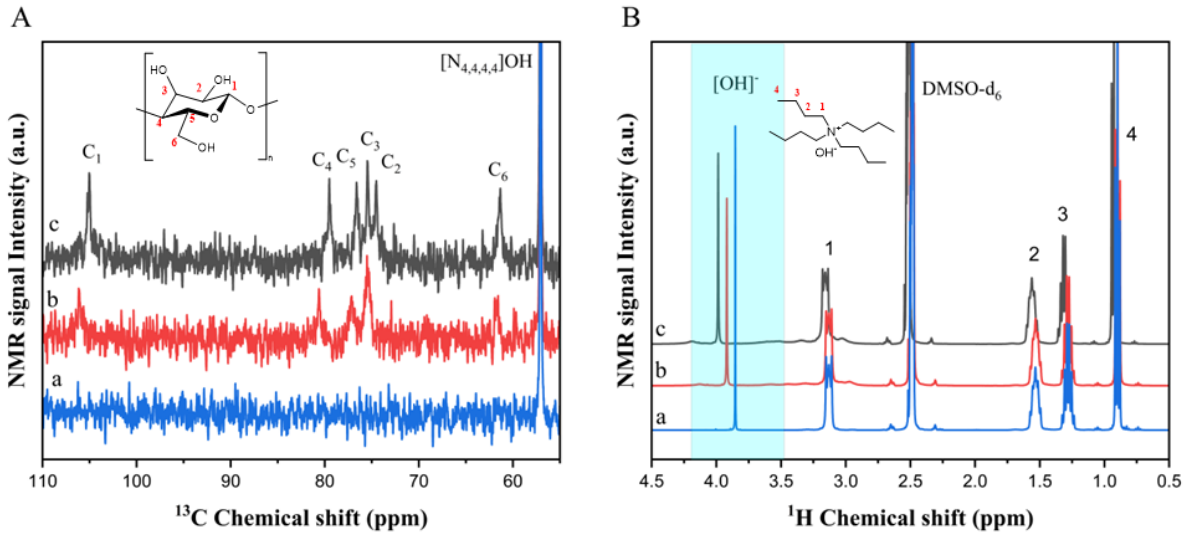

Figure 25. ^{13}C and ^{1}H-NMR spectroscopy of a) [N$_{4,4,4,4}$]OH, b) 200mg/mL, and c) 300mg/mL of MCC dissolved in [N$_{4,4,4,4}$]OH

To further investigate the dissolution mechanism of cellulose in OHS, the ^{1}H-NMR [N$_{4,4,4,4}$]OH solution with varying cellulose concentrations was used, as shown in Figure 26. A gradual shift of the hydroxide anion of [N$_{4,4,4,4}$]OH to higher regions, proportional to the cellulose concentration. The $[OH]^-$ peak of pure [N$_{4,4,4,4}$]OH at δ=3.85 ppm shifted to 3.91 and 3.98 ppm, respectively, for 200 mg/mL and 300 mg/mL concentrations of MCC. A similar phenomenon was observed in the research of Zhong and colleagues.[116] The higher chemical shift was due to the decrease in the electron density around the H atom of the $[OH]^-$ anion. The increase in cellulose, which leads to more hydrogen bonding between the $[OH]^-$ anion and the hydroxide groups of cellulose, is the reason for the downshift of the $[OH]^-$ anion signal. This also confirms that the $[OH]^-$ group of OHS plays a significant role in cellulose dissolution.

In general, the experiment proved that swelling MCC in DMSO enhanced the dissolution ability of OHS. The negative impact of the high viscosity of pure OHS was eliminated, indicating that the cationic structure influences the dissolution process. Additionally, [N$_{4,4,4,4}$]OH was the most effective solvent among the examined OHS and was used for further experiments with cellulose material.

3.3 Evaluation of Kraft cellulose dissolution

In this section, Kraft cellulose (KC) is used to replace MCC, allowing for a comparison of the efficiency of pure $[N_{4,4,4,4}]OH$ and the influence of the swelling step. Using similar experimental conditions applied to MCC, the impact of DP was examined. MCC is related to short polymer chains and low DP value cellulose material, which was tested with a high amount of dissolved MCC.[85] KC is produced from Kraft pulp of wood, which retains very long polymer chains, residual hemicelluloses, and lignin.[117, 118] The DP of KC is in the range of 800 to 1500, or even up to over 2000, depending on the type of blended wood.[119, 120] The results will provide information that will be used for the development of cellulosic material later.

Scanning electron microscopy (SEM) was used to examine the structures of MCC and KC. Figure 26 illustrates the noticeable morphological differences between these two cellulose materials.

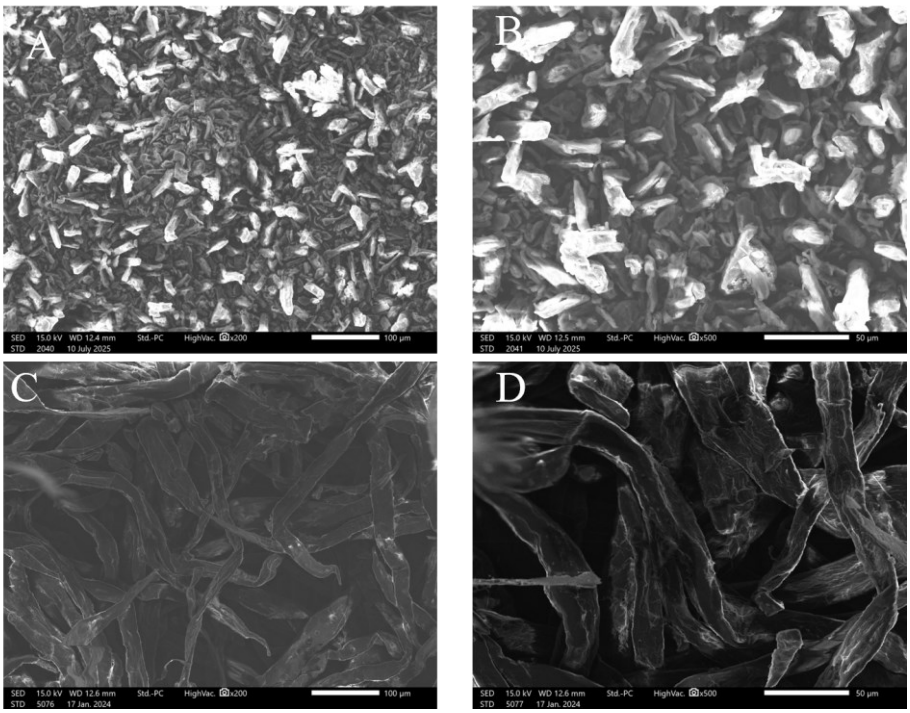

Figure 26. SEM analysis A,B) MCC, and C, D) KC at 200 and 500 magnifications

Under SEM observation, the MCC appeared as discrete, rod-like particles with a uniform size distribution. The length of the MCC particles is under 30µm. In contrast, KC has a fibril morphology characterised by a flattened fibre shape. It comprises

elongated, entangled fibres with irregular widths and rough surfaces. The length of the KC fibrils was considerably longer than that of the MCC.

The KC dissolution capacity of $[N_{4,4,4,4}]OH$ solution from 40 to 60 wt.% concentration of with and without swelling step indicated in Figure 27. The total amount of KC dissolved under all tested conditions and concentrations was less than that of MCC. $[N_{4,4,4,4}]OH$ solution can only dissolve up to 50 mg/mL of KC, compared to 150 mg/mL of MCC. During the swelling process, a notable increase in KC dissolution was observed, with 350 mg of KC was dissolved by 1 mL of 60 wt.% $[N_{4,4,4,4}]OH$ solution. This finding aligns with previous studies examining the impact of cellulose DP on dissolution.[121-123] Short-chain cellulose has fewer intermolecular forces between chains, making it easier for solvent molecules to penetrate and separate the chains. In contrast, longer chain cellulose is more difficult to dissolve due to its stable structure, resulting in reduced solvent penetration and lower dissolving efficiency compared to shorter chains.[124, 125] The fibre morphology, such as particle size, also decides how easily the solvent can penetrate the cellulose material.[126] Figure 26 displays the notable difference in particle sizes between MCC and KC. This may explain why less KC dissolved compared to MCC.

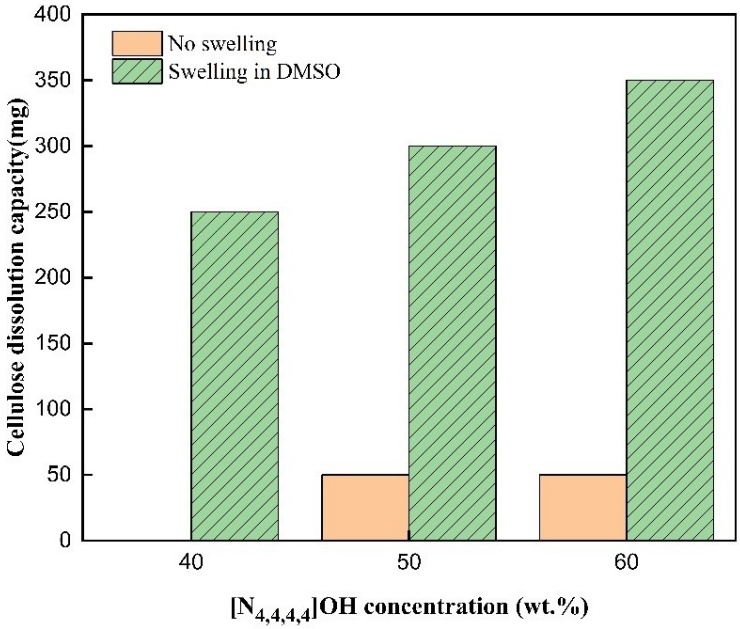

Figure 27. Comparison of dissolution capacity of pure $[N_{4,4,4,4}]OH$ from 40 to 60 wt.% and includes swelling in DMSO

3.4 Observation of swelling and dissolution behaviour of cellulose

After examining the solution of KC using microscopy, unusual shapes of cellulose fibres were observed (Figure 28). This raises questions regarding how cellulose changes during dissolution, which is not yet fully understood. Therefore, a microscope was used to investigate the swelling and dissolution of cellulose in onium hydroxide solutions after swelling at room temperature. This equipment allows for the continuous monitoring of changes in cellulose morphology. The procedure was also conducted at room temperature, which simplified the observations.

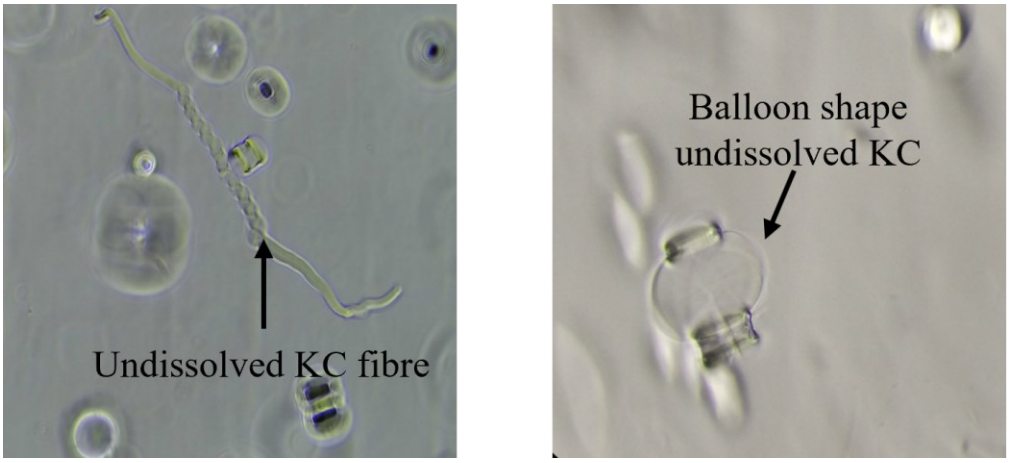

Figure 28. Undissolved fibre in KC solution observed under optical microscopy

3.4.1 Swelling of cellulose material in DMSO

The morphologies of KC and MCC are shown in Figure 26. This indicates that KC has long fibrils, whereas MCC appears as rod-like particles. The difference in morphology between the two cellulose materials results in distinct swelling behaviours for each type.[127]

Figure 29 shows images of the Kraft fibre at different times after DMSO was added. When DMSO contacted the fibre, it penetrated from the outer layer to the inner structure of the fibre. It then gradually occupied spaces inside the fibre structure. Bubbles appeared at several locations on the fibre. Over time, the size of the bubbles decreased before they disappeared because DMSO occupied all the spaces. Additionally, the lumen of the KC fibre can be observed, while it does not appear under SEM measurements. In

contrast, solvent penetration into MCC was not observed because it occurred much faster than in KC fibre.

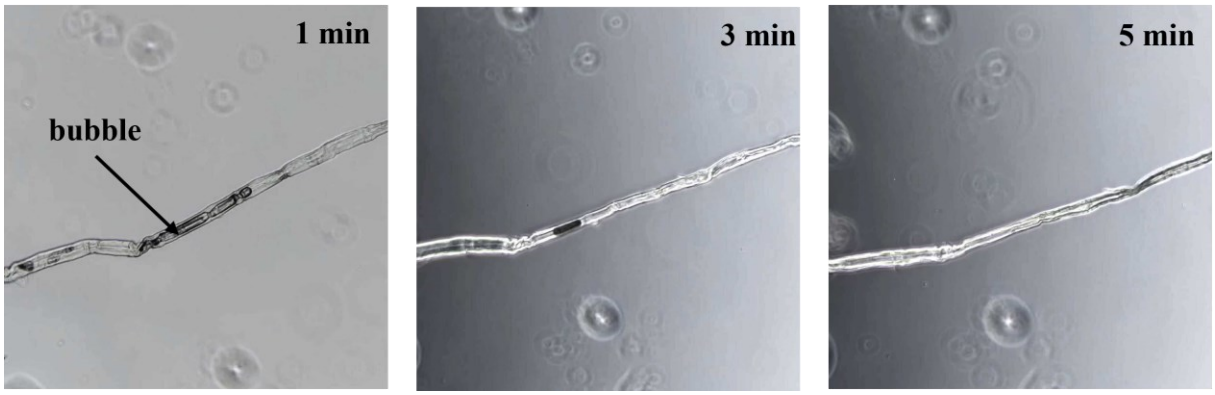

Figure 29. KC fibre in DMSO solution at the beginning of swelling in DMSO

Subsequently, the swelling stages of the cellulose material were observed. Figure 30 shows images of the MCC and KC in DMSO at various time points. The changes in diameter of both cellulose materials were recorded.

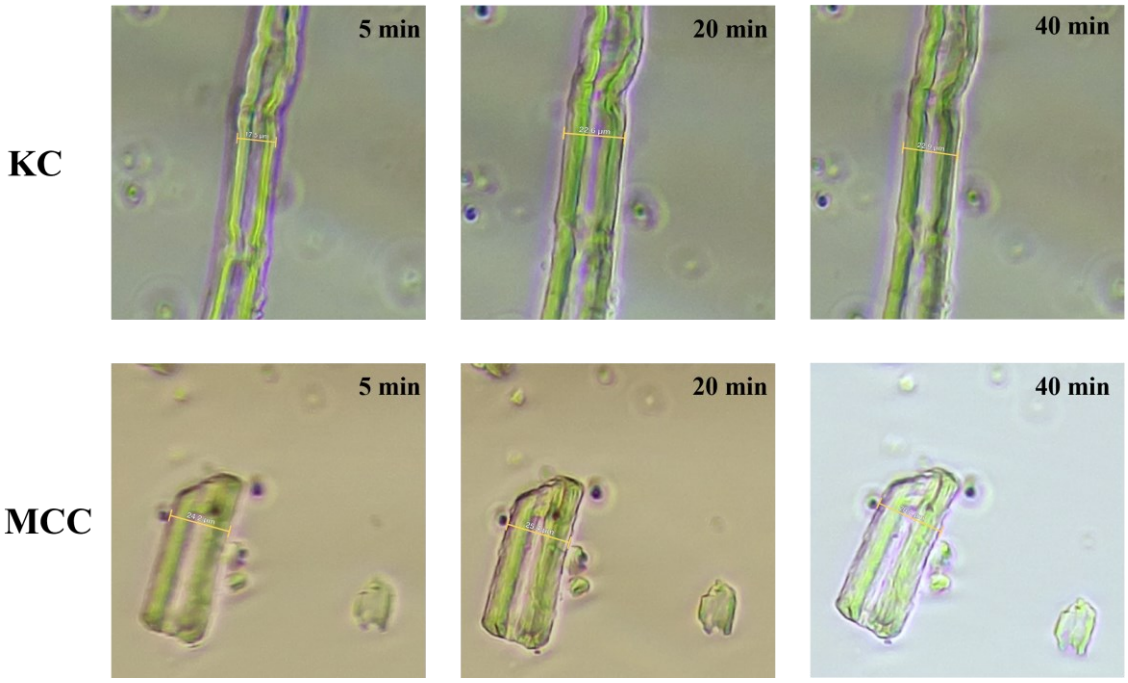

Figure 30. KC and MCC at different periods during swelling in DMSO

Comparing the diameter of KC fibre after 5 minutes and 40 minutes, it increased from 17.5 to 22.9 µm, a 1.3-fold increase. Meanwhile, the diameter of MCC increased from 24.2 µm to 26.2 µm, representing a 1.08-fold increase. This indicates that KC fibres are more effective at swelling in DMSO than MCC, primarily due to their morphology. [127-

[129] Additionally, MCC is known to be obtained after the amorphous region, which is mostly removed after the production process.[130] Meanwhile, long native fibres typically have more complex structures with crystalline and amorphous domains distributed along their length. The amorphous regions have a less ordered structure, allowing more DMSO to diffuse into the inner layer more easily than the crystalline regions. Therefore, the KC fibre can absorb more DMSO, resulting in a higher swelling capacity than that of MCC. Notably, the expansion of S2 layers during the swelling process is more easily observable than that of other layers.

Microscopy observations revealed three stages in the swelling of cellulose in DMSO. Initially, DMSO diffused and occupied all the space within the cellulose structure. Subsequently, increasing amounts of solvent inside the cellulose chains led to fibre expansion, marking the beginning of the swelling process. DMSO inserts itself between cellulose chains, interrupts the inter-chain hydrogen bonds without dissolving, loosens the tight hydrogen-bond network, and causes the chains to move apart to accommodate the solvent molecules.[131] Finally, during the swelling equilibration, when the fibre can no longer absorb more solvent, the fibre's diameter reaches its maximum value. Figure 31 illustrates the swelling mechanism of the cellulose fibre in the DMSO solution.

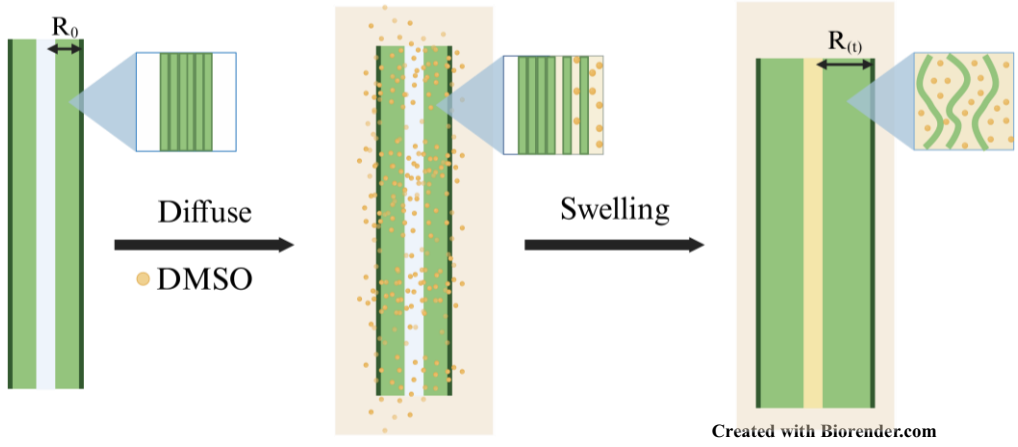

Figure 31. Swelling process of cellulose material in DMSO

3.4.2 Cellulose dissolution phenomenon

After the swelling behaviour ended, the dissolution of both MCC and KC was observed. $[N_{4,4,4,4}]OH$ was used as a dissolving agent, which was dropped directly onto cellulose.

Cellulose dissolved immediately upon contact with the OHS. The dissolution process was recorded for further analysis. Different phenomena were observed.

The first phenomena was observed is the disintegration of MCC into multiple smaller particles, then these particles rapidly dissolved. This dissolution pattern resembles the fragmentation of raw plant fibres, as discussed by Cuissinat and Navard.[132] This study suggested that the fragmentation of cellulose fibres results from the rapid permeability and effectiveness of the solvent, which creates internal stress fractures within the fibre structure. There are pre-existing weak zones (amorphous regions, spaces between bundles, or lumen voids) along the fibre.[132, 133] This can be seen in Figure 32A before fragmentation occurs. These regions facilitate solvent penetration more than other areas, increasing internal stress and leading to fibre fragmentation, after which the cellulose dissolves into smaller pieces.

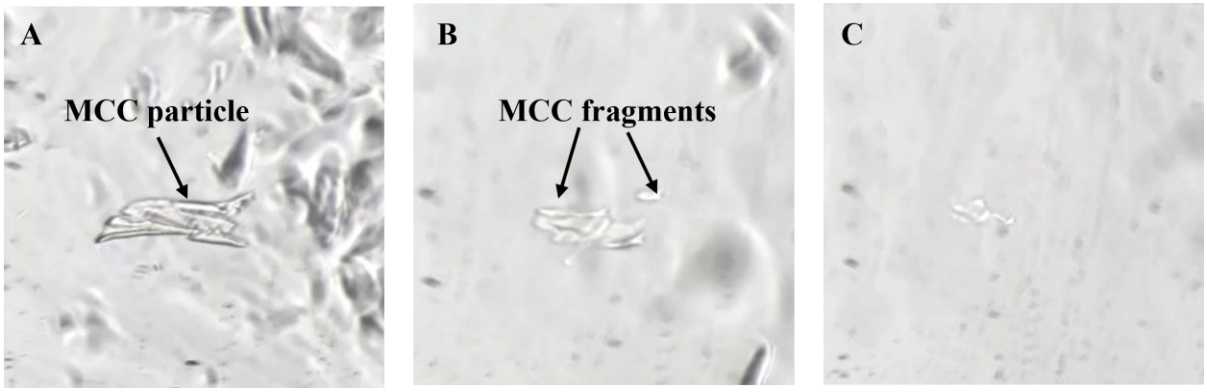

Figure 32. Observation of MCC dissolution by the fragmentation phenomenon

Another dissolution phenomenon is where the MCC gradually became smaller to the centre of the particle. MCC is a cellulose material with a high degree of crystallinity, whose crystallinity region is dominant.[134] The crystalline region has a higher-order structure, which makes it more difficult for the solvent to penetrate the inner layer of the MCC. Therefore, the outer section is solubilised first, before the interior is attacked and dissolved. As a result, these MCC particles did not break into smaller fragments, like previous observations. The shape of the MCC particles became more rounded on both sides, as illustrated in Figure 33. A similar phenomenon was observed in KC dissolution, where the fibril became shorter over time.

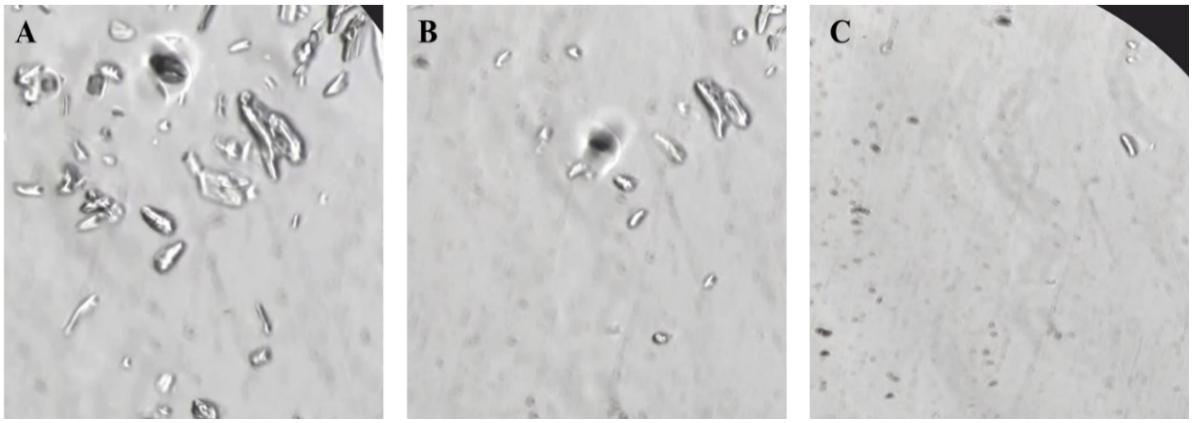

Figure 33. Observation of MCC particle changes over time, which gradually becomes smaller in the centre of the particle

While observing the dissolution of the KC fibre, two phenomena were detected. The first phenomenon is known as the ballooning phenomenon, where a part of the fibre expands like a balloon before breaking.[109, 135] The morphology of the fibre changed during the ballooning phenomenon, as shown in Figure 34. This phenomenon is typically observed in alkaline media, first reported by Nägeli's research in 1864.[136] Since then, several researchers have investigated this dissolution phenomenon.[132] .

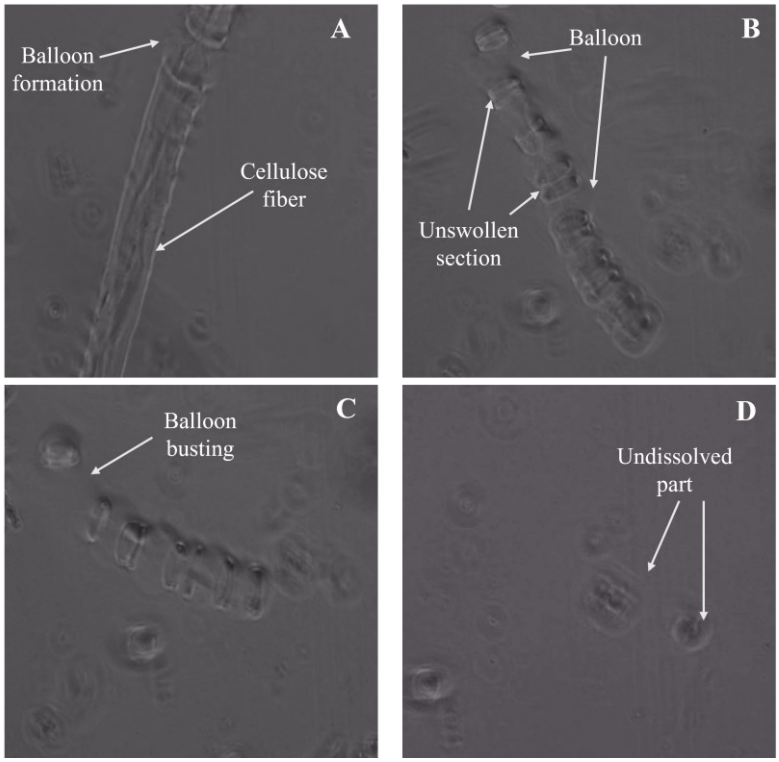

Figure 34. Kraft cellulose fibre in different stages by the ballooning dissolution phenomenon

Based on previous research, the ultrastructure of cellulose fibres can be explained by the ballooning phenomenon. As mentioned, cellulose fibres have amorphous (loose structure) and crystalline (highly structured) regions, which are distributed along the fibre.[137] This leads to the uneven dissolution of cellulose fibres. The amorphous regions are assumed to dissolve more easily because of their loose structure. This region absorbs solvents and expands gradually (transversely to the fibre axis), creating a balloon shape along the fibre length. Simultaneously, the accommodation of the solvent inside the balloon increased the internal pressure. When the outer layer of the cellulose fibre cracks or tears, the balloon bursts, and all the fluid inside diffuses into the medium. After the balloons burst, the outer layer (primary and S1 layer) of the balloons remained attached to the unswollen section and quickly dissolved. The unswollen section between the balloons formed a ring-like shape. The residual section then dissolves slowly. This section is considered a crystalline (highly structured) region, which is harder to dissolve. Therefore, this section dissolved after the balloons disappeared. Finally, the entire cellulose structure disintegrated into a uniform solution. The cellulose dissolution phenomenon via the ballooning effect is illustrated in Figure 35.

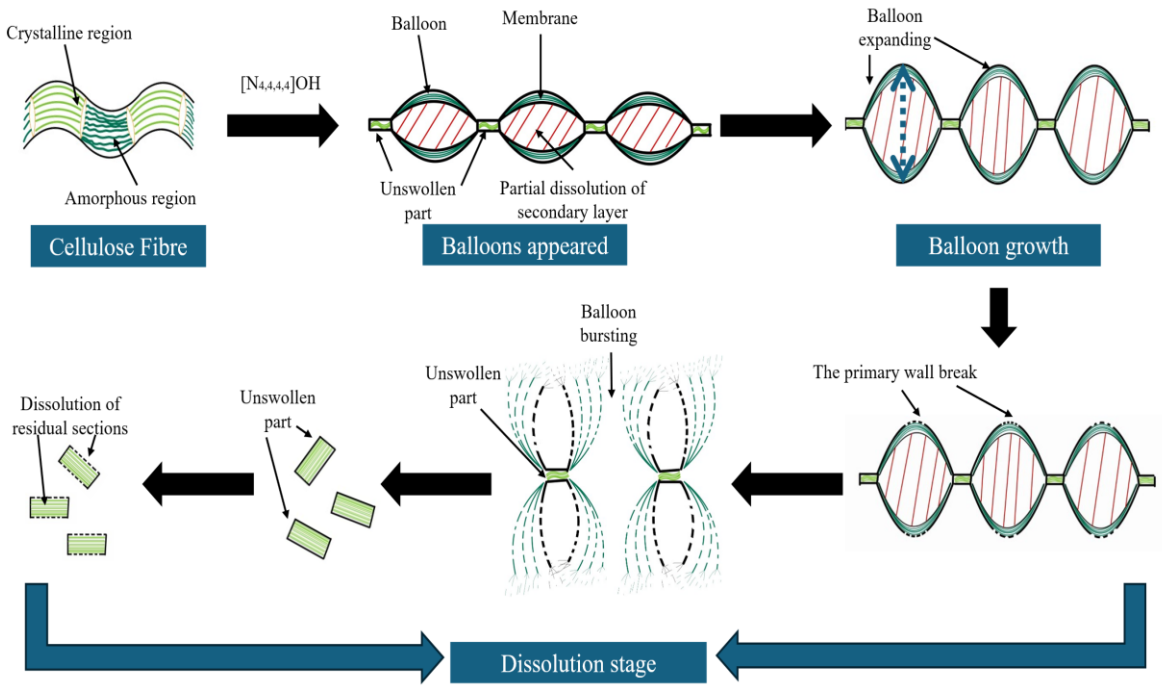

Figure 35. Diagram of cellulose dissolution through the ballooning effect

Another dissolution phenomenon was observed during the Kraft cellulose dissolution. Interestingly, the Kraft fibre did not exhibit ballooning at any stage; instead, the outer layer was solubilised first, and then the fibril was split from the main fibre immediately afterwards. Figure 36 show cellulose fibres at different stages of dissolution. Compared to the ballooning effect, dissolution was slower and more difficult to observe. During this process, smaller fibril structures split on both sides of the main fibre, making the cellulose fibre resemble "a whisk broom". Therefore, this dissolution phenomenon is called the "whisk broom effect".

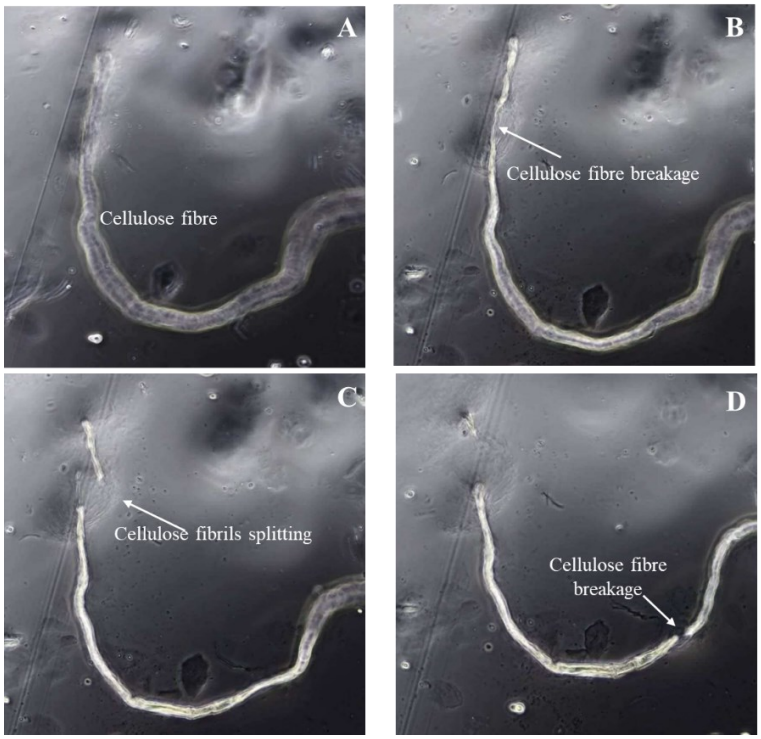

Figure 36. Observation of Kraft cellulose dissolution by whisk broom phenomenon

Based on these observations, the author proposed that the whisk broom dissolution phenomenon occurs in three stages. This phenomenon is a consequence of the complex hierarchical structure of cellulose, in which single cellulose chains bundle into nanoscale fibrils, which then aggregate to form larger structures, such as fibres. Dissolution begins at the primary wall and other outer structures interacting with $[N_{4,4,4,4}]OH$. This phenomenon differs from the ballooning effect, where $[N_{4,4,4,4}]OH$ dissolved the secondary first. It could begin at the end of the fibre or at a location with a thinner outer layer. The outer layer was dissolved, revealing the inner structure of the fibre.

Subsequently, finer fibrillar strands appeared and split to form a whisk broom-like structure. This phenomenon occurs along the fibre axis and could be related to slight untwisting.[138] At the final stage, the fibrillar strands are dissolved. A schematic of the whisk broom effect is illustrated in Figure 37.

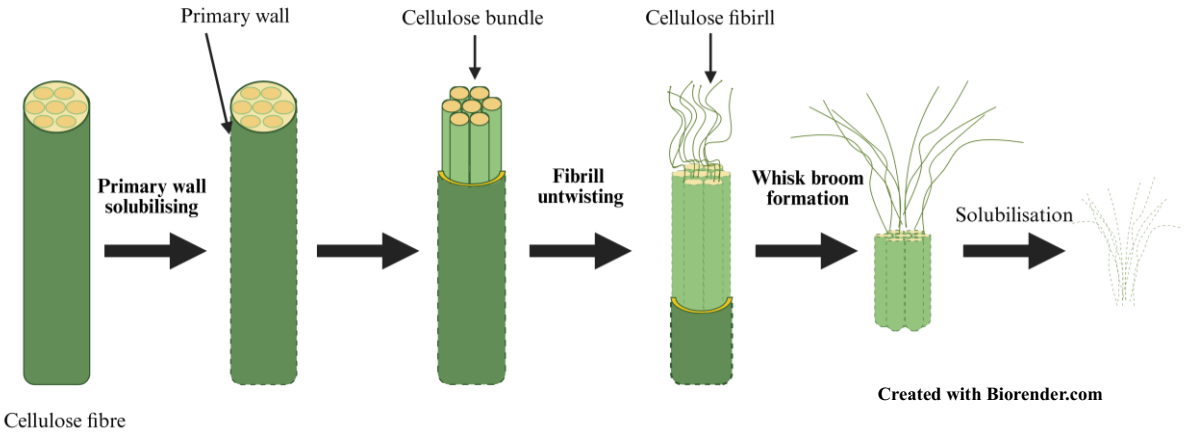

Figure 37. Diagram of cellulose dissolution through whisk broom effect

According to previous studies, the dissolution of cellulose depends on the type of cellulose pulp.[132, 138, 139] However, the KC material used in this study consisted of two types of pulp fibres: northern bleached softwood and hardwood Kraft pulp (NBSK and NBHK). Therefore, two dissolution phenomena were observed. The fibre of NBSK is known to have a larger diameter with a thick cell wall compared to NBHK.[140] The cell wall thickness may account for the differences in the dissolution phenomenon. The "ballooning effect" is believed to have first occurred in the S2. The thick outer layer of this fibre reduced the extent of dissolution. Moreover, in the whisk broom process, it is clearly visible that the outer layer dissolves before the inner layer. The thinner outer layer could be the reason for this dissolution phenomenon. Therefore, the thickness of the primary layer of the cellulose fibre could influence the cellulose dissolution process.

3.5 Production of regenerated cellulose from Kraft cellulose using the modified MDCell process

3.5.1 Production of regenerated Kraft cellulose film.

Our group developed the MDCell method in 2020. A high amount of MCC, up to 20 wt. % was dissolved by [$P_{4,4,4,4}$]OH 50wt.% solution to obtain cellulose solution.[78] By using the casting method, the cellulose solution was cast and then immersed in a propylene

carbonate (PC) bath and quickly solidified. The regenerated cellulose (RC) has good quality and is successfully applied to a designed filtration system for wastewater treatment. This RC membrane exhibited good physical properties in an aquatic environment. However, after drying, the film becomes brittle and inflexible, thereby limiting its application.

A new regenerated cellulose film was developed based on the MDCell method, with minor modifications to the procedure. KC replaced MCC, and this cellulose material needs to swell in DMSO before $[N_{4,4,4,4}]OH$ 40wt. % added. The details of the production process are illustrated in Section II.d. The modified MDCell process for generating a regenerated Kraft cellulose (RKC) film is shown in Figure 38.

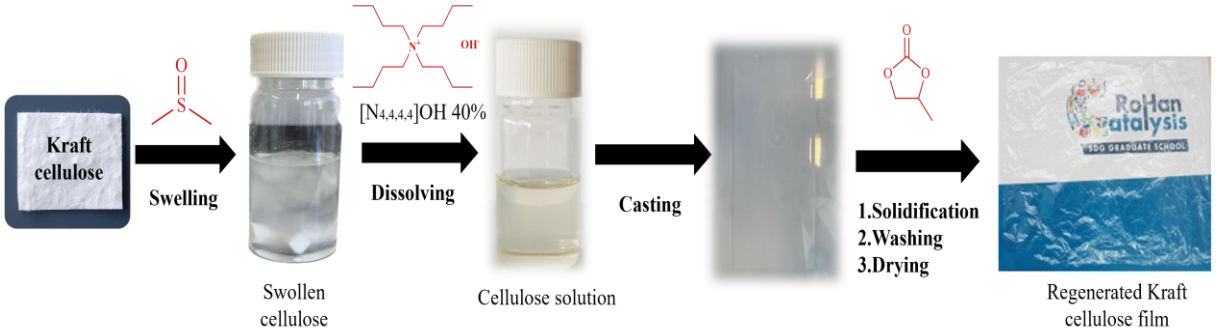

Figure 38. Schematic for generating the regenerated Kraft cellulose film by the modified MDCell process

The obtained RKC films were colourless, homogeneous, and exhibited high transparency. Films cast at under 500µm were more flexible, flatter, and firmer. The chemical, morphological, mechanical, and biodegradability properties of RKC films were thoroughly examined. Subsequently, the application of this film will become clearer.

3.5.2 Characterisation of regenerated Kraft cellulose film

The structural and chemical characteristics of the Kraft cellulose and regenerated Kraft cellulose films were analysed. First, CHNS elemental analysis was used to determine the percentages of carbon, hydrogen, nitrogen, and sulphur in the samples, as shown in Table 4. The results showed that no nitrogen or sulphur was detected in the regenerated

film. Therefore, the $[N_{4,4,4,4}]^+$ cation and DMSO were removed entirely from the RKC film after washing.

Table 4. The CHNS elemental analysis of regenerated Kraft cellulose film

Sample	C(%)	H(%)	N(%)	S(%)
RKC	40.82	6.55	-	-

FT-IR was used to analyse the changes in the chemical structure of Kraft cellulose compared to the regenerated Kraft cellulose film after applying the modified MDCell method. Owing to the complexity of components such as hemicellulose or lignin, MCC with higher cellulose purity was used for comparison with Kraft cellulose. The FT-IR spectra of PC, KC, MCC, regenerated KC (RKC), and MCC (RC) are shown in Figure 39.

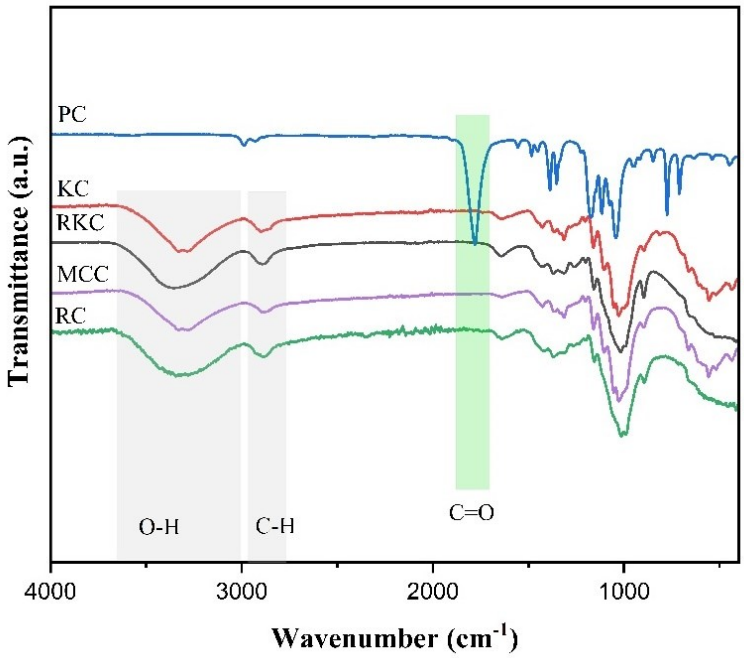

Figure 39. FT-IR spectra of PC, MCC, KC, and regenerated KC and MCC

The FT-IR spectra of the cellulose materials both show a broad absorption band from 2900 to 3600 cm^{-1}, which is attributed to the O-H stretching vibrations of hydroxide groups. This also indicates the complexity of the hydrogen bonds in the cellulose material. Additionally, the band at 2980 cm^{-1} corresponds to the C-H stretching

vibrations. This band primarily arises from the aliphatic methylene (CH_2) group in the cellulose backbone. The peak at 1645 cm^{-1} in the FTIR spectrum of the cellulose material is typically attributed to the OH bending vibration of absorbed water molecules.[141] The strong band at 1022 cm^{-1} is assigned to the C-O-C stretching in the cellulose backbone. Other frequency bands at 1425, 1370, 1313, and 1157 cm^{-1} are attributed to -CH_2 vibration, -CH bending, CH_2 wagging, and C-O-C anti-symmetric stretching, respectively. Furthermore, the signal at 892 cm^{-1} represents the β-glycosidic linkages between glucose and cellulose.

A very strong carbonyl absorption band at 1788 cm^{-1} was observed in the spectra of PC, but it is not visible in the spectra of RKC and RC. This indicates that PC was not present in the regenerated cellulose material. The results show that the chemical composition of the cellulose material from both MCC and KC remained unchanged after the MDCell process was applied.

X-ray diffraction (XRD) measurements were performed to analyse the crystallinity of the cellulose material both before and after the regeneration process (using Mo radiation). The XRD pattern of MCC showed four main diffraction peaks at 2θ angles of 6.8°, 7.3°, 10.2°, and 15.7°. These peaks correspond to d-spacings of 5.98 Å, 5.56 Å, 3.98 Å, and 2.59 Å, respectively, and are attributed to the (110), ($1\bar{1}0$), (002), and (004) planes of the cellulose Iβ crystal structure.[142-144] Additionally, a shoulder was observed near 2θ = 9.3°, which is associated with (012) and (102) reflections; however, its significance is unclear. The XRD pattern of KC was very similar to that of MCC, exhibiting the same major crystalline peaks, which indicates that both materials have the cellulose I polymorph. However, the KC pattern displayed additional signals, suggesting the presence of impurities in this material.

The XRD pattern of the regenerated MCC (RC) sample shows three main diffraction peaks at 2θ = 5.3°, 9.2°, and 9.94°. These peaks correspond to the ($1\bar{1}0$), (110), and (020) planes and match the pattern of the cellulose II polymorph.[145] This indicates that the original cellulose I was transformed into cellulose II after the regeneration process. In contrast, the RKC sample displayed a single peak at 2θ = 9.54°, corresponding to the

(110) and (020) planes. Additionally, the XRD pattern of RKC shows two peaks at 2θ = 15.9° and 16.5°, which did not appear in RC. French et al.[142] and Carolina et al.[146] reported that these peaks were related to the (004) planes of cellulose II after the regeneration process, but they are not always observed in all types of regenerated cellulose samples.

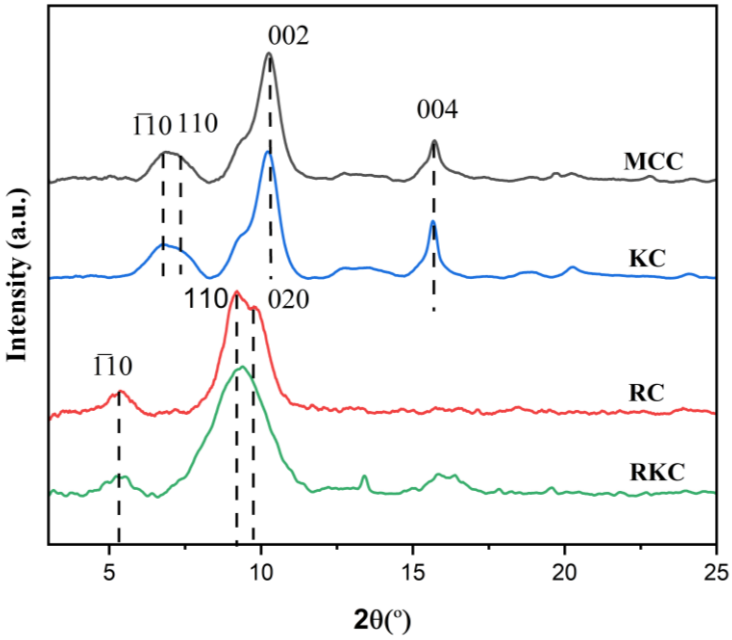

Figure 40. XRD pattern of MCC,KC, RC and RKC

The XRD diffraction peaks of the regenerated cellulose were both broadened and reduced in intensity for both MCC and KC. Therefore, the crystallinity index was employed to determine the crystallinity of each cellulose material, as reported by Segal et al.[147] The crystallinity index of MCC reduced from 82.4% to 74.2%, and that of KC decreased from 71.5% to 65.3%. This indicates that the dissolution and regeneration processes disrupted the original and higher-order structures of native cellulose, increasing the amorphous regions where the polymer chains were less regularly arranged. The result agrees with the previous research of Nguyen et al.[78]

SEM and AFM measurements were used to investigate the topography of the regenerated Kraft cellulose film. Micrographs of the cross-section and surface area of the RKC film are shown in Figure 41. The surface of the RKC film was very smooth, dense, and highly uniform. However, several straight lines were observed on the surface of the film. This could be due to the surface contacting the glass plate, which is easily

scratched by physical contact and leads to an uneven surface. The cross-sectional SEM images of the RC film illustrate that this material is composed of a multilayer of thin seeds.[78, 148, 149]

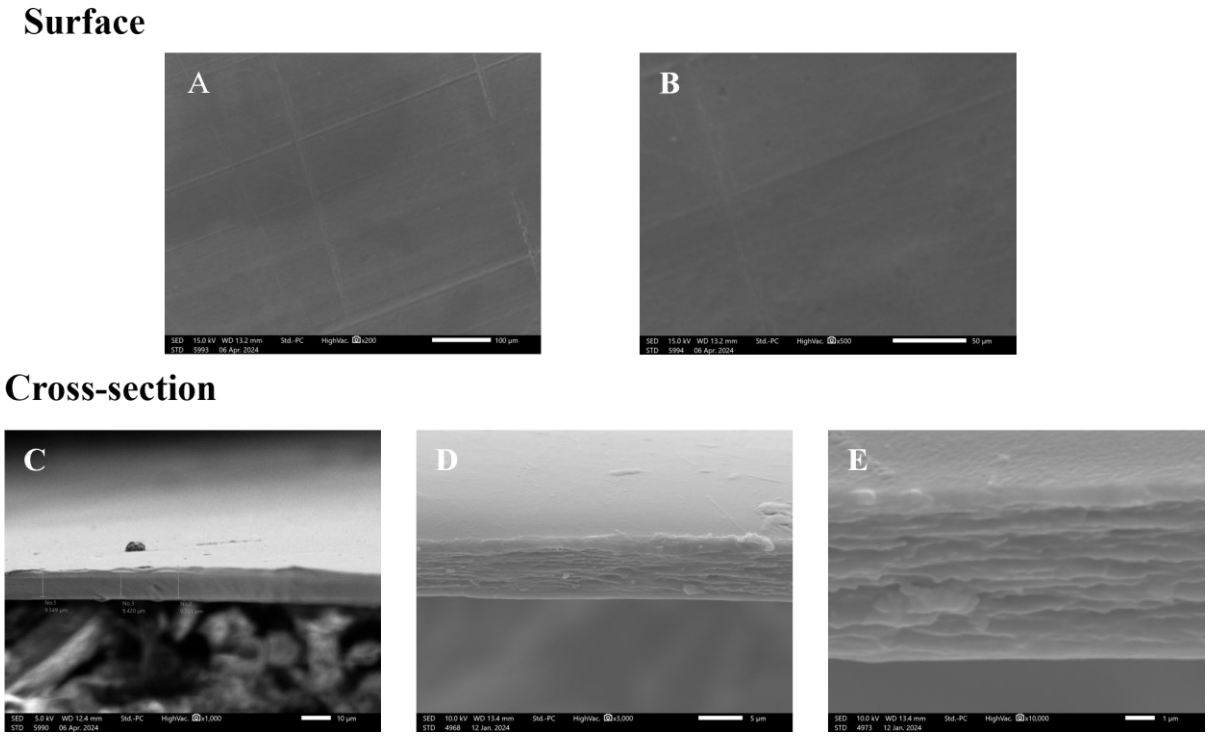

Figure 41. SEM analysis of the surface and cross-sectional area of RKC film at different magnifications.

Figure 42 shows AFM images of the RKC film at different magnifications. The surfaces of the RKC films were smooth and homogeneous. Additionally, some impurity particles were detected in the AFM images. Furthermore, the side that contacted the glass plates (bottom side) had some straight lines, but they were not observed on the other side (top side). This also influences the roughness of the films. The mean roughness of the top side was S_a =4.1 nm, whereas that of the bottom side was 3.2 nm, indicating that the bottom side had a smoother surface than the top side. The movement of the cellulose solution before dipping into the PC bath led to unevenness on the top side compared to the bottom side. The mean roughness between the two sides of the film was not significantly different, indicating a rapid reaction between the cellulose solution and PC.

The high-resolution AFM measurement reveals a ribbon-like morphology of the RKC film, with a typical width of 20–25 nm and a length of 50 nm.

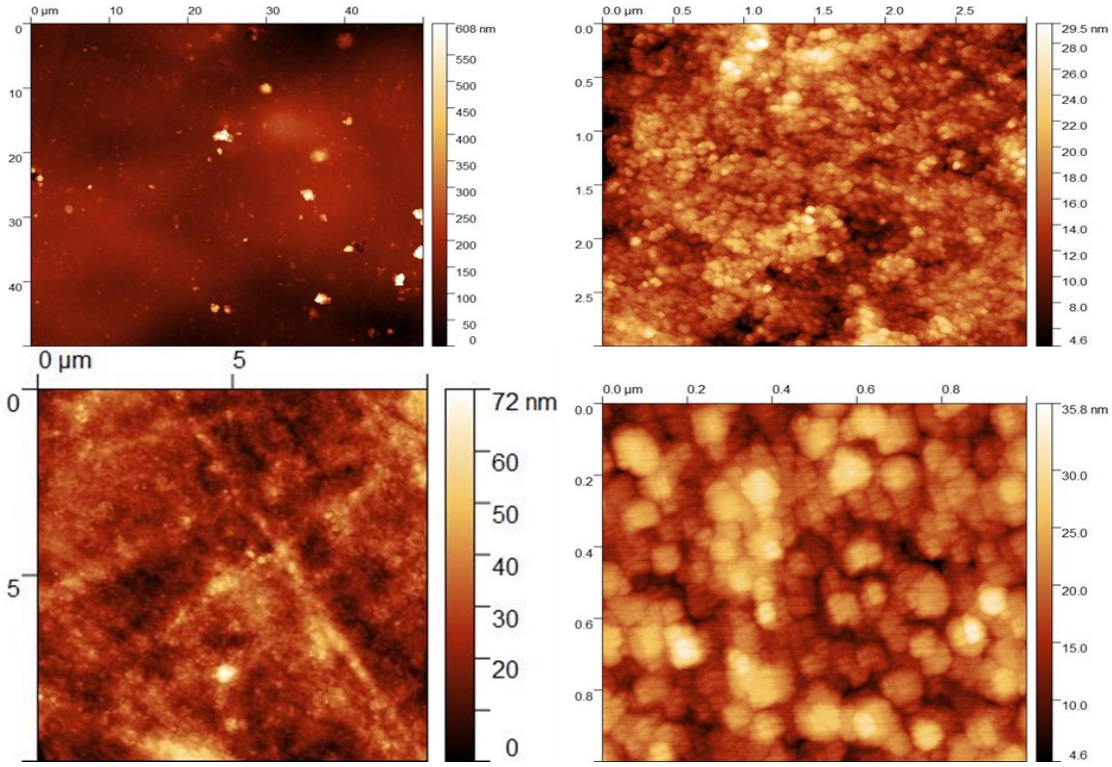

Figure 42. AFM measurement of RKC film at different magnifications

Regenerated Kraft cellulose thin films of different thicknesses were produced using various casting blades (300, 500, and 750µm) to create RKC300, RKC500, and RKC750 films. The effect of thickness on the physical properties of the RKC film, including its mechanical strength and transparency, was analysed. Cellophane and Polylactic acid (PLA) films are biopolymer films used for comparison with our film. Table 5 lists the thickness and transparency of RKC after drying, as well as those of cellophane and PLA.

Table 5. Thickness and transparency of RKC, cellophane and PLA

Type of film	Thickness (µm)	Transparency (%)
RKC300	10 ± 2	83 ± 2
RKC500	15 ± 3	79 ± 3
RKC750	22 ± 3	74 ± 3
Cellophane	15 ± 2	89 ± 2
PLA	25 ± 1	85 ± 1

The results showed that the film thickness decreased significantly by approximately 97% across all three RKC samples. Additionally, the transparency of the RKC film was high, reaching approximately 83% (RKC300), which is comparable to that of commercial cellophane and PLA. It was noted that increased thickness negatively impacted the transparency of the cellulose film, with transparency reducing from 83% to 74% when the cast thickness was increased from 300 to 750µm. Furthermore, a greater thickness diminishes the film's flexibility, making it more brittle.

Tensile measurements were performed to analyse the mechanical properties of the films, as shown in Figure 43. Cellophane had the highest tensile strength (247 ± 12.1 MPa) and elongation (32 ± 3.5%), whereas PLA had the lowest tensile strength (45 ± 2.8 MPa). The RKC films with different thicknesses had an average tensile strength of 141 MPa and an elongation of approximately 10%. The thickness of the film also affected the tensile strength of cellulose, and the RKC750 film had the lowest tensile strength (113 ± 23.1 MPa) compared to the two other thinner RC films (153 ± 31.1 and 156 ± 29.6 MPa). Additionally, RKC films and cellophane indicate the natural brittleness of the cellulosic base material, with no yield point evident in the stress-strain curve. The stress increases rapidly at the beginning and then more slowly thereafter.[150] The stress-strain curve of PLA showed different behaviours, where the yield point appeared very clearly, and the stress was reduced after that. The curve indicates that PLA is a ductile material.[151]

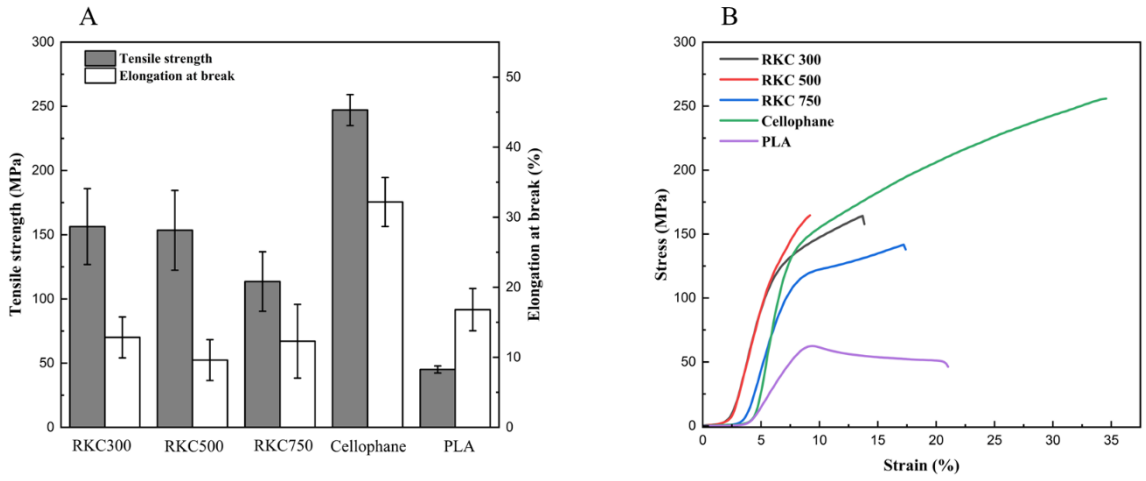

Figure 43. A) Tensile strength and elongation at break, B) Tensile stress-strain curve of RKC film in different thickness, cellophane and PLA

Regenerated cellulose films are reported to have excellent biodegradability.[152] In this study, the biodegradability of our regenerated cellulose film was compared with that of cellophane, polyethene low-density (PE-LD), PLA, and paper. These materials have been used worldwide for a long time. The study was conducted in plant soil (Figure 44) and under Baltic Sea (Figure 45). Visual changes in each type of film were recorded at specific times.

Two methods were applied to the soil environment: buried soil and soil surface (details are illustrated in Section III.n). The samples were examined in 5 weeks, and the morphological changes of all film samples are shown in Figure 44.

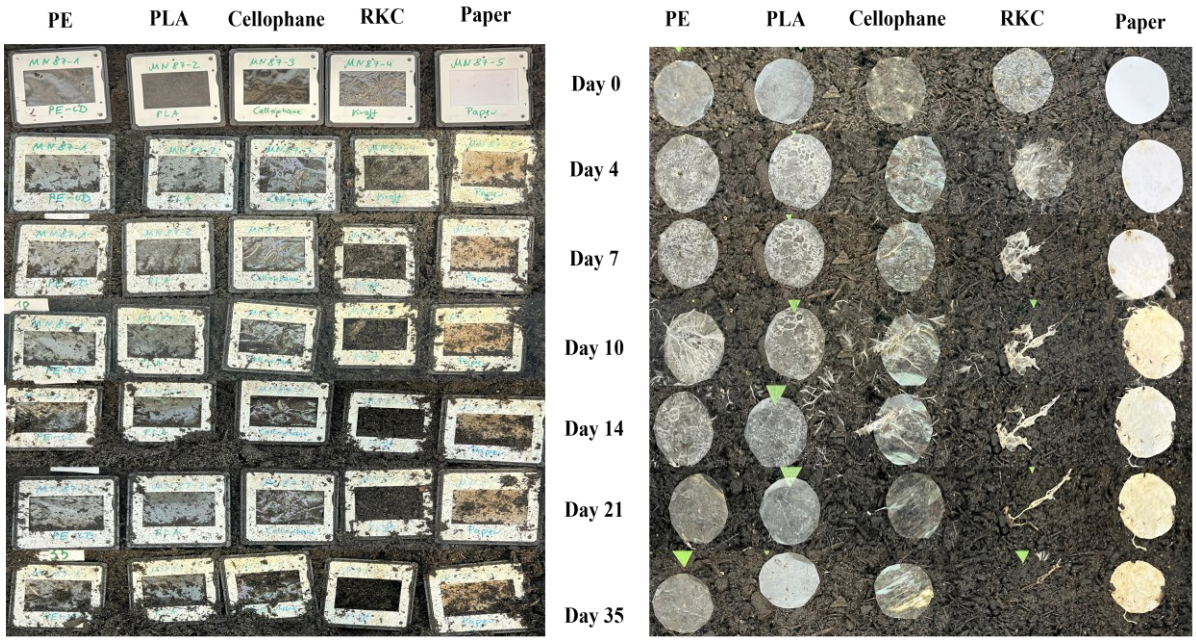

Figure 44. The morphological changes of PE, PLA, cellophane, RC and paper in A) soil buried, and B) on the soil surface after 5 weeks

After 35 days, it was difficult to observe changes on the surfaces of the cellophane, LD-PE, and PLA films. The paper sample showed minor damage on its surface. In both experiments, the RKC films were biodegraded entirely. In the buried soil experiment, tiny holes and cracks appeared on the surface of the RKC film after 4 days. The size of the holes increased on days 7 and 10. Finally, the RC film was fully decomposed after 14 days. In the surface experiment, after 4 days, tiny holes and large pieces were visible on the top right side of the RKC film. Additionally, mould or fungi developed on the soil surface and the RKC film. By day 7, they began growing on the surface of the paper.

More than half of the RKC was consumed by the organism. In the next 2 weeks, RKC film gradually degraded on the soil surface, then totally degraded after 21 days.

The observation of the degradation process of the soil experiment showed similar changes in the morphology of the film at both the buried soil and soil surface experiment. According to previous research, the biodegradation of cellulose film follows three main stages: biodeterioration, fragmentation, and assimilation.[152-154] In the biodeterioration step, microorganisms grow on the film's surface and around the median. Their population is increasing rapidly, leading to chemical and physical changes. Microorganisms can penetrate the pores of polymer structure and provoke cracks. Several studies have suggested that soil moisture plays a role in biodegradation.[48] The polymer structure slowly swells by absorbing moisture from the medium, making it easier for microorganisms to enter the polymer matrix. In the fragmentation stage, enzymes are considered the primary agents, breaking down the longer chain cellulose polymer into shorter chain structures, which are the monomers and oligomers. Microorganisms secrete specific enzymes that diffuse into the polymeric matrix and break the 1,4-glycosidic bond of cellulose. Endoglucanase, Cellobiohydrolase, and β-glucosidase are the most well-known enzymes that naturally decompose cellulose and other polysaccharide materials.[155] The assimilation process is the final step of the biodegradation process, in which microorganisms convert cellulose monomers or oligomers to produce energy, biomass, CO_2, and water.[152, 156] As a result, cellulose films are completely degraded. Soil type, moisture content, pH, and temperature also affect the biodegradation process in the soil environment. Compared with the soil-buried experiment, the film on the soil surface degraded more slowly. The film only contacted the soil on one side, resulting in a lower growth of the microorganism population.

To further investigate the biodegradability of the material in nature, all samples were examined under sea conditions. Figure 45 shows images of the material changes weekly under the Baltic Sea. There were no signs of decomposition in the PE and PLA films, while the cellulosic materials were degraded during testing. In the first week, there were no significant changes in the morphology of any samples, except that the paper began to show signs of degradation. After two weeks, all samples showed some colour

changes, turning light grey and green. Additionally, the samples became slippery and slightly slimy to the touch, indicating microbial growth and mineral deposits on their surfaces. By the fourth week, the colour of the cellophane and RKC films darkened and fragmented into smaller pieces. The RKC film completely disappeared after five weeks, and the cellophane was also nearly gone by that time.

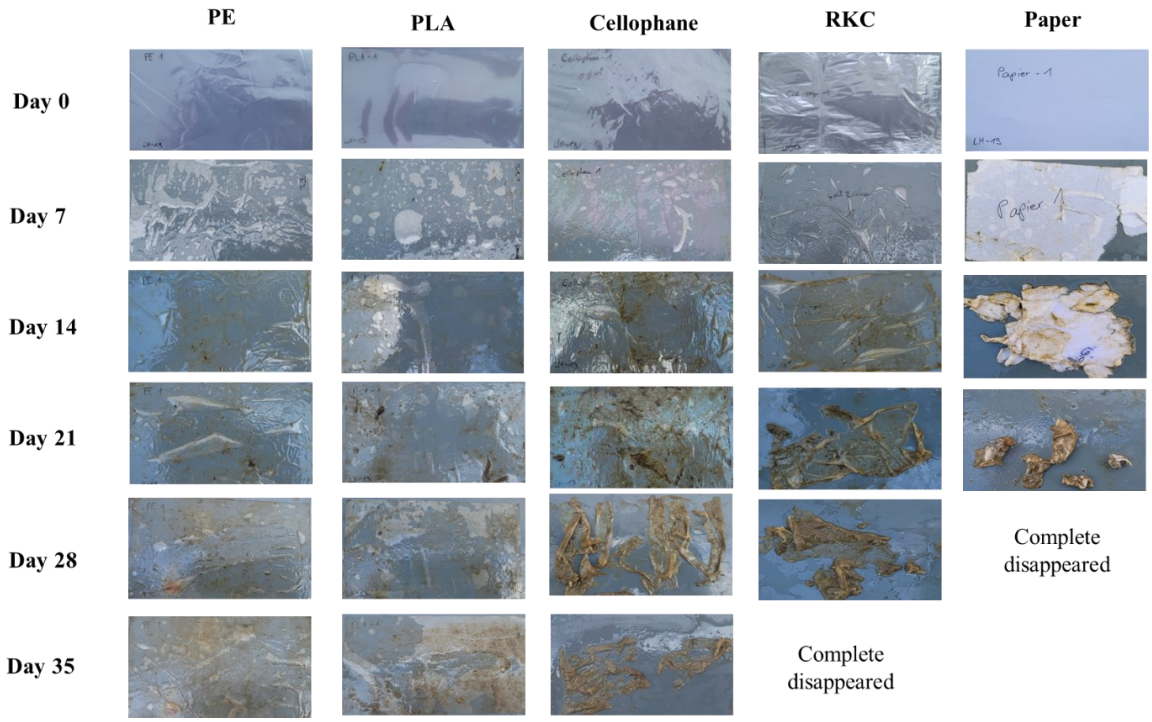

Figure 45. The morphological changes of PE, PLA, cellophane, and paper under the Baltic Sea after 5 weeks.

Compared to the buried soil experiment, all cellulosic materials decomposed more rapidly in the sea environment. The study by Royer et al.[157] reported similar results for the decomposition time of cellulose material in the sea environment. This study showed that their cellulose material broke down after about a month on the sea surface and seafloor. While other materials, such as PLA, PET, and PP, were tested, it was observed that they did not suffer significant damage, even after being exposed to the sea environment for 231 days. Another study indicated that the type of water greatly affects the biodegradation of cellulosic materials material.[158] The experiment compared the biodegradation of MCC, cotton, rayon, polyester/cotton (50:50), and polyester by immersing these samples in lake and sea water for 35 days. MCC exhibited the highest biodegradation properties, with their mass reduced by 81% in the lake water

environment, while the reduction in seawater was 71%. Bacterial activity was also confirmed to be involved in biodegradation in the water environment.

The modified MDCell procedure provides a rapid method for producing regenerated cellulose thin films from Kraft cellulose. The RKC film exhibits good physical properties, such as high transparency and strong mechanical properties, which are compatible with those of cellophane or PLA. Additionally, the cellulosic film displayed excellent biodegradability in both soil and seawater environments.

3.6 Lithium chloride: a novel plasticiser for cellulose film.

In the previous section, the RKC film was successfully produced using the MDCell method. It exhibited good mechanical properties. However, the strong intermolecular hydrogen bonds cause the RKC film to become stiff and brittle, particularly when the film is thick. The use of plasticisers is one method that has been applied to improve the flexibility and reduce the toughness of the cellulose-based film.[159-161] Glycerol (Gly) and polyethene glycol (PEG) are two traditional plasticisers that have been applied in processing cellulose film.[161, 162] Recently, we found that lithium chloride (LiCl) used in a post-treatment with cellulose film can increase the flexibility of thicker films, similar to that of plasticisers.

3.6.1 Plasticising process for regenerated cellulose film

There are different methods for plasticising cellulose films. However, immersing the regenerated film in a plasticiser solution is a quick way to produce a plasticised cellulose film.[163, 164] This method is more suitable for our regenerated film than mixing directly with plasticisers at the liquid stage. The addition of glycerol, PEG, or LiCl accelerated the solidification of our cellulose solution, making it too quick to form films. To assess the effect of LiCl on the mechanical properties of the film, glycerol, PEG, and potassium chloride (KCl) salts were used for comparison. The plasticising of the regenerated cellulose followed the procedure shown in Figure 46.

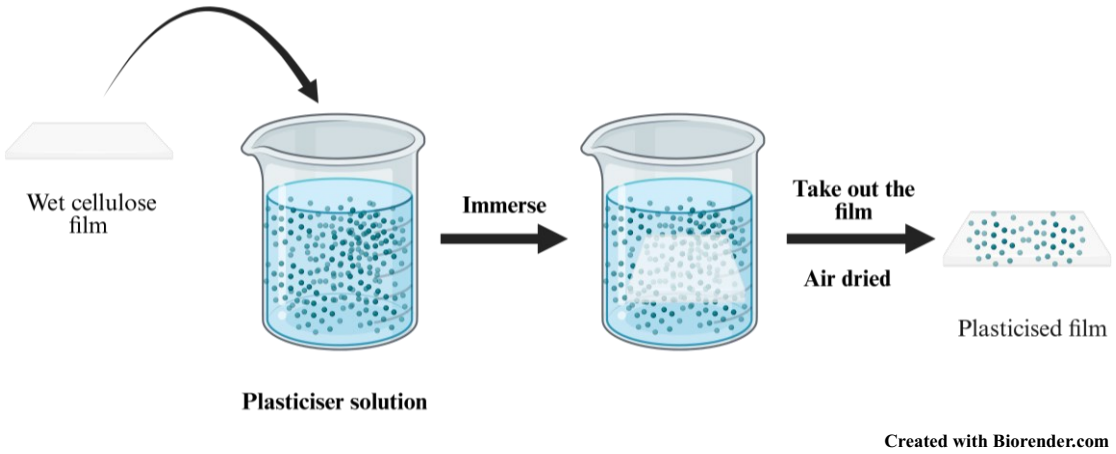

Figure 47. Preparation of plasticised regenerated cellulose film

The regenerated wet cellulose film was immersed in a 1 w/v% solution of glycerol, PEG, and KCl, while different concentrations (0.25, 0.5, 1, and 2 w/v%) of LiCl were prepared. The samples were immersed overnight before drying. They were named RKC-K1, RKC-Li1, RKC-Gly1, and RKC-PEG1 according to the solution in which they were immersed: KCl, LiCl, glycerol, and PEG. Only the cellulose-lithium films had RKC-Li0.25, RKC-Li0.5, RKC-Li1, and RKC-Li2. The images of the plasticised film are shown in Figure 47. Except for the RKC film immersed in KCl, which became blurry and had a rough surface, the other treated RKC films were transparent, firm, and flexible.

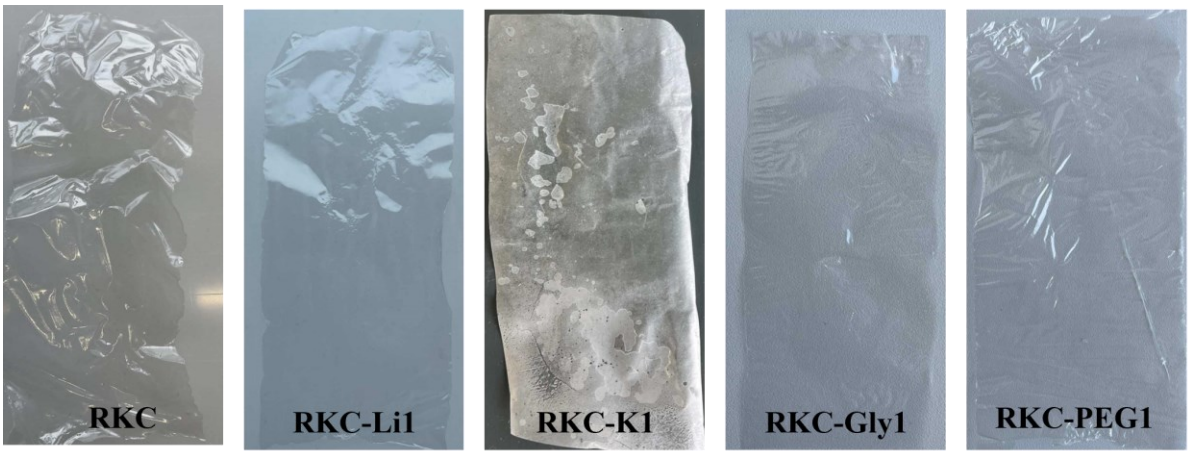

Figure 46. Morphology of plasticised RKC films

3.6.2 Characterisation of plasticised cellulose film

Investigating the compatibility of the plasticiser with the RKC film is crucial. The morphology of the film is shown in Figure 47. It noted that only the RKC-K1 film appeared, with a rough, cloudy surface. It is possible that KCl recrystallised after the

drying process and formed on the surface of the film. In contrast, the other films exhibited homogeneity with high transparency. Additionally, these films exhibited firmness and flexibility, especially when compared to the RKC film. This demonstrates the high compatibility of glycerol, PEG, and LiCl with the RKC film.

Inductively Coupled Plasma (ICP) measurements were used to quantify the lithium concentration inside the RKC-Li films, and the results are shown in Table 6. It indicated that he lithium concentration increased proportionally with the concentration of the immersed LiCl solution.

Table 6. The ICP measurement of the Lithium element inside the RKC-Li film

Type of film	Li(%)
RKC	0
RKC-Li0.25	0.53
RKC-Li0.5	1.21
RKC-Li1	1.83
RKC-Li2	2.75

FT-IR was employed to analyse the chemical structure of plasticised RKC immersed in a 1w/v% plasticiser solution, which is shown in Figure 48. The main functional groups of the plasticised RKC films were almost identical to those of the pure RKC film. A wide band at approximately 3600-3000 cm^{-1} was observed for the O-H stretching of cellulose, glycerol, and PEG. The band between 3000 and 2800 cm^{-1} is mainly attributed to the C-H stretching vibration of cellulose and glycerol, while that presented for the CH_2 stretching in the PEG backbone.[165] The presence of plasticiser inside the cellulose structure could be the reason for the slight shift of the peak in this region. Meanwhile, an absorption peak appeared at approximately 1640 cm^{-1}, attributed to the hydroxyl group of absorbed water within the cellulose film.[141] The intensity of this peak for the RKC-Li1 film was higher than that of the other films. This may be linked to the high hygroscopicity of LiCl, which allows more water to be absorbed within the cellulose film. In the spectra of RKC-PEG1, a small signal at 1350 cm^{-1} indicated the CH_2 wagging of PEG, which proved that PEG was plasticised on the cellulose film.[166] Additionally, a band at 925 cm^{-1} was only present in the spectra of the RC-Gly1 film,

indicating the presence of glycerol in the cellulose matrix.[167, 168] The characteristic bands for LiCl and KCl are difficult to identify in the FTIR spectra.

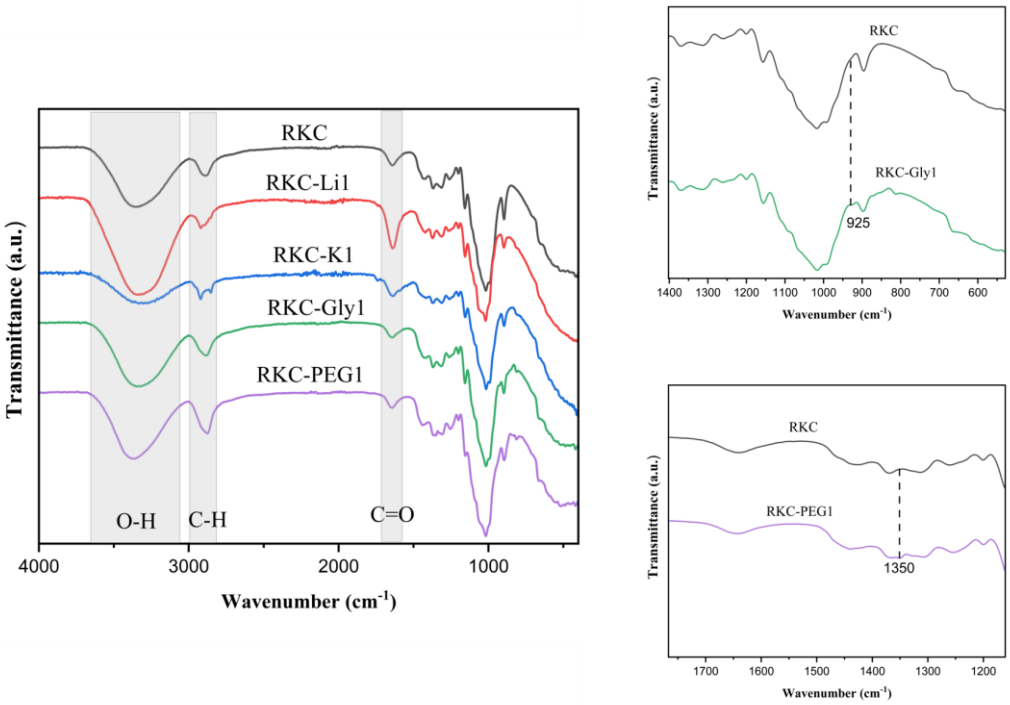

Figure 48. FT-IR spectra of plasticised RKC film

SEM measurements were used to examine the morphology of the film, and the surface and cross-section are shown in Figure 49.

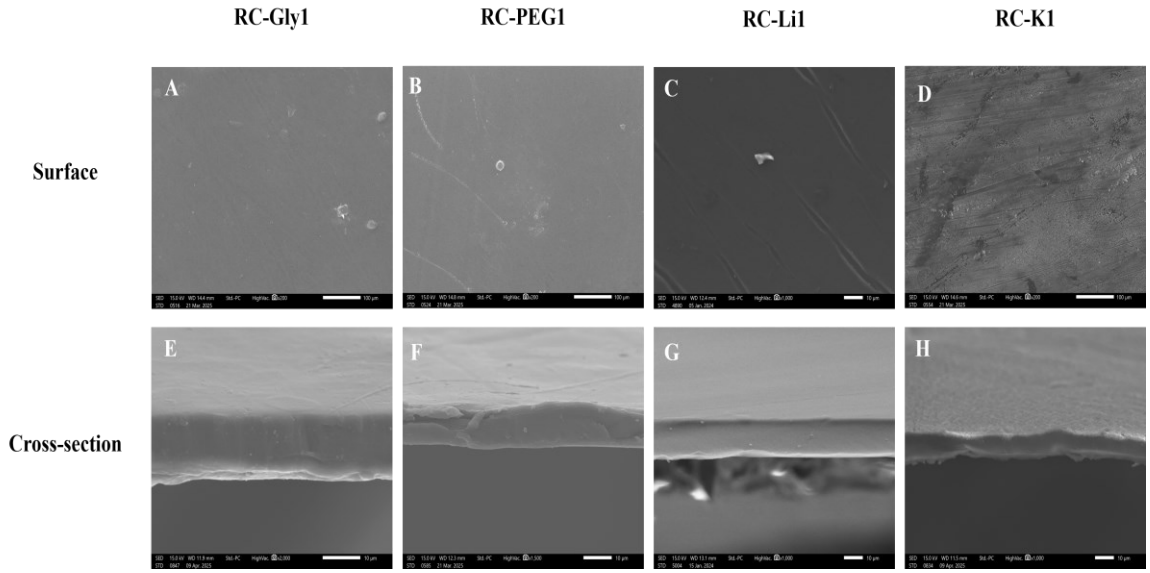

Figure 49. SEM analysis of surface area and cross section area of plasticised film

The morphologies of RKC-Li1, RKC-Gly1, and RKC-PEG1 were similar to that of RKC film. The surfaces of both films are homogeneous, smooth, and highly uniform,

with no phase separation observed. Additionally, the cross-sectional area of these films was very dense and compact, and aligned layers of RKC film were not observed in plasticised sample. The cubic structure of KCl was detected on the surface of RKC-K1, distributed on the film surface, and formed salt layers on both sides of the film. The RKC-K1 cross-section shows three distinct layers, with a cellulose film in the middle of the salt layer. No LiCl crystals were detected in the RKC-Li1 film.

The mechanical properties of the regenerated cellulose films that were immersed in 1% solution of KCl, LiCl, glycerol, and PEG are demonstrated in Figure 50. The tensile strength and elongation at break of the pure regenerated cellulose film were 153 ± 31 MPa and 10 ± 3%, respectively. The high tensile strength and low elongation at break values indicate the stiffness and brittleness of the film. The effects of glycerol and PEG were observed, resulting in slightly more flexible mechanical properties. This is indicated by the reduction in tensile strength to 111 MPa for RKC-Gly1 and 98 MPa for RKC-PEG1. The percentages of elongation of RKC-Gly1 and RKC-PEG1 were 21% and 17%, respectively. Plasticisers diffuse into the cellulose matrix and can form hydrogen bonds with cellulose molecules, reducing the cohesive forces between cellulose chains and allowing them to move more easily.[169]

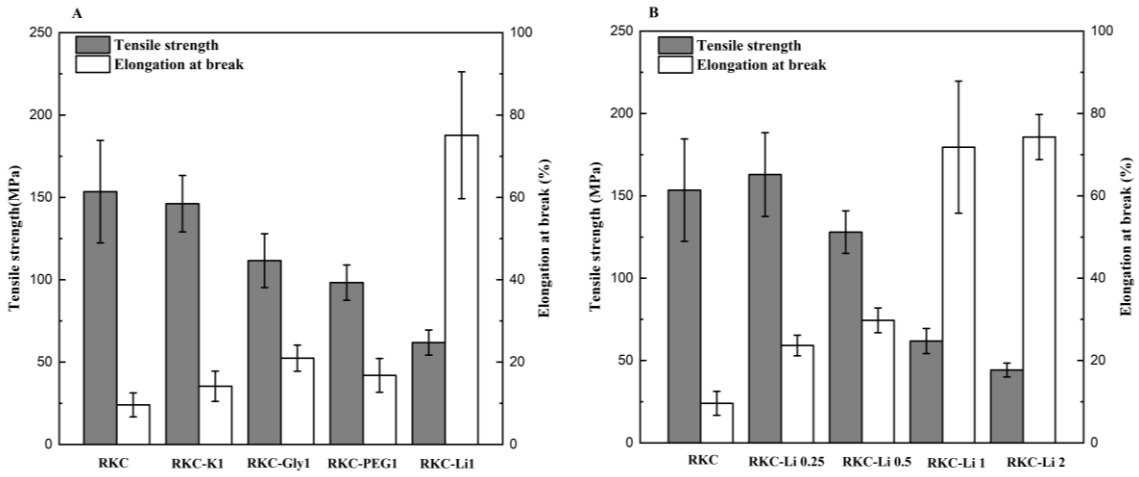

Figure 50. The tensile strength and elongation at break A) plasticised RKC film in 1w/v% solution B) in different LiCl concentration

Additionally, it is noted that the impact of LiCl on the RKC film was more clearly observed than that of glycerol and PEG at the same concentration. The elongation at

break of RKC-Li1 increased significantly to 75% which is over seven times higher than that of the pure regenerated film. In contrast, the tensile strength and elongation of the RKC-K1 film were similar to those of the RKC film. This result shows KCl is less compatible with cellulose film compared to the tested agents.

An increase in LiCl concentration was correlated with a decrease in tensile strength and an increase in elongation at break of the films, resulting in increased flexibility. Additionally, LiCl can absorb moisture during storage because of its high hygroscopicity. Thus, a lithium film with a higher lithium concentration can retain more water inside the cellulose structure, making the film more flexible.[170] Subsequently, the RKC-Li2 film exhibited the highest elongation at break and lowest tensile strength compared to all other lithium films.

Table 7 lists several physical properties of the RKC film that was immersed in a plasticised solution. There was no significant impact on the transparency of the regenerated cellulose film when immersed in glycerol and PEG, with values similar to those of the original samples. This result aligns with previous research indicating that traditional plasticisers, such as glycerol and PEG, can penetrate and form hydrogen bonds with the cellulose network.[169, 171] The plasticisers and cellulose create a uniform matrix without phase separation, which does not diminish the transparency of the film. The transparency of the RKC-Li and RKC films was also similar, at 76% and 80%, respectively. This result shows the minor impact of LiCl on film transparency. In contrast, the transparency of the RKC-K film was 52% due to the formation of KCl particles on its surface. This salt has low hygroscopicity, which recrystallises at relative humidity (RH) lower than 85%.[172] The RH value of LiCl is 11.3% at 25°C, indicating that LiCl is in the deliquescence stage.[173, 174] Moreover, the ionic radius of K is approximately 1.38 Å, whereas that of Li is approximately 0.76 Å. Thus, the bulkiness of the cationic atom and the low water affinity of KCl could be the reason for the lower compatibility of this chloride with the cellulose film.

Table 7. The value of thickness, transparency and WVTR of RKC film that is immersed in different solutions

Type of film	Thickness (µm)	Transparency (%)	WVTR ($g/m^2 h$)
RKC	15 ± 3	79 ± 1	10.8 ± 0.1
RKC-Gly1	17 ± 2	82 ± 1	7.5 ± 0.5
RKC-PEG1	17 ± 2	81 ± 1	8.6 ± 0.5
RKC-Li1	18 ± 3	76 ± 3	7.7 ± 0.5
RKC-K1	20 ± 3	52 ± 8	7.0 ± 0.1

The influence of plasticisers on the water vapour transmission rate (WVTR) is presented in Table 7. The WVTR of all plasticised films is smaller than that of the cellulose films, which means that less water vapour can penetrate. The WVTR of the RKC-K1 film was 7.0 g/m^2h, which was the lowest value among the four plasticised films. During the experiment, droplets were formed on the film surface inside the cup. This could be due to the high humidity inside the water cup (considering 100%) being higher than the relative humidity of KCl (RH ~85%), which leads to the dissolution of the salt. The salt absorbed the water vapour and formed a layer on the surface of the film, resulting in reduced vapour transport. Similarly, droplet formation on the film surface occurred with the RKC-Li1 film. This can explain the reduction in the WVTR of the film immersed in the inorganic salt solution. In contrast, no droplets were observed on the surfaces of RKC-PEG1 and RKC-Gly1. However, the film became increasingly softer during the experiment. Glycerol and PEG are hydrophilic and attract water. [175, 176] Thus, the film was plasticised with glycerol, and PEG interacted with water vapour, with some trapped inside the cellulose matrix, leading to a smaller WVTR than that of the pure cellulose film. Tarque et al.[177] assumed that the low glycerol concentration might interact better with the bio-polymer chain, leading to a dense and highly compact polymer structure. Consequently, less vapour can diffuse and the WVTR value decreases. The efficiency of reducing the water vapour transmission of the plasticised agent was KCl>Gly>LiCl>PEG.

The soil burial experiment was conducted to examine the influence of the plasticiser on the degradation of the cellulose film. Figure 51 shows the morphological changes in the

films during the experiment. The degradation of the film depends on biological factors such as fungi, bacteria, and microorganisms, and other conditions such as the type of soil and humidity. In the soil environment, the interaction of microbial organisms with biopolymers is the main factor leading to polymer degradation. The enzyme from the microbial organism breaks the polymer chain into a shorter chain before converting it into CO_2 and water.

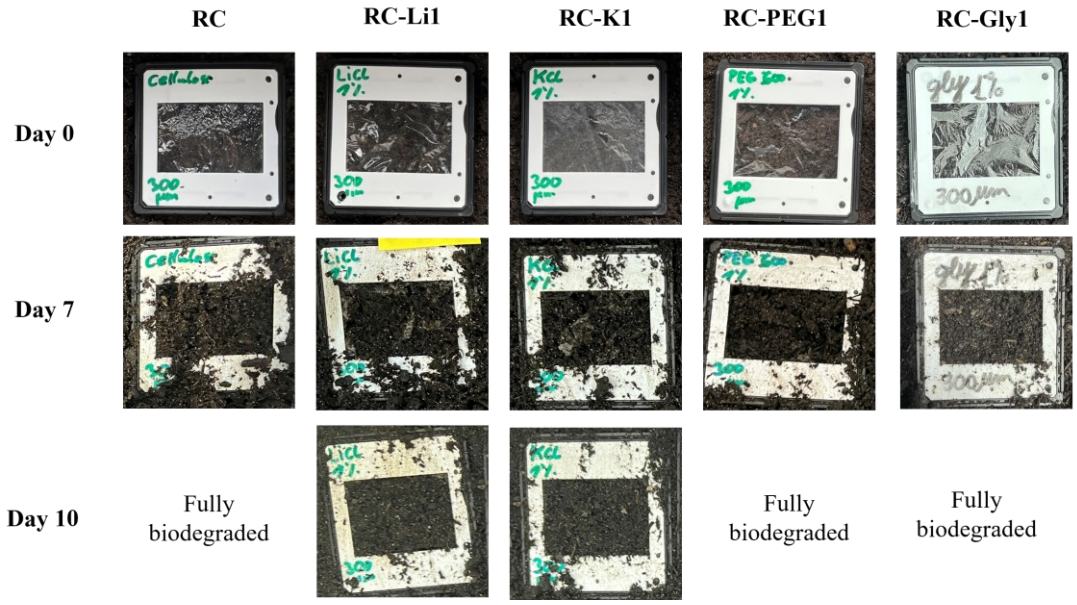

Figure 51. The morphological changes of the plasticised RKC film during the soil burial test

As shown in Figure 51, the plasticised RKC films were degraded after 10 days of the experiment. RKC, RKC-Gly1, and RKC-PEG1 completely decomposed after 7 days, which was faster than the decomposition of the RKC-Li1 and RKC-K1 films. This is due to potassium salt and lithium, which were found to significantly decrease the bacterial community because they increase the salinity and toxicity of the environment.[178-180] The results show that the microbial community required more time to degrade the RKC-Li1 and RKC-K1 films. In contrast, glycerol and PEG (low molecular weight) are considered low-toxicity, biodegradable materials.[181, 182] Additionally, the concentration of glycerol influences the biodegradation rate of the biopolymer film in soil by increasing the moisture inside the film.[177] This indicates that immersing the RKC film in a low concentration of glycerol and PEG had less impact on the biodegradable

properties of the film. Hence, RKC, RKC-Gly1, and RKC-PEG1 were totally degraded in the test in similar periods.

Overall, LiCl had a significant impact on the mechanical properties of the RKC film, as evidenced by the substantial increase in elongation. The RKC film immersed in 1 w/v% LiCl also exhibited better performance than other traditional plasticisers such as glycerol and PEG. However, the RKC-Li1 film required more time to degrade in the soil-buried experiment, indicating that it negatively influenced the biodegradability of the RKC film.

3.7 Solubilisation of chitosan in onium hydroxide solution.

Abe et al.[79] indicated that tetraethylammonium hydroxide ($[N_{2,2,2,2}]OH$) and tetrapropyl ammonium hydroxide ($[N_{3,3,3,3}]OH$) could dissolve 0.2wt. % of chitin after two weeks, then chitosan is obtained by precipitating the chitin solution with ethanol. Recently, chitin was reported to be soluble in $[N_{4,4,4,4}]OH$ solution under microwave irradiation, and chitosan was obtained using ethanol.[81] This indicates that onium hydroxide is a potential dissolution solvent for chitosan, which enables the combination of cellulose films produced by MDCell process.

3.7.1 Evaluation of chitosan dissolution in onium hydroxide

A similar strategy, which was used to evaluate the cellulose dissolution ability of pure OHS, was applied to chitosan, consisting of two processes: screening and quantification (Figure 17). Different concentrations of six types of OHS were used to test chitosan solubility. However, according to Abe's research, the testing time for chitosan solubility was increased to seven days, while other conditions and procedures were kept the same.[79] Low molecular weight chitosan (LMW-CS) was used in the solubilisation experiment first. After the quantification process was completed, the optimal onium hydroxide solution was identified and used for further experiments (details are provided in section I.c).

Chitosan was successfully dissolved by onium hydroxide as predicted. The dissolution time of chitosan was significantly higher than that of cellulose. For example, 5mg/mL of MCC in $[N_{4,4,4,4}]OH$ 50 wt.% solubilised within 5 minutes, while the same

concentration of LMW-CS needs around 6 hours. This also occurs in other onium hydroxides. Depending on the cationic structure and onium content, the 5 mg/mL chitosan needs several hours to several days to dissolve. In comparison with chitin dissolution by $[N_{3,3,3,3}]OH$ in the study of Abe, chitosan dissolved faster with higher concentration under similar room temperature conditions.[79] The images of chitosan solutions are shown in Figure 52. Similarly, the chitosan solution changed from a light yellow to a honey-like appearance, depending on the concentration of chitosan.

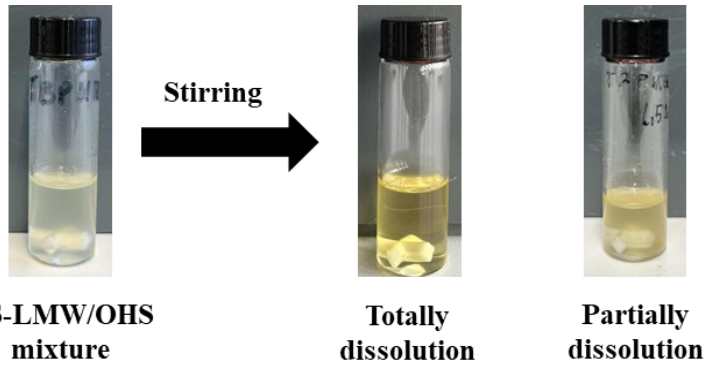

Figure 52. Chitosan/OHS mixture at beginning, fully dissolved , and partially dissolved.

Figure 53 shows the LMW-CS dissolution limits of the six tested onium hydroxides at different concentrations. This indicates that, except for the $[N_{1,1,1,1}]OH$ solution, the other tested type OHS were able to dissolve chitosan at room temperature. In all examined solvents, $[N_{4,4,4,4}]OH$ 60 wt.% showed the highest chitosan dissolution, which could dissolve up to 80mg/mL. The high viscosity caused by the high concentration of OHS in the dissolution, similar to cellulose, was also observed with the chitosan material.

The onium concentration and the cationic structure also influence the solubility of chitosan in OHS, similar to cellulose and chitin. [79, 82, 84] LMW-CS is less soluble in OHS than MCC but more soluble than chitin under the same conditions. For example, 1mL of $[P_{4,4,4,4}]OH$ 60 wt.% can dissolve up to 150mg of MCC, whereas chitosan solubilization was found to be very limited (10mg). Conversely, chitosan shows greater solubility than chitin in OHS under identical conditions.[87] Compared to $[N_{4,4,4,4}]OH$ solutions at the same concentration, $[P_{4,4,4,4}]OH$ acted as a less effective solvent. As mentioned, the dissolution of cellulose in this solvent is highly affected by

amphiphilicity, which must be optimised to achieve the highest dissolution capacity. Chitosan is known as a hydrophobic material, whereas cellulose is hydrophilic material.[183] The amphiphilicity between those two materials could be a reason that leads to the dissolution capacity differences.

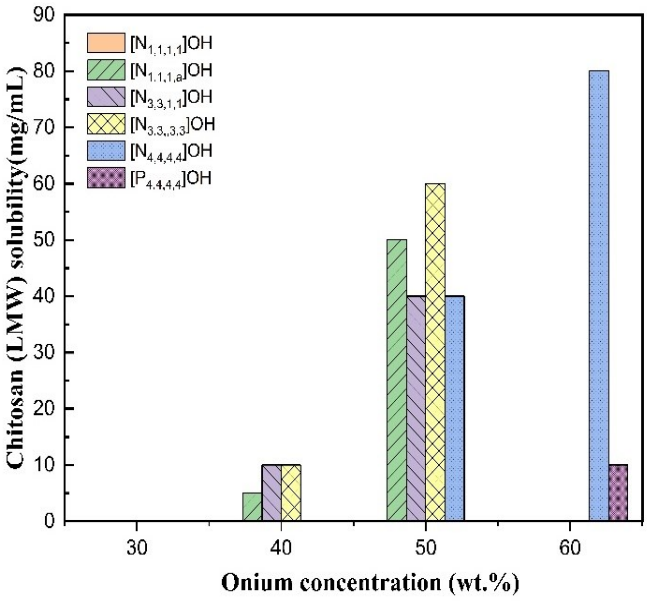

Figure 53. LMW-CS dissolution limit in six types of onium hydroxide

The dissolution strategy applied for cellulose was also applied, with DMSO used as a swelling agent or co-solvent with $[N_{4,4,4,4}]OH$ to promote the dissolution of chitosan. Pre-swelling in DMSO or a combination of DMSO/$[N_{4,4,4,4}]OH$ did not work with chitosan. Kurita et al.[184] examined the swelling behaviour of chitosan in DMSO. This study indicated that chitosan was only dispersed in DMSO; even after heating to 100°C, the shape of chitosan changed minimally. This could be attributed to the strong hydrogen bonds and hydrophobicity of chitosan. However, the addition of DMSO into chitosan/$[N_{4,4,4,4}]OH$ solution reduces the high viscosity of the solution, similar to the effect observed in cellulose solutions.[86]

The influence of the molecular weight of chitosan on the dissolution limit of $[N_{4,4,4,4}]OH$ 60wt.% indicated in Table 8. Medium- and high-molecular-weight chitosan (MMW-CS and HMW-CS) were used to estimate the dissolution capacity of this solvent. As the molecular weight increased, the dissolution capacity of the onium hydroxide solution

decreased. This behaviour is similar to that of cellulose, where longer polymer chains tend to entangle more and are more hydrophobic, which slows down swelling and disentanglement. Therefore, molecular weight is a key factor influencing chitosan dissolution, and high-Mw chitosan is considerably more difficult to dissolve under identical conditions.[185] Furthermore, longer chitosan chains exhibit greater hydrophobicity than shorter chains, resulting in an extended dissolution period. For instance, 5 mg/mL concentration of HMW-CS takes 3 days to prepare, whereas the same concentration of LMW-CS obtained after approximately 6 hours.

Table 8. Dissolution limit of different molecular weight chitosan in $[N_{4,4,4,4}]OH$ 60wt.% under room temperature

Type of chitosan	LMW-CS	MMW-CS	HMW-CS
Dissolution limit (mg/mL)	80	60	30

The influence of temperature was examined as an influencing factor in this study. The dissolution capacity of $[N_{4,4,4,4}]OH$ 60wt.% at various temperatures is shown in the Figure 54. The results indicated that 110 mg/mL was the highest concentration of $[N_{4,4,4,4}]OH$ solution achieved when heated above 50°C.

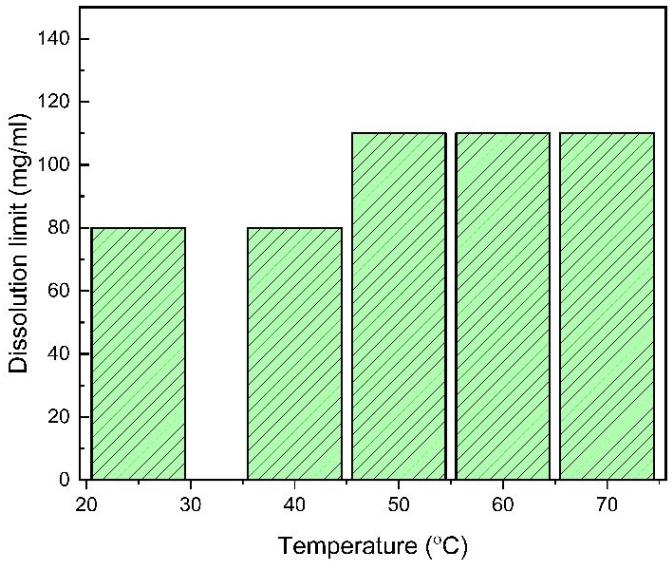

Figure 54. LWC-CS dissolution limit of $[N_{4,4,4,4}]OH$ 60 wt% at various temperatures

Below 50°C, the high viscosity of $[N_{4,4,4,4}]OH$ 60wt.% hinders the movement of the stirring bar, resulting in reduced dissolution ability and limiting the maximum dissolution of this solvent at 80mg LMW-CS. Figure 55 indicates the chitosan 100 mg/mL solution obtained by heating to 50°C and 70°C after 4 hours. The colour of the chitosan solution turned dark when heated to 70°C for an extended period, whereas it still retained a honey-like colour at 50°C. The dark colour of the chitosan solution was due to the decomposition of tetraalkyl ammonium hydroxide by Hofmann elimination. Therefore, the temperature limit for the heating process was set at 70°C for a maximum of 4 hours.

Figure 55. Obtained chitosan 100mg/ml solution by heating at 50 °C and 70 °C after 4 hours

Different chitosan/$[N_{4,4,4,4}]OH$ 60 wt.% (5, 50 and 100 mg/ml) ratios were prepared to investigate the influence of temperature on dissolution time. Table 9 lists the time required for chitosan to solubilise in $[N_{4,4,4,4}]OH$ at various temperatures. This indicates that higher temperatures significantly decrease the chitosan dissolution time. This can lower the viscosity of the solution and improve the dissolution efficiency of chitosan in OHS. For instance, a 50 mg/ml chitosan solution took approximately 3 days to dissolve at room temperature. In contrast, the same amount of chitosan dissolved in only 20 min at 70°C, making it more than 200 times faster.

Table 9. Dissolution time of 5, 50 and 100 mg/mL of chitosan in [$N_{4,4,4,4}$]OH 60 wt.% at different temperatures

Chitosan concentration (mg/mL)	Temperature (°C)				
	25	40	50	60	70
	Dissolution time				
5	6h	1h	30mins	5 mins	5 mins
50	2-3 days	**x**	2h	40 mins	20 mins
100	-	**x**	4h	3h	2h

-: not measured, **x**: partial dissolved

Liquid-phase NMR spectroscopy was performed to analyse the chemical structure of chitosan. Using [$N_{1,1,1,a}$]OH as a dissolving agent, six carbon signals of the chitosan structure appeared in the ^{13}C-NMR spectra (Figure 56), whereas they were not fully detected with other solvents. Six signals of glucosamine are detected at 102.2, 79.5, 77.4, 74.3, 61.7, and 58.2 ppm, which were attributed to C_1, C_4, C_5, C_3, C_6, and C_2, respectively. The signals related to the acetyl group were not detected in these NMR spectra, possibly because of the high DDA value of the chitosan sample (DDA ≥ 75% according to the provider). As a result, the signal intensity of this group was too low to be detected by NMR spectroscopy.[186]

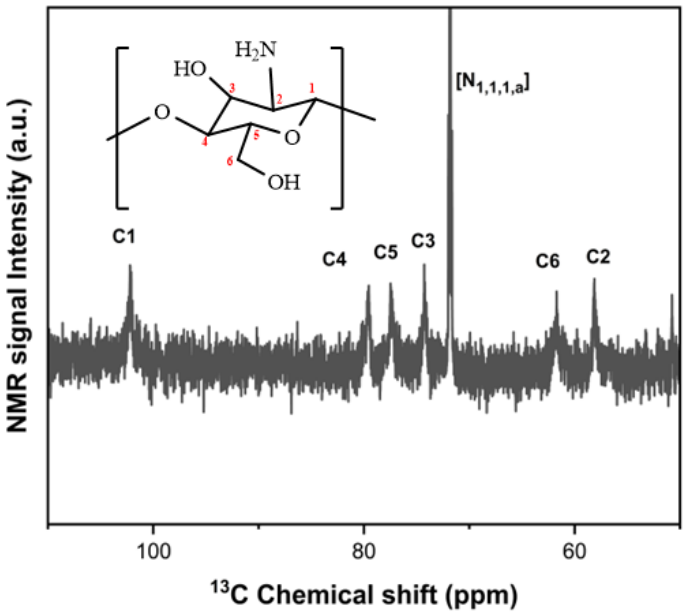

Figure 56. ^{13}C NMR spectra of chitosan in [$N_{1,1,1,a}$]OH

Different concentrations of chitosan solution were prepared in $[N_{4,4,4,4}]OH$ solution to better understand how OHS can dissolve chitosan (Figure 57). However, the position of the C_2 carbon in chitosan overlaps with the signal of the $[N_{4,4,4,4}]^+$ cation, resulting in only five carbon signals being observed in the ^{13}C-NMR spectrum. This also indicates that the intensity of the carbon signals is proportional to the chitosan concentration.

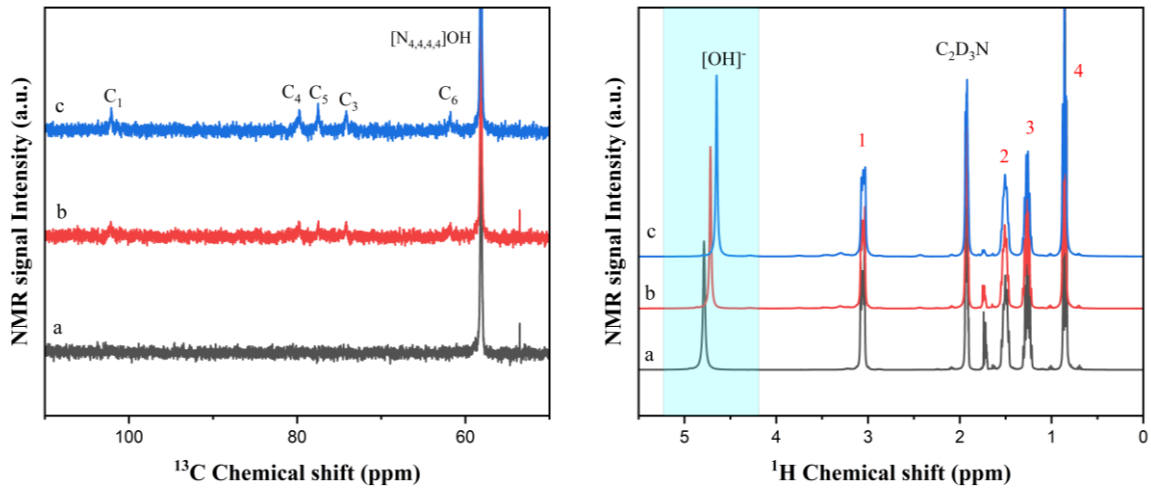

Figure 57. ^{13}C and ^{1}H NMR spectra of chitosan in different concentrations of chitosan with $[N_{4,4,4,4}]OH$ a) pure $[N_{4,4,4,4}]OH$, b) 50mg/ml, c)100mg/ml

^{1}H-NMR spectra show a slightly shift in the $[OH]^-$ signal at different chitosan concentrations. The peak of pure $[N_{4,4,4,4}]OH$ appeared at $\delta = 4.79$ ppm, which then shifted to lower regions at $\delta = 4.71$ and 4.66 for chitosan concentrations of 50 and 100 mg/mL, respectively. The downfield shift of the hydroxide proton indicates a decrease in the electron density as the chitosan content increases. This is most likely due to the formation of hydrogen bonds between the hydroxide anion and the hydroxyl groups of chitosan.[187, 188]

Water and ethanol have been used as anti-solvents for chitosan and other polysaccharides, respectively. When excess anti-solvent was added to the chitosan solution, the interaction between chitosan and the $[OH]^-$ groups was disrupted. Consequently, chitosan precipitated from the polymer solution (Figure 59). The precipitated chitosan was washed with ethanol at least three times, and the pellet and supernatant obtained after the process were used for further analysis.

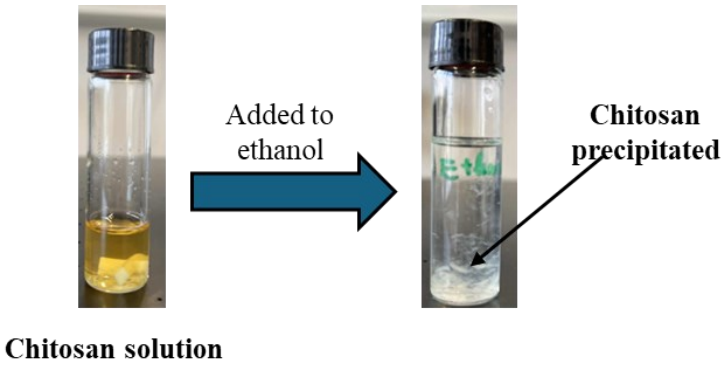

Figure 58. Chitosan precipitations in ethanol

The ethanol was removed from the supernatant by rotary evaporation, and the recovery of $[N_{4,4,4,4}]OH$ was determined. NMR measurements were applied to analyse the recovery of $[N_{4,4,4,4}]OH$ after the solidification process, as shown in Figure 59.

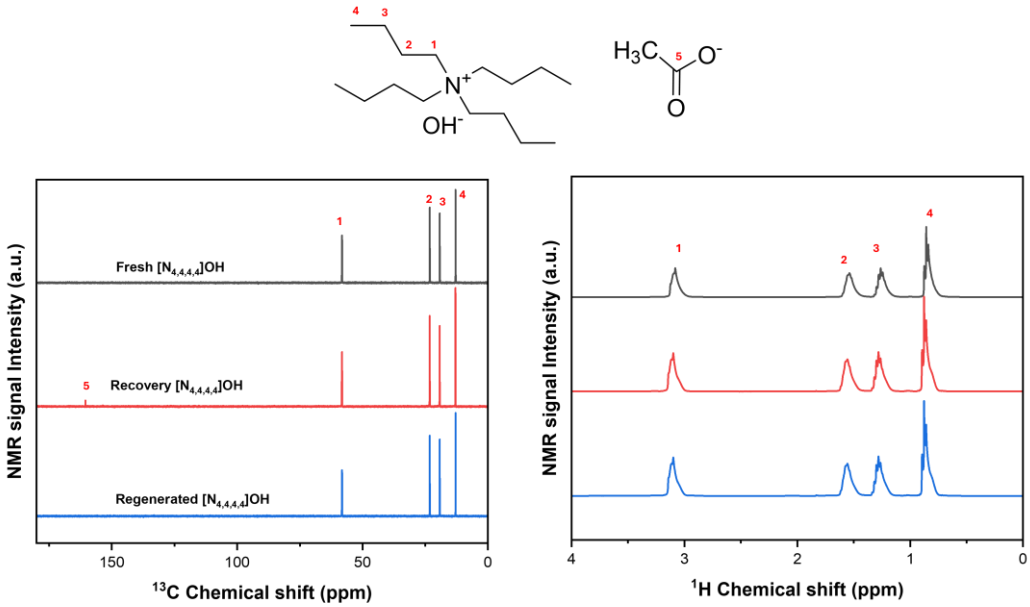

Figure 59. ^{13}C and ^{1}H NMR spectra of fresh, recovered and regenerated $[N_{4,4,4,4}]OH$

A new peak at 160.5 ppm was detected in the ^{13}C-NMR spectra of the recovered $[N_{4,4,4,4}]OH$ compared to the fresh solution, indicating the presence of acetyl groups after the process. This suggests that deacetylation occurs simultaneously with the dissolution process. The same new peak was also observed in the ^{13}C-NMR spectra of the recovered $[N_{4,4,4,4}]OH$ after chitin deacetylation, as reported in a previous study by Dinh et al.[81]

Thus, OHS must be regenerated for subsequent use. To regenerate [$N_{4,4,4,4}$]OH after the chitosan dissolution process was complete, the ionic exchange column was set up. After the regeneration process was completed, the peak at 160 ppm disappeared, indicating that the acetate ion was removed. The ^{13}C-NMR spectra of the regenerated and fresh [$N_{4,4,4,4}$]OH were similar, confirming the successful regeneration.

3.7.2 Characterisation of regenerated chitosan powder

The precipitated chitosan was dried overnight at 80°C in an oven. The samples were then ground into powder for further analysis. The mass of the regenerated chitosan collected after the dissolution and regeneration processes was 76 ± 5%.

The CHNS analysis was performed for CS and RCS, revealing the mass concentrations of carbon, hydrogen, and nitrogen (Table 10).

Table 10. The CHNS elemental analysis of chitosan (LMW) and regenerated chitosan

Sample	C(%)	H(%)	N(%)	S(%)
CS	39.2	6.6	6.4	-
RCS	41.2	6.9	6.8	-

Subsequently, FT-IR spectra were used to analyse the chemical structures of the CS and RCS powders, as shown in Figure 60. No new peak was detected in the RCS spectra, confirming that dissolution in OHS did not alter the chemical structure of chitosan. The broad absorption band in the 3200–3500 cm^{-1} region is attributed to O-H and N-H vibrations and extensive hydrogen bonding in the chitosan network. The peaks at 2920 and 2870 cm^{-1} are associated with C-H symmetric and asymmetric stretching, respectively. Additionally, the peaks at 1650 cm^{-1} (C=O stretching of amine I) and 1320 cm^{-1} (C-N stretching of amine III), related to the N-acetyl group, were still present in the chitosan structure. The band at approximately 1590 cm^{-1} is assigned to the bending vibration of the primary amine ($–NH_2$) group. In addition, several bands associated with the pyranose rings of the polysaccharide material, including C-O-C glycosidic bonding and C-O stretching, appeared at approximately 1150 and 1020 cm^{-1}. Moreover, the peak

at 890 cm^{-1} is assigned to a β-glycosidic linkage, which is similar to that found in cellulose.

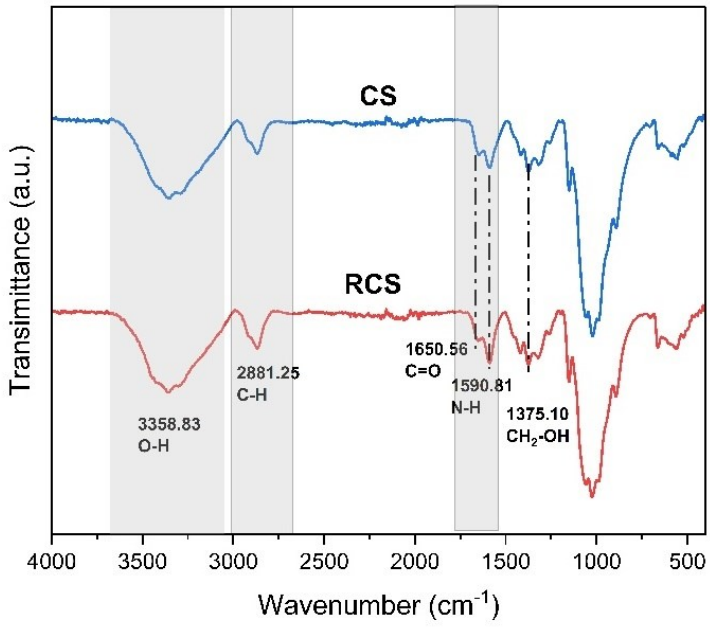

Figure 60. FT-IR spectra of CS and RCS regenerated in ethanol

To obtain further information, XRD analysis was employed to observe the changes in the crystallinity of chitosan after regeneration in ethanol, as illustrated Figure 61 (Cu radiation was used for measurement). The XRD pattern typically displays two characteristic diffraction peaks: one at 2θ = 10.2° (010), attributed to a less ordered region, and a more prominent peak at 2θ = 20.2° (200).[189] Notably, there were no changes in the diffraction peaks of chitosan after regeneration. However, the XRD pattern of the regenerated chitosan showed a significant reduction in the intensity and broadening of the 10.2° peak. Conversely, the peak at 20.2° remained very sharp compared to that of the original chitosan. In addition to the chitosan peaks, a peak was detected at 28.5°, corresponding to calcium carbonate ($CaCO_3$). The presence of $CaCO_3$ could be attributed to its being the primary component of crustacean exoskeletons and a crucial resource for producing chitosan. The crystallinity index of CS and RCS powder was measured by the method of Forcher et al. [190], showing a slight decrease from 76.5% to 71.7% after CS regeneration.

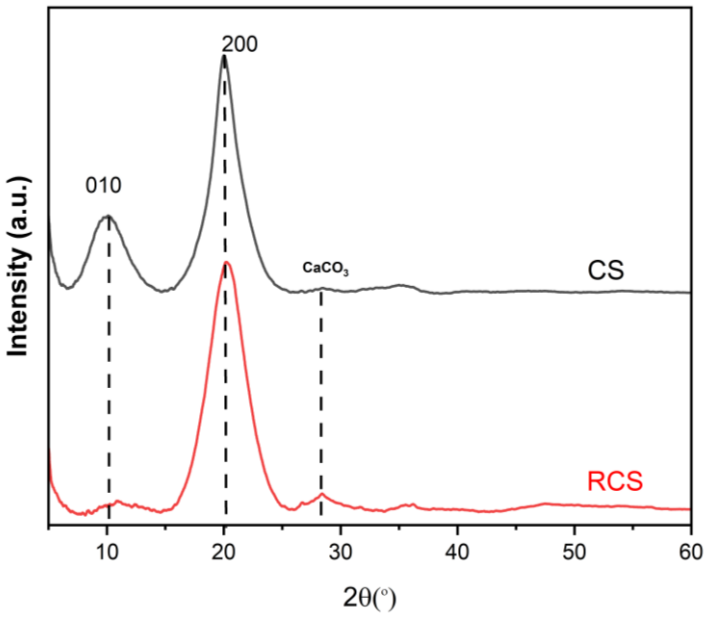

Figure 61. XRD pattern of CS and RCS

3.7.3 Production and characterisation of regenerated chitosan film by MDCell process

To produce a cellulose/chitosan blended film using the MDCell procedure, the chitosan solution must first be solidified in PC. The concentration of chitosan is a crucial factor that influences the quality and mechanical stability of films during production. Therefore, different chitosan solutions were prepared to determine suitable concentrations for chitosan film production.

The results showed that chitosan dissolved in $[N_{4,4,4,4}]OH$ 60 wt.% could solidify in the PC solution across a wide concentration range. However, a stable and good chitosan film was produced only at concentrations above 80 mg/mL. Below this concentration, the film was very weak and lacked physical stability, making it unsuitable for generating films using the MDCell procedure. Additionally, compared to the cellulose solution, the solidification time of the 100 mg/mL chitosan solution in the PC bath was significantly longer, taking approximately 3 hours for the chitosan solution to fully gel and detach

from the glass plate. After regeneration, the obtained chitosan film appeared compacted, as shown in Figure 62.

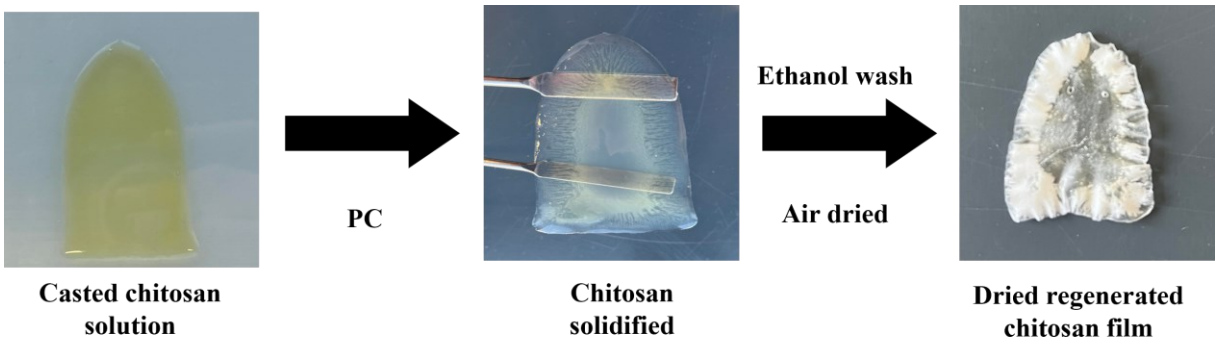

Figure 62. Regenerated chitosan film produced by modified MDCell process

In producing a film using the MDCell process, water is used to remove unreacted agents from the RKC film after it has been regenerated from the PC bath. However, water is unsuitable for chitosan films, as the film tends to break apart during washing. Furthermore, when water is used to produce chitosan films, it breaks into smaller pieces after air drying, as shown in Figure 63. In contrast, replacing water with ethanol results in a chitosan film that remains stable and is easier to process. The RCS film also remains compact after air drying (Figure 62).

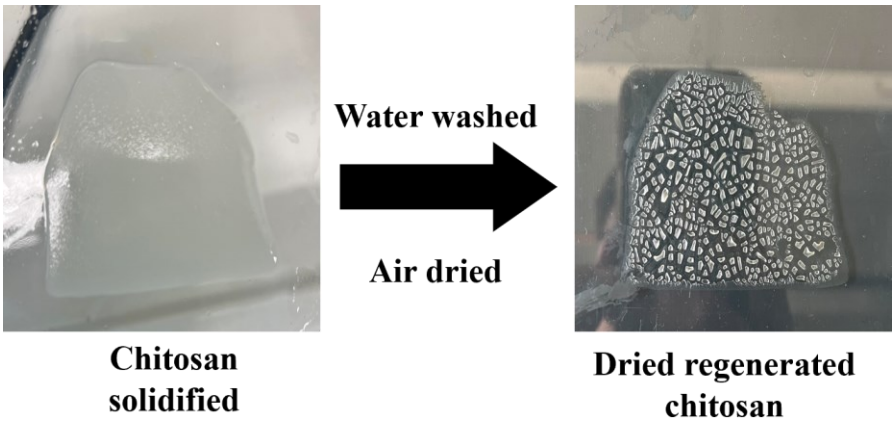

Figure 63. Chitosan solidified in water and after air dried

FT-IR was used to analyse the chemical structure of the RCS powder after regeneration with PC and washing with ethanol (Figure 64). No new signals were detected, indicating that RCS have no differences to CS before dissolution and regeneration in PC. This also

confirms that the regeneration phenomenon in a PC solution of chitosan has a mechanism similar to that of cellulose, as proposed in the previous section.

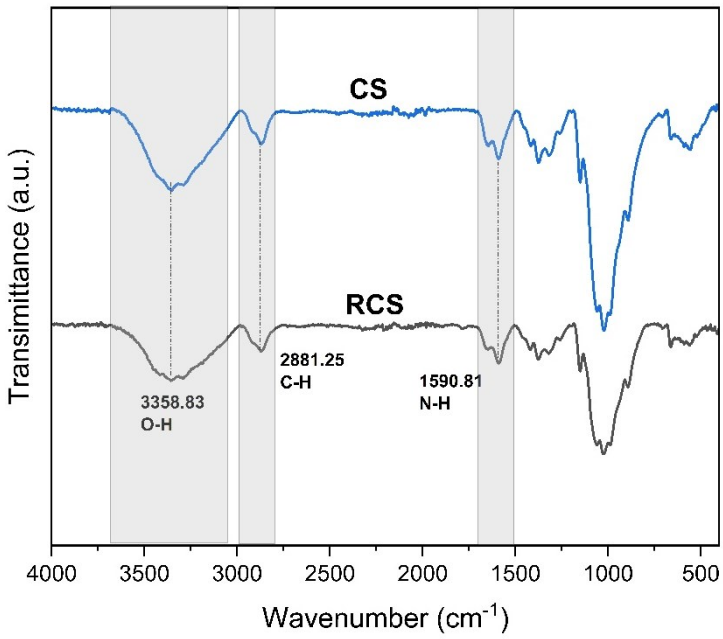

Figure 64. FTIR spectra of CS and RCS powder regenerated by MDCell process

The SEM measurement was used to analyse the morphology of the RCS film, which is shown in Figure 65.

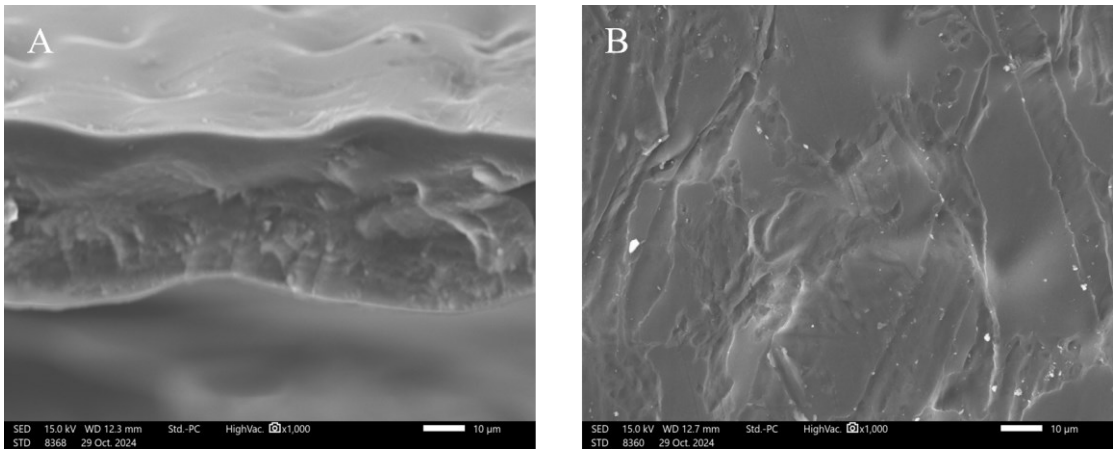

Figure 65. SEM analysis RCS film A) surface and B) cross-sectional area

It can be observed that the surface of the chitosan film appears not to be particularly smooth and flat, and it does not exhibit any cracks. The uneven chitosan surface may be due to the long solidification time of chitosan in the PC bath and the evaporation of ethanol during the drying process. Additionally, tiny particles were observed on the surface of the chitosan films. This could be attributed to undissolved chitosan powder

or impurity particles such as $CaCO_3$ (detected in XRD spectra of chitosan powder in Figure 61). The cross-section of the pure chitosan film appeared very dense and uniform. Compared to the RKC film, the cross-section of the RCS film did not show the aligned structure.

3.7.4 Proposed chitosan dissolution mechanism in onium hydroxide solution

Based on the above analysis, it was confirmed that both the cation and anion of OHS contribute to the dissolution of chitosan. The cation $[OH]^-$ continues to play a crucial role in the dissolution process of chitosan. Previous research has suggested that the obtained chitosan increases proportionally with treatment time in an ammonium hydroxide solution.[79, 80] Thus, it is agreed that the deacetylation reaction occurred after the dissolution process was complete. Consequently, the $[OH]^-$ groups not only participate in the dissolution but also in the deacetylation process, which involves the reaction of the remaining acetamido group in chitosan. The deacetylation mechanism is indicated in Figure 66.[191]

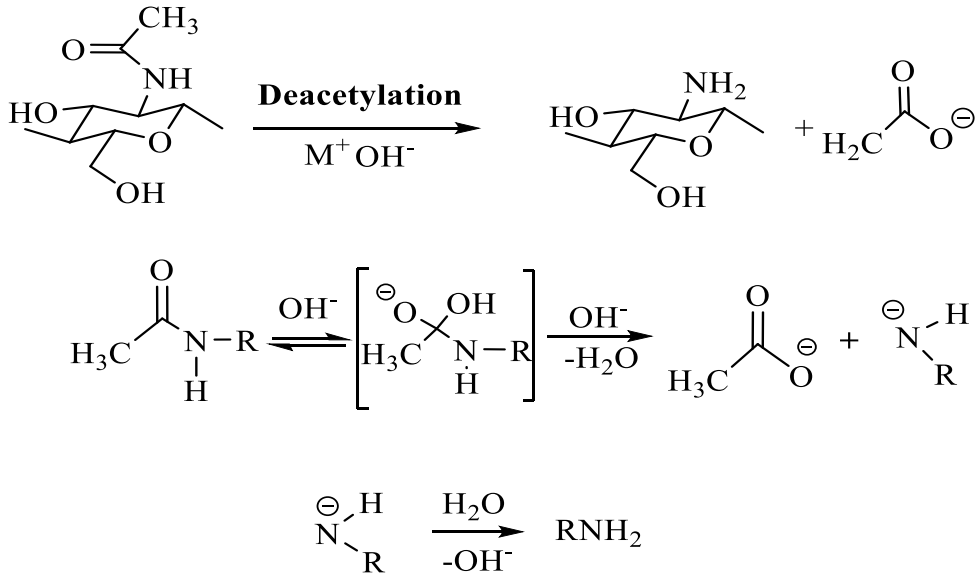

Figure 66. Deacetylation mechanism of chitin/chitosan

The proposed dissolution of chitosan in OHS is illustrated in Figure 67. This indicates that the $[OH]^-$ of OHS plays a central role in disrupting the hydrogen bond network of chitosan, leading to its dissolution. The cation aggregates on the chitosan fibre,

preventing the chains from interacting, leading to solidification.[81, 188, 192] As a result, the chitosan solution remains stable for a long time.

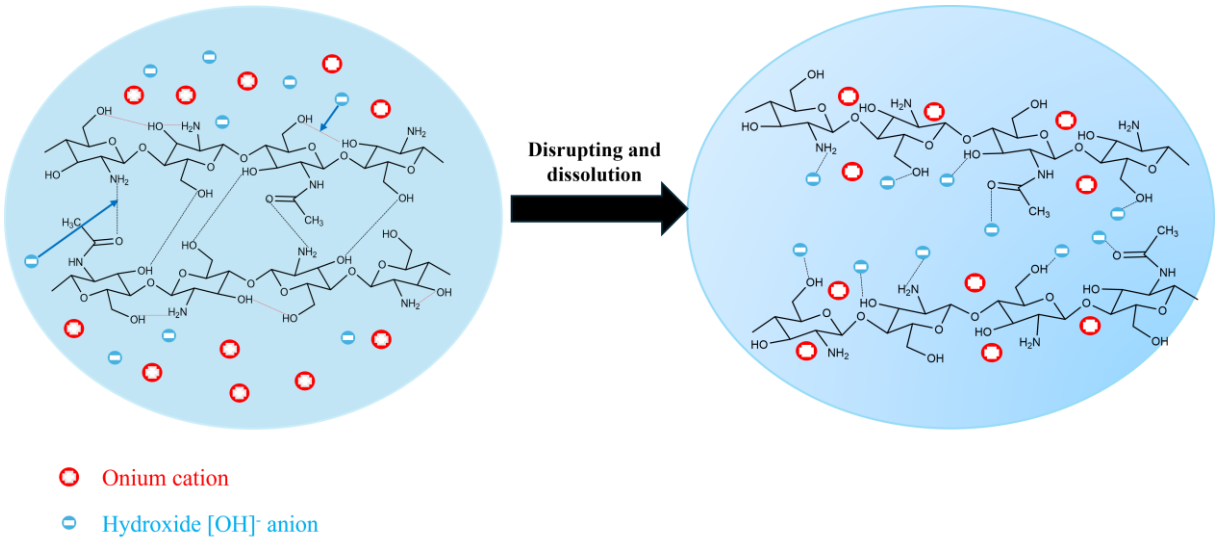

Figure 67. Proposed chitosan dissolution mechanism by onium hydroxide solution

Additionally, the solubility of chitosan in OHS significantly depends on water content and cationic structure, similar to cellulose. However, the greater hydrophobicity of chitosan compared to cellulose led to differences in the optimal dissolution of these two materials. According to our results, the OHS must have an Nw value between 8 and 12 to dissolve chitosan effectively.

3.8 Production of regenerated cellulose/chitosan film

3.8.1 Production of cellulose/chitosan film by the modified MDCell process

In the previous section, chitosan was successfully dissolved in the $[N_{4,4,4,4}]OH$ solution, and the RCS film was generated using the modified MDCell procedure. In this section, chitosan is combined with cellulose to create regenerated cellulose/chitosan films.

Different ratios of MCC and LMW-CS solutions were prepared by directly dissolving them in $[N_{4,4,4,4}]OH$ 60 wt.%. These polymeric solutions were both clear and transparent, showing a homogeneous distribution and dissolution (Figure 68). The colour of the cellulose/chitosan solution changed from clear to yellow as the chitosan concentration increased.

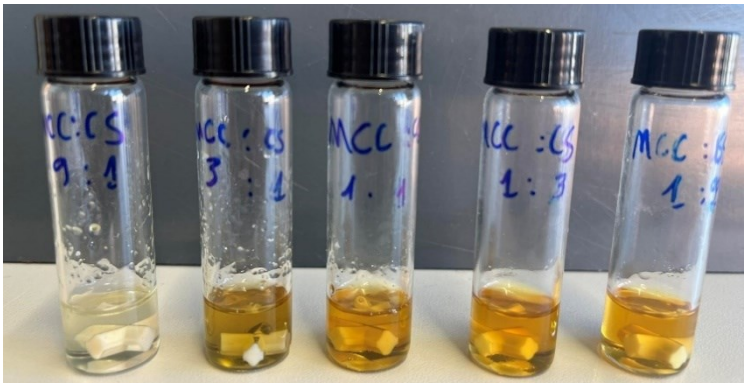

Figure 68. MCC/LMW-CS dissolved by [$N_{4,4,4,4}$]OH 60wt.% solution (the concentration of chitosan rising from left to right: 10, 25, 50, 75, and 90%)

The cellulose/chitosan solution was cast and immersed in the PC solution, resulting in a solidified gel with cellulose/chitosan in different ratios. The solidification time for each cellulose/chitosan ratio is indicated in Figure 69. The results show that the solidification time is proportional to the chitosan concentration in the mixture, increasing from 15 minutes to approximately 3 hours as the chitosan concentration increased from 10% to 90%.During the production process, the blended cellulose/chitosan film exhibited better durability when the chitosan content was below 50%. Higher chitosan content resulted in weaker mechanical properties of the film. Additionally, films with less than 50% chitosan content could be washed with water and remained intact after drying. In contrast, films with higher chitosan content broke during the same procedure described in the section. Therefore, a 50% chitosan ratio will be used as the maximum to produce thin blended films.

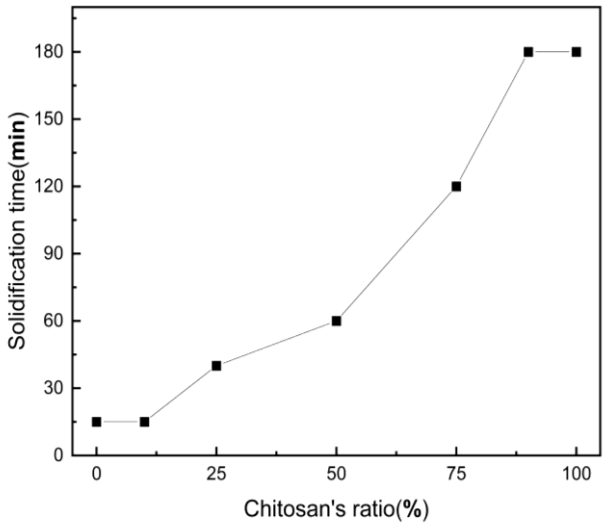

Figure 69. The solidification time of MCC/LMW-CS in different ratios in PC

When MCC was replaced with KC, a different strategy was applied to prepare the cellulose/chitosan solution. Cellulose and chitosan were prepared separately before mixing. The procedure for generating the regenerated KC and chitosan-blended film is illustrated in Figure 70 (detailed process is described in Section II.h).

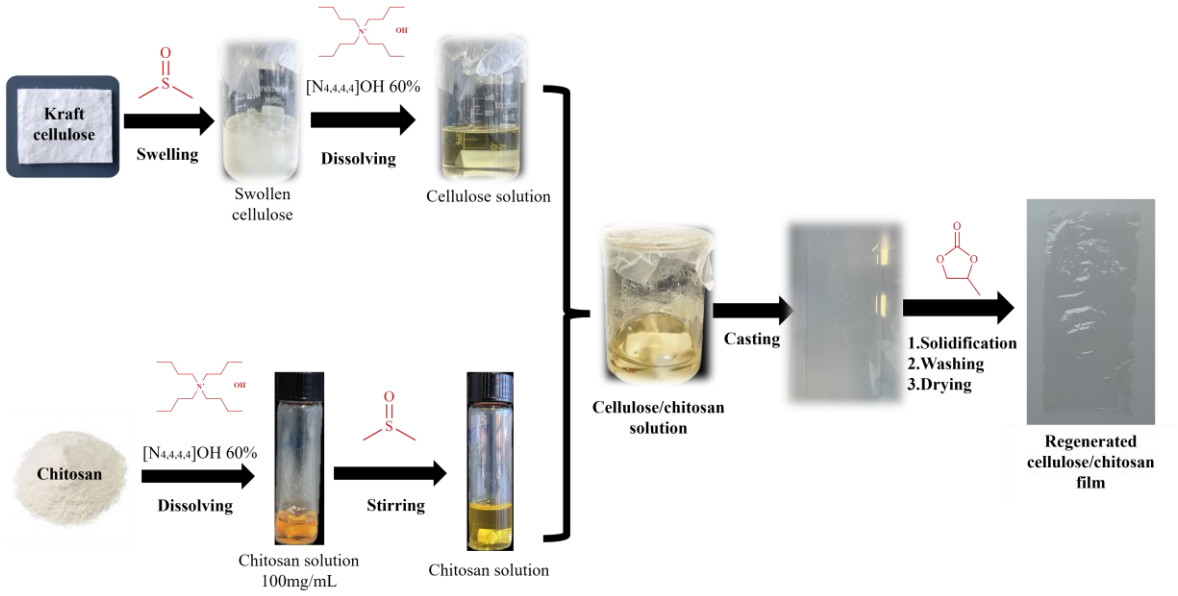

Figure 70. Procedure for preparing regenerated Kraft cellulose/chitosan films

After complete drying, the regenerated Kraft cellulose/chitosan (RKC/RCS) films were compact and homogeneous (Figure 71). Compared with the RKC film, the RKC/RCS film appeared blurry and was not very transparent. It noted that the film has wrinkles similar to those of RKC film at the same casted thickness.

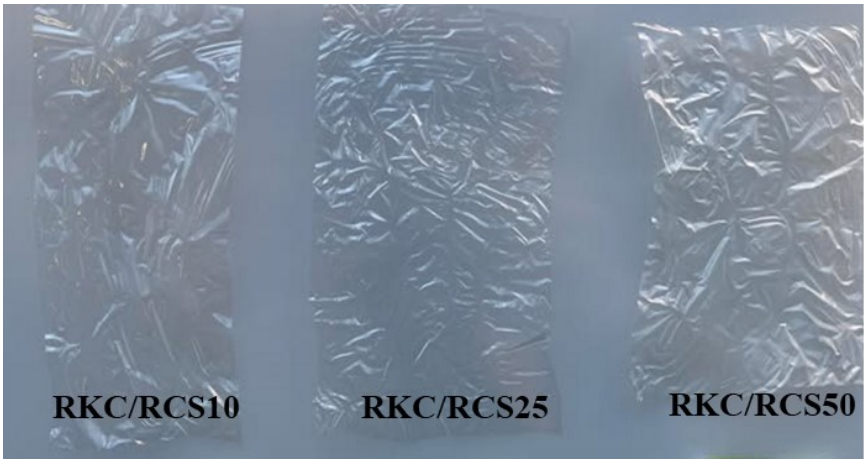

Figure 71. The morphology of RKC/RCS films

Additionally, the solidification time of the KC/LMW-CS solution in PC is significantly reduced compared to that of the MCC/LMW-CS solution, decreasing from one hour to

approximately 10 minutes at a 50-50 ratio. Then RKC/RCS films will be characterised by chemical, mechanical and physical methods to investigate the influence of chitosan on the RKC films.

3.8.2 Characterisation of regenerated cellulose/chitosan films

CHNS elemental analysis was used to determine the elemental ratio of the regenerated cellulose/chitosan material (Table 11). Sulphur was not detected in any of the film samples. With an increase in the chitosan ratio in the blended material, the percentage of nitrogen was higher. These results indicate that cellulose and chitosan cooperate in the polymer structure and co-solidify in the PC solution.

Table 11. The CHNS elemental analysis of RKC/RCS films

Type of film	C(%)	H(%)	N(%)	S(%)
RKC/RCS10	41.66	6.27	0.32	-
RKC/RCS25	41.05	6.03	1.36	-
RKC/RCS50	42.51	6.60	3.03	-

The FTIR spectra of pure regenerated cellulose, chitosan, and cellulose/chitosan blended films are shown in Figure 72. Both cellulose and chitosan are polysaccharides that share many common functional groups, as indicated by the previous results of FT-IR spectra of RKC and RCS. The presence of amine and N-acetyl groups (DDA always lower than 100%), which characterise the chemical structure of chitosan, distinguishes it from cellulose. Thus, the distinct regions between cellulose and chitosan are located between 1550 and 1650 cm^{-1}, which is attributed to the amine and N-acetyl groups. The peak at approximately 1657 cm^{-1} represents the C=O stretching of residual N-acetyl, as indicated in the RCS spectra. Meanwhile, the cellulose spectra exhibit a broad peak, similar to that of chitosan, which appears at approximately 1640 cm^{-1} and responds to water absorbed into the polymeric structure.[193] It is noted that the N-H bending from amide II around 1590 cm^{-1} shows high intensity in the RCS spectra. The intensities of these peaks decreased proportionally with the reduction in chitosan content in the

blended films, and it can not detected in the spectra of the RKC/RCS10 film. The studies by Stefanescu et al.[194] and Yang et al.[56] , which reports a similar trend for their cellulose/chitosan materials.

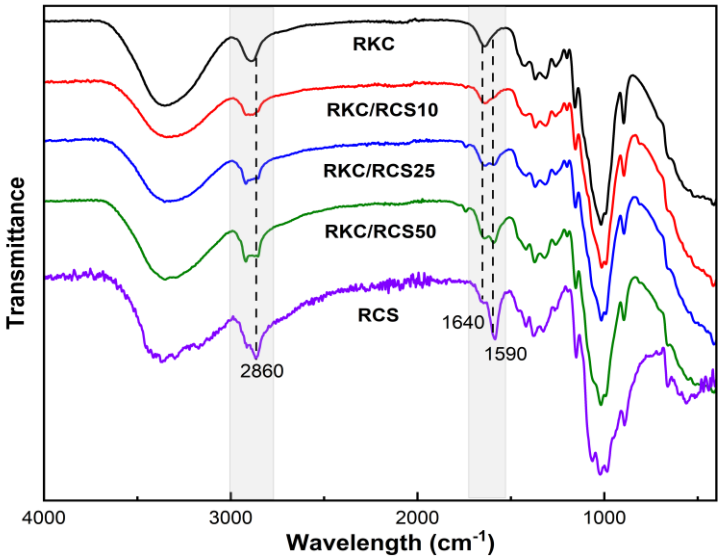

Figure 72. FT-IR spectra of RKC, RCS and RKC/RCS in different ratios films

Furthermore, two peaks were observed at approximately 2850–2920 cm^{-1} in chitosan and the blended material. The peak at 2920 cm^{-1} is generally assigned to the anti-symmetric stretching of the CH_2 group. The lower wavenumber peak, at approximately 2850 cm-1, is attributed to the symmetric vibration of the CH_2 group in the glucosamine and N-acetylglucosamine units of chitosan. The intensity of this peak was also proportional to the chitosan concentration, similar to the amide II peak at 1590 cm^{-1}. This evidence can be used to prove that cellulose and chitosan are well blended in the polymeric structure.

The X-ray diffraction patterns of RCS, RKC, and RKC/RCS at different concentrations are presented in Figure 73. The XRD patterns of regenerated chitosan showed two main diffraction peaks at 5.1° and 9.2°, corresponding to (010) and (200) crystallographic planes, respectively.[195] RKC has three main diffraction reflections at 5.4° ($\bar{1}$10), 9.2° (020), and 16.1° (004), corresponding to cellulose II crystallinity.

It is noted that RKC/RCS sample displayed a sharp and broad peak at 2θ = 9.2°. As shown in the XRD patterns of regenerated cellulose and chitosan, there are peaks that cause overlap in the lattice of the blended material. Additionally, there is a lower

intensity and narrower peak around 5.4° indicate the influence of the component material concentration in the blended samples. The XRD patterns of RKC, RKC/RCS10, and RKC/RCS25 show diffraction peaks in this region at 5.4°, 5.3°, and 5.3°, respectively. When the chitosan concentration reaches 50%, as indicated by the RKC/RCS50 spectra, this peak shifts to around 2θ = 5.2°, which is closer to the diffraction peak of pure regenerated chitosan at 2θ = 5.1°. Moreover, all the XRD patterns of blended cellulose/chitosan indicated a signal at 16.1° (004), corresponding to the cellulose II pattern, which is not present in the pure chitosan spectrum.

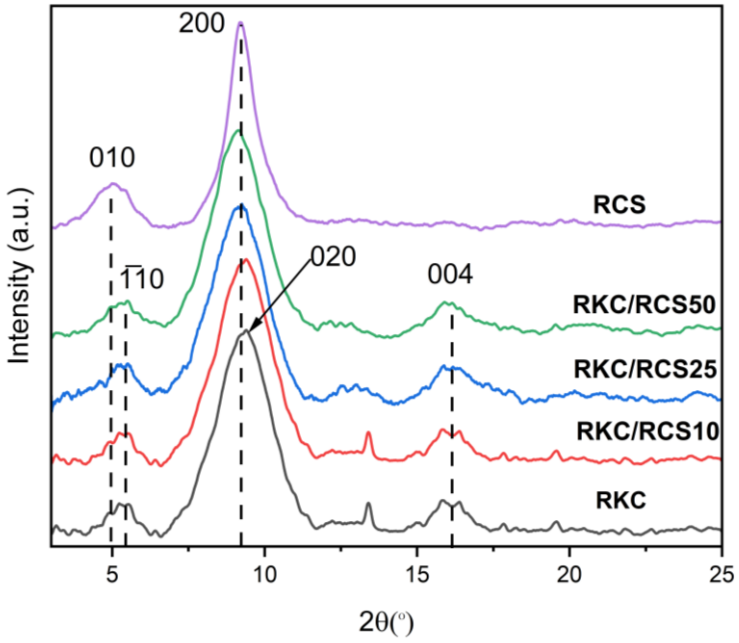

Figure 73. XRD pattern of RKC, RCS and RKC/RCS in different ratios

The surfaces and cross-sections of the RKC/RCS films at different concentrations are shown in Figure 74. The morphology of pure regenerated cellulose appeared homogeneous and thin, with a flat surface. When combined with chitosan, the surface of the films remained very homogeneous, but tiny particles were easily observed. This could be due to the presence of impurities, such as $CaCO_3$. Additionally, the blended cellulose/chitosan cross-section appeared dense and homogenous, and no phase separation was detected in any the of samples. However, the layered structure of cellulose was difficult to observe in the blended film. Morphological changes occurred at low concentrations of chitosan. The cross-section of RC/RCS10 appeared very

compact, dense, and less aligned. However, the layered structure was still observed in the cross-sectional images of RKC/RCS50. Hasegawa et al.[196] explained this phenomenon, which is highly related to chitosan. Typically, pure cellulose has a lamellar structure, and chitosan tends to fill the interstitial space among the lamellar structures of cellulose. As a result, the crystalline structure of cellulose was affected, resulting in a less ordered structure of the blended material. The similar morphology of cellulose/chitosan films was also found in the research of Yang et al.[56] and Cheng et al.[197] .

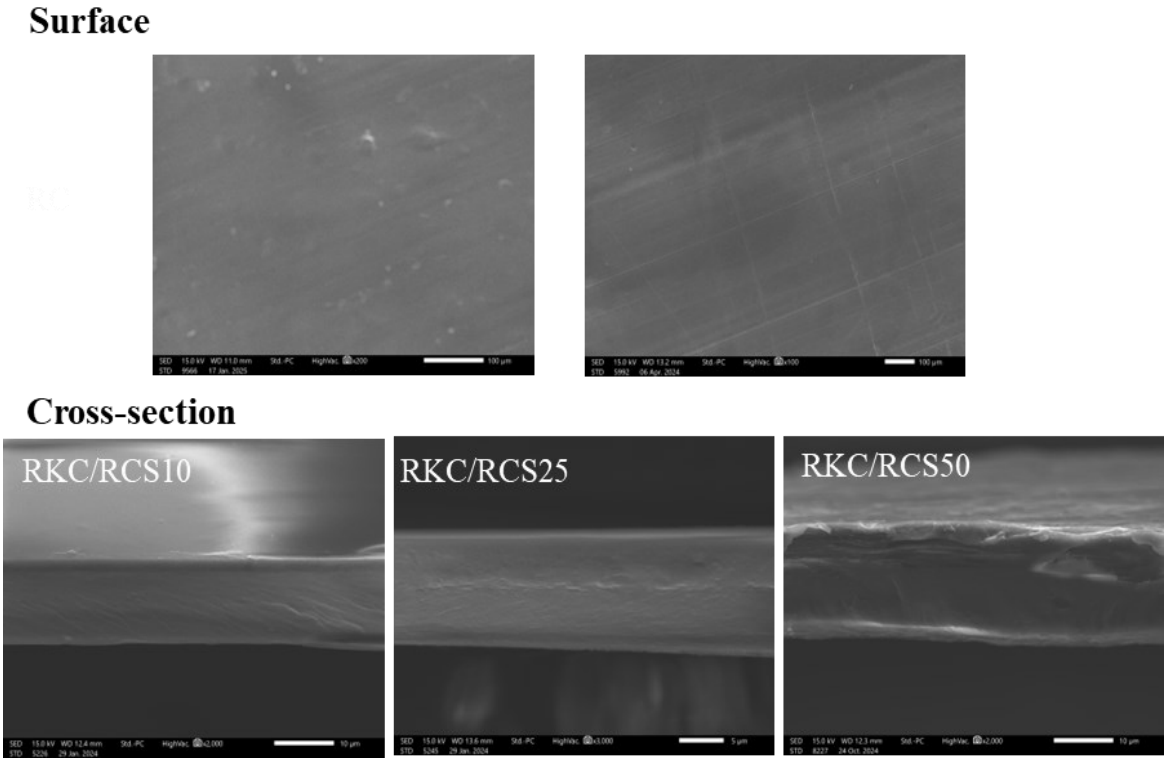

Figure 74. SEM analysis of surface and cross-sectional area of RKC/RCS film

The AFM image of the surface RKC/RCS50 film at different magnifications is indicated in Figure 75. Numerous impurity particles were detected on the surface of the RKC/RCS50 film using AFM. Additionally, straight lines also appeared on the blended film, as shown in the RKC film (Figure 42). The roughness of the bottom side of the film was measured as Sa = 21 nm, while the roughness of the top side was Sa = 13 nm. This indicates that the blended film is rougher than the pure cellulose film, with roughness values of 4.1 and 3.2 nm on the top and bottom sides, respectively. The

roughness of the RKC/RCS50 film exceeds that of the RKC film, which could be attributed to $CaCO_3$ or other impurities within the chitosan. (Figure 61).

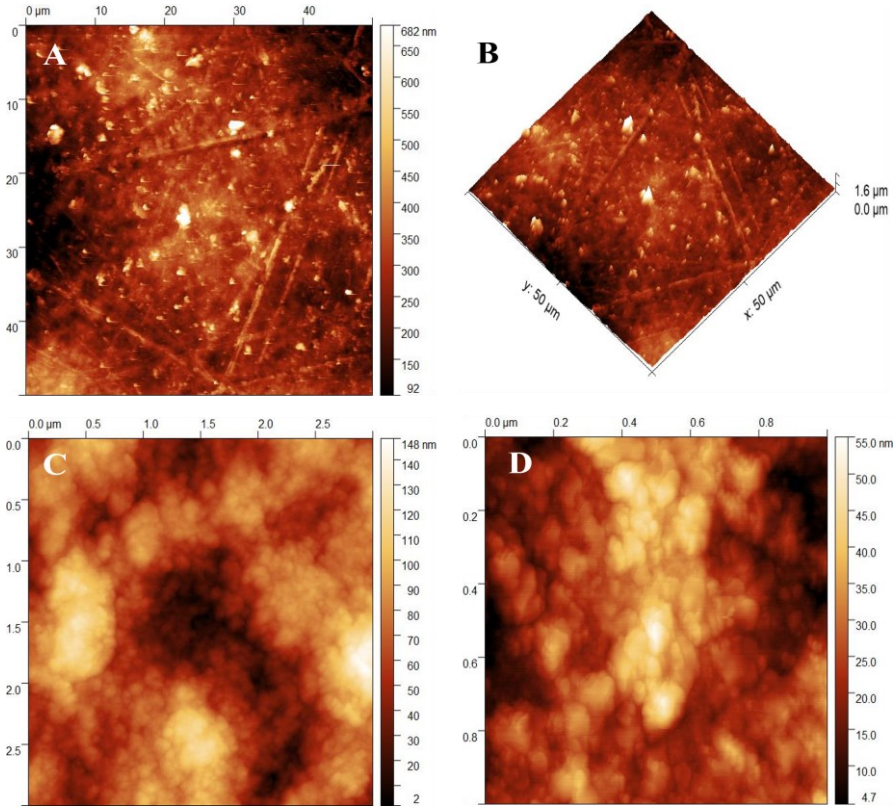

Figure 75. AFM analysis of RKC/RCS50 film at different magnifications: A) 50x50µm, B) high surface area at 50x50µm, C) 3x3µm, and D) 1x1µm.

High-resolution AFM images revealed the morphological differences between the RKC/RCS50 film and the RKC film. As mentioned, AFM detected the ribbon-like structure, measuring 20-35 nm in width and 50 nm in length in the RKC film. Meanwhile, platelets, approximately 200 nm long and between 200 and 100 nm wide, were found in the RKC/RCS50 film. Additionally, no ribbon structure was observed in the blended film sample. This suggests that chitosan altered the original structure of cellulose. Additionally, the platelet structure found in blended film has a larger size than the ribbon structure of pure cellulose, which could contribute to the rougher surface of the blended film.

The thickness, transparency, and WVTR of the cellulose/chitosan blended film are listed in Table 12. The films had a relatively consistent thickness, approximately 15µm for every blended film.The film transparency decreased with increasing chitosan concentration. The transparency of the RKC film was 79%, and the values of

RKC/RCS10, RKC/RCS25, and RKC/RCS50 were 65, 41, and 43%, respectively. These results align with previous measurements of SEM and AFM images, which indicated the presence of impurities on the surface of the blended films. As the chitosan concentration increased, more $CaCO_3$ was introduced into the blended films, resulting in a reduction in transparency.

Table 12. The thickness, transparency, and WVTR of RKC and RKC/RCS films

Type of film	Thickness (µm)	Transparency (%)	WVTR (g/m^2 h)
RKC	15 ± 3	79 ± 3	10.7 ± 0.1
RKC/RCS10	16 ± 2	65 ± 1	9.1 ± 0.3
RKC/RCS25	17 ± 3	41 ± 1	8.9 ± 0.5
RKC/RCS50	15 ± 2	43 ± 2	7.7 ± 0.3

The water vapour transmission rate (WVTR) is a quantitative measure of the amount of water vapour passing through a material over a specific period. It is a vital physical parameter for cellulose-based materials used in food packaging. Different types of materials can create a controlled humid environment for food storage. Therefore, selecting suitable materials is crucial to prolong storage life and minimise flavour loss during production. The WVTR parameter was utilised to evaluate the impact of each material component on the others over an extended period. The WVTR of the RKC film and other RKC/RCS films are listed in Table 12.

The cellulose/chitosan blended film prepared using the MDCell method showed a lower WVTR than the pure regenerated cellulose film. The WVTR of the pure regenerated cellulose film was 10.7 g/m^2 h, indicating that the pure cellulose film allowed more water vapour to pass through than the cellulose/chitosan film. The values for RC/RCS10, RC/RCS25, and RC/RCS50 were 9.1, 8.9, and 7.7 g/m^2 h, respectively, indicating that blending chitosan into the cellulose structure immediately influences the

polymer structure. At 50% chitosan in the blended film, the WVTR decreased from 10.7 to 7.7 g/m² h, which is approximately 28% less. Numerous studies have reported similar trends when chitosan is incorporated into their materials. For instance, Reis et al.[198] indicated that their cellulose material showed better trapping of water vapour when coated with chitosan. The WVTR of their coated chitosan Kraft cellulose was 6.06 g/m^2 h, while the value for the uncoated material was 10.73 g/m^2 h. Similarly, Shapi et al.[199] observed a reduction in the WVTR of their starch film when chitosan was incorporated.

Cellulose is a hydrophilic material with numerous free hydroxide groups that can easily interact with water molecules. Hence, water vapour is easily transported through the film. When chitosan is introduced into cellulose material, its amino (-NH_2) forms strong hydrogen bonds with the hydroxide group of cellulose. This led to the polymer matrix being tied up and the structure of the blended material becoming denser, as observed in the SEM image. Hence, the compact structure of cellulose/chitosan limits water diffusion and permeation. Consequently, moisture requires more time to escape the polymer matrix, thereby reducing the WVTR.

Figure 76 shows the contact angles between the water droplet and surface of RKC, RKC/RCS50 and RCS film. It is noted that the contact angle between water and RKC film is around 39°, indicating the hydrophilicity of the cellulosic material. [200] While the contact angle of pure regenerated chitosan is attributed to its hydrophobic property, because its angle is larger than 90°.[201, 202]

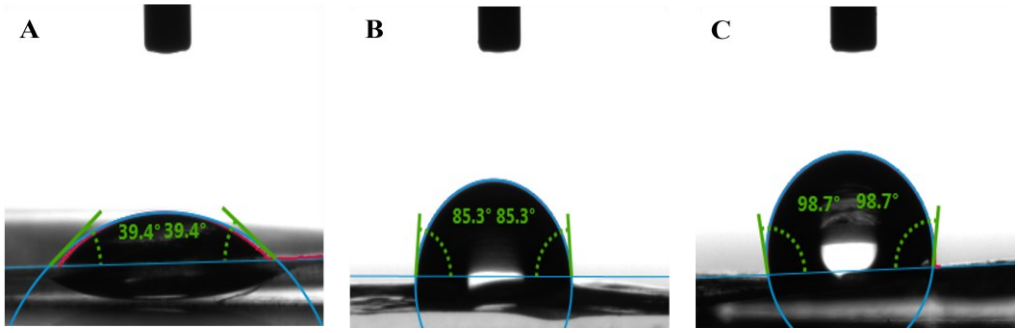

Figure 76. Water contacting angle images of: A) RKC, B) RKC/RCS50, and C) RCS film

Table 13 lists contact angles of the front and back sides of the regenerated cellulose/chitosan films at different ratios. The results show that chitosan incorporated

into the polymeric structure of cellulose leads to changes in the wettability of the cellulose films. The contact angle of the RKC/RCS films was relatively higher than that of the RKC films, indicating lower hydrophilicity and higher hydrophobicity.

Table 13. The contact angle of cellulose/chitosan in different concentrations

Side of the film	Contacting angle (°)				
	RKC	RKC/RCS10	RKC/RCS25	RKC/RCS50	RCS
Back	37 ± 4.7	73 ± 15.8	53 ± 10.6	71 ± 10.4	91 ± 11.3
Front	59 ± 7.0	88 ± 6.0	67 ± 8.2	74 ± 12.5	96 ± 3.5

Tensile strength measurements were conducted on films with varying cellulose/chitosan ratios to evaluate their mechanical properties. Figure 77 shows the tensile stress-strain curve and the changes in tensile strength and elongation at the break of the films.

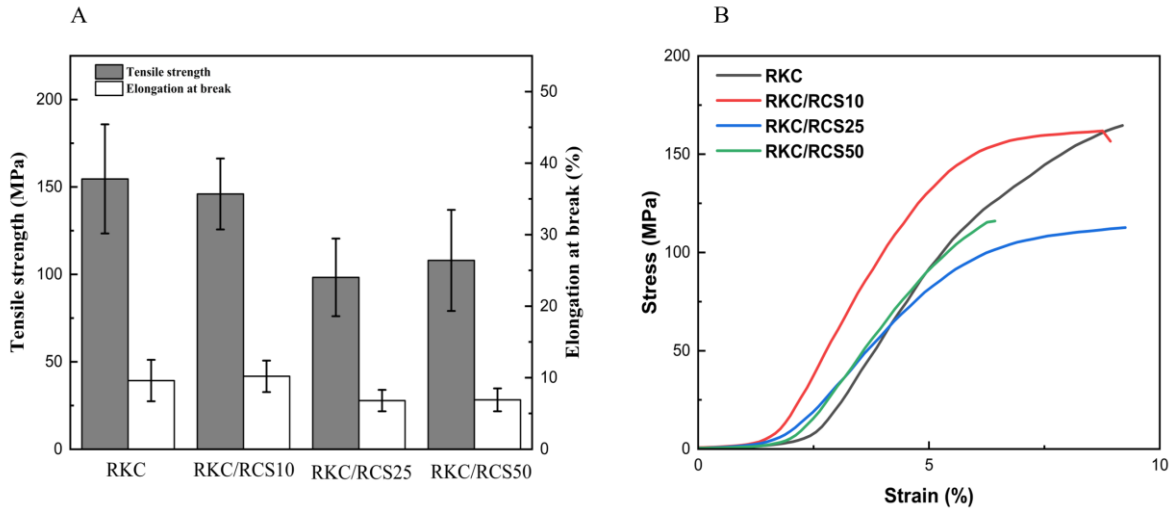

Figure 77. A) Tensile strength and elongation at break, B) Tensile stress-strain curve of RKC and RKC/RCS blended film at different ratios

The absence of yield points in the stress-strain curves of the films indicates their brittleness. The regenerated cellulose exhibited the best mechanical properties, with a maximum tensile strength of approximately 154 ± 31 Mpa and an elongation at break of approximately 10 ± 3%. At a 10% chitosan concentration, a slight decline in the maximum tensile strength was observed, dropping to approximately 145 ± 20 MPa.

When the chitosan content increased to 25% and 50%, the tensile strength decreased from 70 to 120 MPa, and the elongation from 4% to 8%. Nonetheless, the mechanical properties of the cellulose/chitosan blended films remained good even at higher chitosan levels. However, it is generally recognised that increasing the chitosan content deteriorates the mechanical properties of the composite. Yang et al.[56] suggested that higher chitosan levels disrupt the microstructure of the polymer, making it less aligned and more loosely packed. While Hasegawa et al.[196] proposed that the decrease in cellulose domain size when combined with chitosan negatively affects the mechanical properties of blended film compared to pure cellulose film

Three samples of each cellulose/chitosan blended film were tested and compared with previous studies on soil degradation. Figure 78 shows the gradual changes in the blended film over 28 days. The shapes of the films changed very little during the first 7 days. Very small holes appeared on the surface of the RKC/RCS10 film. Significant changes were observed from day 10 onwards, and all three samples of this film were completely degraded after 14 days. The films containing 25% and 50% chitosan took longer to decompose in the test. All RKC/RCS25 samples disappeared after 21 days, while RKC/RCS50 samples disappeared after 28 days.

Compared to the original RKC film, the incorporation of chitosan into the cellulose polymer structure changed the film's biodegradability in soil. The biodegradation process is complex and involves various aspects.[203,204] Chitosan content is one aspect that needs to be considered. Othman et al.[205] observed a longer degradation time in the soil for the starch and chitosan nanoparticle (CNP) film compared to the pure starch film. While the starch film fully decomposed after 8 days, only minor damage was observed in the composite starch/chitosan film. This study also showed that increasing the CNP ratio resulted in lower weight loss of the composite film. Specifically, the composite film with 25% CNP had a weight loss of 49.3%, whereas the films with 10, 15, and 20% CNP exhibited weight losses of 90.9%, 80.7%, and 65.5%, respectively.

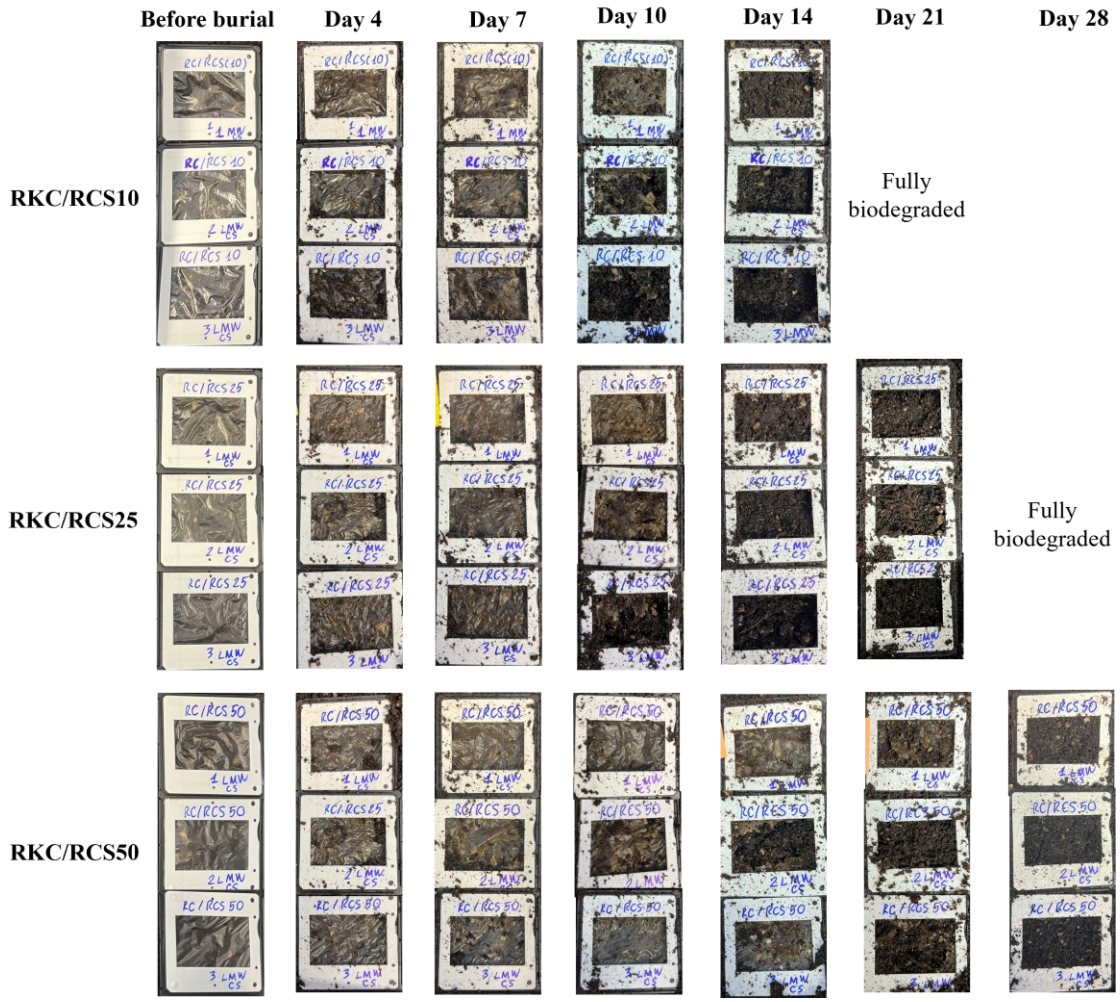

Figure 78. The morphological changes of RKC/RCS films at different ratios in soil buried experiment

Biodeterioration, fragmentation, and assimilation are the three main stages of biodegradation in the soil environment, as proposed in the RKC film experiment. [152-154] It begins with the hydration process, during which the film starts to swell and the microorganisms begin to grow inside film.[48] Enzymes from microorganisms are the primary agents that break down the polymer chains of polysaccharide materials such as cellulose and chitosan. Chitosanase, isozymes, and proteases are the three enzymes that break down the chitosan chain into shorter chains, producing carbon dioxide, water, and ammonia.[206] Chitosan is the component that affects the biodegradability of the RKC film, extending its decomposition time in the soil environment, depending on its ratio. Other properties of chitosan, such as molecular weight, crystallinity, and DDA, also influence the degradability of both pure chitosan and its composite products.[207, 208]

In summary, the cellulose/chitosan solution can be easily prepared using $[N_{4,4,4,4}]OH$ at a 60 wt.% solution through two methods: co-dissolution or mixing cellulose and chitosan solutions. By modifying the MDCell process, blended regenerated cellulose/chitosan was successfully produced. The films appeared dense and uniform. The ratio of the components within the films affected their transparency, WVTR, and biodegradability. As the chitosan concentration increased, the biodegradation time of the blended film in the soil environment increased proportionally. Similarly, films with higher chitosan content inhibited water vapour transmission more than those with lower chitosan content, with the WVTR of RKC/RC being 28% lower compared to RKC film.

4 SUMMARY

In this PhD study, the cellulose dissolution ability of various onium hydroxides at different concentrations was assessed, highlighting the effects of cationic structure and water content. A pre-swelling step in DMSO significantly enhanced the dissolution capacity of onium hydroxide by reducing the high viscosity of pure onium hydroxide. Moreover, the presence of DMSO extended the dissolution range of onium hydroxide solutions, enabling higher concentrations of onium solutions to dissolve cellulose compared to pure solutions. The swelling behaviour of MCC and KC was easily observed and documented using optical microscopy because dissolution occurred rapidly at room temperature. The $[N_{4,4,4,4}]OH$ exhibited the best cellulose dissolution capacity and was employed to produce a cellulose film via a modified MDCell process.

Kraft cellulose material was used to produce regenerated Kraft cellulose. The film exhibited good mechanical properties, high transparency, and excellent biodegradability. The RKC film completely degraded in soil within two weeks and in the Baltic Sea environment within five weeks. This suggests that the regenerated cellulose film made by the MDCell process has high potential for packaging applications and can be compared to fossil fuel-based plastics or other bio-based films.

The flexibility of the RKC films was greatly enhanced by immersing them in LiCl solutions. LiCl improves this property at low concentrations compared to traditional plasticisers like glycerol and polyethylene glycol. However, the presence of LiCl in the film reduces its biodegradability in soil environments.

The solubility of chitosan in onium hydroxide solvents was examined. Compared to chitin at room temperature, a higher yield of chitosan was obtained. $[N_{4,4,4,4}]OH$ at 60 wt.% could dissolve up to 80mg of LMW-CS at room temperature, increasing to 110mg at 50°C. Subsequently, a homogeneous cellulose/chitosan mixture was successfully produced, allowing the creation of a thin film using the MDCell process. The regenerated cellulose/chitosan film with different ratios was prepared by adjusting the polymer solution. The blended film demonstrates good mechanical properties. The addition of chitosan to the polymer structure modified specific properties of the film,

including WVTR and biodegradability. This blended film shows great potential in packaging applications. Additionally, the homogeneous mixture of cellulose and chitosan also opens an opportunity to develop other blending products depending on the proposed application.

APPENDIX

I. Materials

Tetrabutylphosphonium hydroxide ([$P_{4,4,4,4}$]OH), dipropyldimethylammonium hydroxide ([$N_{3,3,1,1}$]OH) 40 wt.% onium, and trimethyladamantane hydroxide ([$N_{1,1,1,a}$]OH) 20 wt.% in water were purchased from Sachem. Tetrapropylammonium hydroxide ([$N_{3,3,3,3}$]OH) 40 wt. % and tetramethyl hydroxide ([$N_{1,1,1,1}$]OH) 25 wt.% in water were purchased from Sigma Aldrich. Tetrabutylammonium hydroxide ([$N_{4,4,4,4}$]OH) 40 wt.% in water, Polyethene glycol (PEG) 300 purchased from Carth Roth. Microcrystalline cellulose (MCC) 20μm, low molecular weight chitosan (75-85% DDA, 20-300 cp), medium molecular weight chitosan (75-85% DDA, 200–800 cp), dimethyl sulfoxide (99.8%), glycerol (99.5%), and propylene carbonate (PC, 99,7%) were obtained from Sigma Aldrich. Kraft cellulose (KC) was obtained from Mercer. High-molecular-weight chitosan (DDA ≥ 90%, 1000–2000 cp). Potassium chloride (99.5%) was obtained from Fisher Scientific. Lithium chloride (98%) was obtained from TCI. Amberlite IRN-78 ion exchange resin from Alfa Aesar.

Cellulose and chitosan were dried in an oven at 80°C overnight before use. Another chemical, except tetraralkyl-onium hydroxide, were used without further treatment.

II. Preparation method

a. Preparation of onium hydroxide at different concentrations

Six types of onium hydroxides were condensed to different concentrations using the rotary evaporation method at 30mbar and 40°C. Karl Fischer's Titration confirms the water concentration of the onium hydroxide solution, with an error of ±1 wt.%.

b. Screening and quantifying cellulose dissolution in onium hydroxide

MCC was used as the target material to screen the cellulose dissolution ability of OHS at different onium concentrations. First, 5 mg of dried MCC was placed in a 5 mL vial, and 1 mL of onium hydroxide solution was added. The mixture was then stirred at 200 rpm at room temperature. Each solution type was tested for up to 24 hours. If, after this period, the MCC powder settled at the bottom of the vial, it was considered unable to dissolve cellulose. Conversely, if the mixture became transparent and homogeneous, the

vials were used for the quantification process to estimate the maximum cellulose dissolution.

For quantification, MCC was added to the vial to achieve a concentration of 10 mg/mL. If the mixture became transparent, more MCC was added in increments of 10 mg. After 24 h, if the mixture remained blurry or highly viscous, the procedure was terminated. Consequently, the dissolution limit was estimated.

Screening and quantification methods were employed to evaluate the effect of swelling in DMSO on the dissolution process. First, 1 mg of MCC was swollen in 2 mL of DMSO with stirring at 200 rpm for 1h. Then, 0.2 mL of each type of OHS (achieving a 5 mg/mL ratio between MCC and OHS) was added to the vial and stirred at the same speed for up to 24 hours. If the mixture becomes homogeneous, the OHS can be used to estimate the dissolution limit. Different amounts of MCC were swollen in DMSO, with the initial amount recorded before 0.2 mL of OHS was added. The dissolution limit was determined by the ratio between 0.2 mL of OHS and the highest solubilised MCC, at which the cellulose solution was transparent, homogeneous, and without gelation.

c. Screening and quantifying chitosan dissolution in onium hydroxide

The chitosan screening and quantification processes are similar to those of cellulose. LWC-CS was used as the solubilised material, and the experiment was conducted at room temperature for up to 7 days. The most effective OHS was used to examine the effect of chitosan molecular weight on its dissolution capacity. Medium- and high-molecular-weight chitosan (MMW-CS and HMW-CS) were used to assess this effect.

The influence of temperature was also investigated. The mixture was heated up to a maximum of 70°C, increasing in 10°C steps (starting from 40°C), and maintained at each temperature for up to 4 hours. The vials were placed in an oil bath and heated to the appropriate temperature. The chitosan dissolution capacity at each temperature was evaluated by observing the homogeneity of the solution, using a methodology similar to that employed for cellulose. If the mixture became excessively viscous, rendering the stirrer immobile, the process continued at the subsequent evaluation temperature. The

dissolution time was also recorded to illustrate the effect of temperature on this process. Three concentration ratios were used for this assessment: 5, 50, and 100 mg/mL.

d. Preparation of regenerated cellulose film

KC (200 mg) is swollen with DMSO (9 ml) under vigorous stirring for at least two hours. Before use, $[N_{4,4,4,4}]OH$ (40 wt.%) was heated in a 40°C water bath for 20 minutes. To dissolve, 1 mL of $[N_{4,4,4,4}]OH$ (40 wt.%) was added to the swollen Kraft cellulose and stirred at room temperature for 2 hours, ensuring the cellulose dissolved completely. The resulting cellulose solution was then cast onto a glass plate. Different solution thicknesses could be selected before casting by adjusting the casting blade. The highest quality cellulose film was achieved using an automatic casting machine at a casting speed of 5 mm/s. The glass plate was then immersed in a PC bath. The cellulose solution gelled rapidly after a few minutes. The gel was washed at least four times with water to remove residual chemicals. Finally, the cellulose gel was air-dried to produce a regenerated cellulose film.

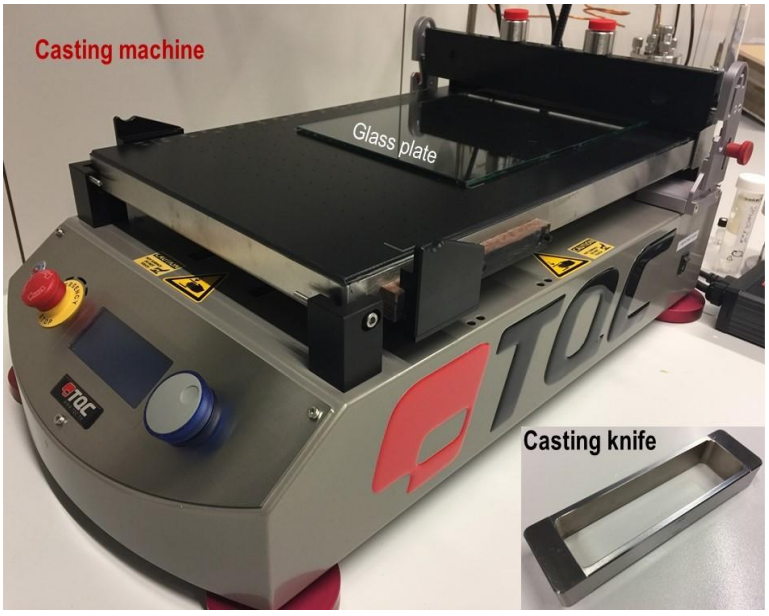

Figure 79. Casting machine and casting knife

e. Preparation of plasticising regenerated cellulose film

The regenerated Kraft cellulose film was produced following the procedure outlined in Section d without drying. Subsequently, the wet films were immersed in plasticised solutions at different concentrations overnight. KCl, Gly, and PEG (1g each) were dispersed in distilled water (100mL) to achieve a 1 w/v% concentration, while various

amounts of LiCl (0.25 g, 0.5 g, 1 g, and 2 g) were prepared. After immersion, the films were removed from the solution and air-dried. Once dried, the films were named RKC-K1, RKC-Li1, RKC-Gly1, and RKC-PEG1 based on the KCl, LiCl, Gly, and PEG solutions, respectively, in which they were immersed. RKC-Li films include four samples: RKC-Li0.25, RKC-Li0.5, RKC-Li1, and RKC-Li2, corresponding to LiCl plasticisation.

f. Recovery and regeneration of onium hydroxide solution

To recover the onium hydroxide after dissolving chitosan, the chitosan solution was added to ethanol to ensure complete solidification. The entire mixture was then centrifuged at 2000 rpm for 5 min. The supernatant and pellet were collected. The pellet was washed with ethanol at least three more times to eliminate all onium hydroxides. The mixture was centrifuged again to collect the supernatant. The supernatant was filtered again using a syringe filter (0.25μm) to remove undissolved particles. Finally, rotary evaporation was used to remove all the ethanol. The collected solvent was then used for further analysis, such as NMR. At the same time, the obtained regenerated chitosan was centrifuged and dried in the oven at 80°C overnight. The recovery of chitosan was calculated as follows:

$$Recovery\ CS\ yield = \frac{m_{regnerated\ chitosan}(g)}{m_{initial\ chitosan}(g)} \times 100\% \qquad (1)$$

To regenerate the onium hydroxide solution, the ionic exchange column was repaired following the setup illustrated by Dinh et al.[81]. First, 30 g of Amberline IRN-78 (hydroxide form) was washed three times with Millipore water to remove impurities and then loaded into a column with a 2 cm inner diameter and a bed volume of approximately 100 ml. Next, the recovery onium, such as $[N_{4,4,4,4}]OH$, was diluted with Millipore water before being loaded into the column. The flow rate was maintained at 2-3 drops per second to initiate the ionic exchange reaction. Millipore water was then added to the column to elute the sample at the same drop rate. Three times the bed volume was used to ensure that the onium hydroxide was eluted from the column. A rotary evaporator was then used to remove most of the water. Karl-Fisher titration was used to confirm the concentration of the onium after the regeneration process.

The recovery yield of the onium hydroxide was calculated using the following equation:

$$Recovery\ OHS\ yield = \frac{m_{regnerated\ OHS}(g)}{m_{initial\ OHS}(g)} \times 100\% \qquad (2)$$

g. Preparation of regenerated chitosan film

LMW-CS was used to produce regenerated chitosan films. $[N_{4,4,4,4}]OH$ 60 wt.% used to dissolve chitosan. The LMW-CS was dried overnight in an oven before use. To prepare the solution, 100 mg of LMW-CS powder is thoroughly mixed with 1 mL of [N4,4,4,4]OH (60 wt.%) at 50°C for at least 4 hours, ensuring complete dissolution and yielding a 100 mg/mL chitosan solution. The regenerated chitosan film was then created through casting, following a process similar to that for the regenerated cellulose film (section). The chitosan solution was cast onto a glass plate with a thickness of 750 µm, and then quickly immersed in the PC bath and left to solidify completely. The resulting chitosan gel was washed at least four times with ethanol to eliminate any remaining unreacted agents. The regenerated chitosan film was obtained after drying in air or by keeping it in ethanol for other purposes.

h. Preparation of regenerated cellulose/chitosan film

KC and LMW-CS were used as the initial materials to prepare the regenerated Kraft cellulose/chitosan film. Cellulose and chitosan were prepared separately before being combined. The cellulose solution was prepared similarly to the method described in the section d , except that a 60 wt. % solution replaced 40 wt.% of $[N_{4,4,4,4}]OH$.

The weight of each component was measured before dissolution based on the cellulose-to-chitosan ratios. Three cellulose/chitosan ratios were used to produce the regenerated films: 90:10, 75:25, and 50:50. The chitosan solution was prepared (described in g), achieving a concentration of 100 mg/mL. The 100 mg/mL chitosan solution was then diluted with DMSO (V_{DMSO} = $4V[N_{4,4,4,4}]OH$) to obtain a 2 w/v% solution. Subsequently, cellulose and chitosan solutions were mixed at room temperature for 1 hour. The 2w/v% cellulose/chitosan solutions (with various cellulose-to-chitosan ratios were obtained by combining the components in different proportions. The solutions

were cast using the same method with a 500 μm casting blade. After solidification in PC, the films were carefully washed with water to remove any residual chemicals. Finally, the films were obtained by air-drying.

III. Characterisation method

a. Fourier Transform Infrared Spectroscopy (FT-IR)

To analyse the chemical structure of the material samples, FT-IR spectra were recorded in the transmittance range of 4000 cm^{-1} to 400 cm^{-1}. A Bruker FT-IR spectrometer was used to measure the samples directly in the ATR mode.

b. Inductively Coupled Plasma Optical Emission (ICP-OES)

ICP-OES is a well-known technique for determining the elemental composition of samples. Powder or small film samples were analysed using a Varian 715-ES ICP-Emission Spectrometer. Each sample was measured twice.

c. CHNS elemental analysis

CHNS was used to quantify the percentages of carbon (C), hydrogen (H), nitrogen (N), and sulphur (S) in the samples. The powder samples were analysed using a Vario Microcube (Firma Elementar). Each sample was measured twice.

d. Nuclear Magnetic Resonance (NMR)

NMR was used to analyse the structure of tetraalkyl onium hydroxide, cellulose, and chitosan. For OHS, the samples were diluted with DMSO-d_6, D_2O, or acetonitrile-d_3. The ^{1}H and ^{13}C NMR were measured at 400MHz by Jeol ECZL 400 (at 25°C)

For the cellulose sample, MCC was swollen in DMSO-d_6 for at least 2 hours at room temperature before OHS was added. To prepare the chitosan sample, LMW-CS was dissolved in OHS at 50°C for 4 h to ensure complete dissolution. Then, acetonitrile-d3 was added with $V_{acetonitril\text{-}d3}=V_{OHS}$. All NMR spectra were analysed using Jeol Jason 5.0.

e. Scanning Electron Microscopy (SEM)

For the thin film measurement preparation, the sample was immersed in liquid nitrogen to freeze. The film broke immediately after it was still frozen when it was removed from

the liquid nitrogen. The specimens were then mounted on SEM stubs using carbon tape and coated with thin gold layers (5 nm) using a Quorum Q150T S Plus sputter coater. A JEOL JMC-7000 BENCHTOP SEM was used to analyse the cross-section and surface of the film at an accelerating voltage of 15 kV.

f. Light Microscopy (LM)

The swelling and dissolution of cellulose were observed using light microscopy. The Echo Revolve 2, equipped with an Olympus lens, was used at various magnifications (from 2x to 20x), and the Echo Pro was utilised to record and analyse samples and phenomena.

Figure 80. Echo Revolve 2 light microscopy

g. **X-Ray diffraction (XRD)**

XRD powder patterns were obtained using a Stoe Stadi P transmission diffractometer with a DECTRIS Mythen2 1K detector, employing Ge(111) monochromatized Mo Kα1 (50 kV, 40 mA, 0.7093 Å) or Cu Kα1 (50 kV,40 mA, 1.5406 Å). The samples were ground into a fine powder and placed between two acetate foils before measurement. Peak positions and profiles were fitted with a Pseudo-Voigt function using the HighScore Plus software package (Panalytical). Phase identification was carried out with the PDF-2 database from the International Centre for Diffraction Data (ICDD).

The crystallinity index of cellulose is calculated using the method of Segal et al.[147], as indicated in the equation:

$$CrI = \frac{I_{002} - I_{am}}{I_{002}} \times 100(\%) \quad (3)$$

CrI is the relative degree of crystallinity (%), I_{002} is the maximum intensity of crystallinity at the (002) diffraction peak of cellulose, while Iam is the intensity of the amorphous region between (002) and (101)

The crystallinity index of chitosan is calculated using the method of Forcher et al. [190], as indicated in the equation:

$$CrI = \frac{I_{200} - I_{am}}{I_{200}} \times 100(\%) \quad (4)$$

I_{200} is the maximum intensity of crystallinity at the (200) diffraction peak of chitosan, while Iam is the intensity of the amorphous region between (200) and (010)

h. Water Vapour Transmission Rate (WVTR)

The wet cup method, described by ASTM E96/E96M-10 with minor adjustments, was used to examine the WVTR of the films. The cup used for the measurement is shown in Figure 81 was 3D printed, which used Dropass's design.[209] Distilled water was added to the cup to create a 2 cm gap between the water level and the surface of the samples. The film was then placed between the cup and gasket and sealed with a screw lid. The cup mount area is 0.002 m^2. A saturated sodium chloride solution bath was used to establish the proper humidity of 73 ± 5% in the desiccator box. The temperature was maintained at 23 ± 2°C during measurement. The cup was placed in the desiccator and weighed every 24 hours for 6 days. Three samples of each film type were used for the measurements.

The WVTR was calculated using the following equation:

$$WVTR = G/tA = (G/t)/A \quad (5)$$

Where:

WVTR = water vapour transmission rate, g m^{-2} h^{-1}

G = mass loss over the measurement period (g)

t = time (h)

A = cup mouth area (m^2)

G/t = slope of the straight line

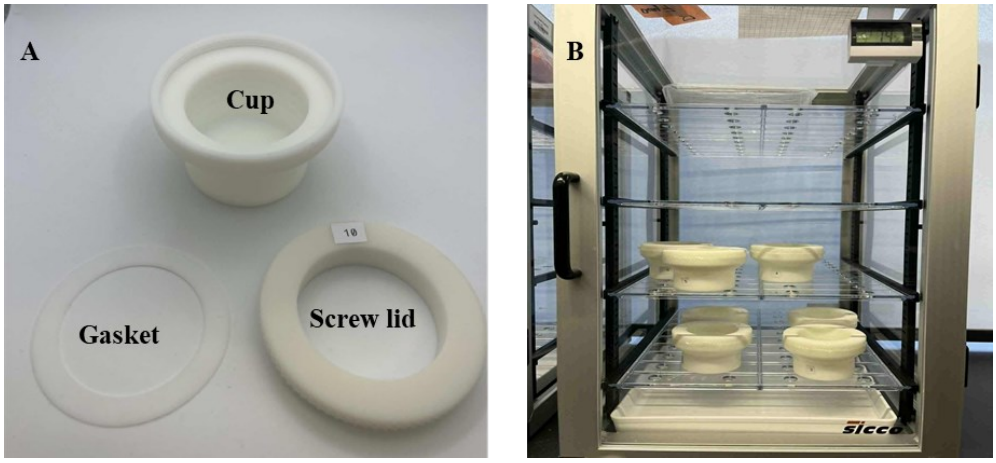

Figure 81. ASTM E96 wet cup set up. A) Test cup, B) Desiccator box

i. Thickness

Five points in different locations of the films were measured to determine their thickness.

j. Transparency

The transparency of the film samples was assessed using an Ocean Insight-USB650 Miniature spectrometer. Measurements were taken at five different points on each sample to evaluate transparency.

k. Tensile strength measurement

The tensile strength was measured at 23°C using Universal testing machine for uniaxial tensile tests, "Zwicki ZN 1.0" (ZwickRoell Gmbh, Ulm, Germany), following the tensile configuration according to DIN EN ISO 527-2. Each sample was prepared in a dog-bone shape (ISO 527-2 type 1BB). The gauge length was 20mm, and the initial length for strain determination was 10 mm. The test was conducted at a speed of 50 mm/min with a preload of 0.005 N. Each type of film sample was measured five times. The measurement was recorded by testXpert III (ZwickRoell GmbH, Ulm, Germany).

l. Atomic Force Microscopy (AFM)

AFM topographies of the RKC and RKC/RCS50 film were measured using Park Systems XE100. To prevent excessive contact with the sample, the device was operated in a non-contact mode, characterised by small cantilever oscillation amplitudes of a few nanometers and a moderate setpoint, while maintaining a constant dither frequency through amplitude modulation. Multiple locations were examined to ensure the accuracy of the observed morphology.

m. Water contact angle measurement

The water contact angle is a technique used to characterise the wettability of the RKC, RCS, and RKC/RCS blended films. The Drop Shape Analyser-DAS25 (KRUSS) was used for the measurements. The high-resolution camera of DAS25 took pictures, and ADVANCE software was used to measure the angle between the film surface and the water droplet. Three measurements were taken for each side of the film (top and bottom).

n. Soil degradation study

A soil burial experiment was conducted in the laboratory to maintain a stable environment at approximately 23°C. The soil used in the experiment was purchased from a supermarket. The soil was watered and mixed several times to ensure even distribution and was allowed to settle for several days before use in the experiment. All films were placed in plastic frames and labelled before being buried. Afterwards, all the samples were buried inside the soil box, which was 5 cm below the surface. Water was added every two days to maintain the soil moisture. Images were captured at specific time points to document changes in the samples throughout the experiment.

Figure 82. Degradation study in the soil environment. A) the soil box, B) the samples are placed on the soil bed, C) soil buried.

o. Sea water biodegradation study

The seawater biodegradation study was conducted at the Marine Science Centre, Rostock, Germany, from April 2024 to June 2024. All samples were cut to the same size (10 × 15 cm). Each sample was then placed in an individual cylinder basket, as shown in Figure 83, with its tag. All samples were kept approximately 50 cm below the sea surface. The samples were checked weekly to observe morphological changes.

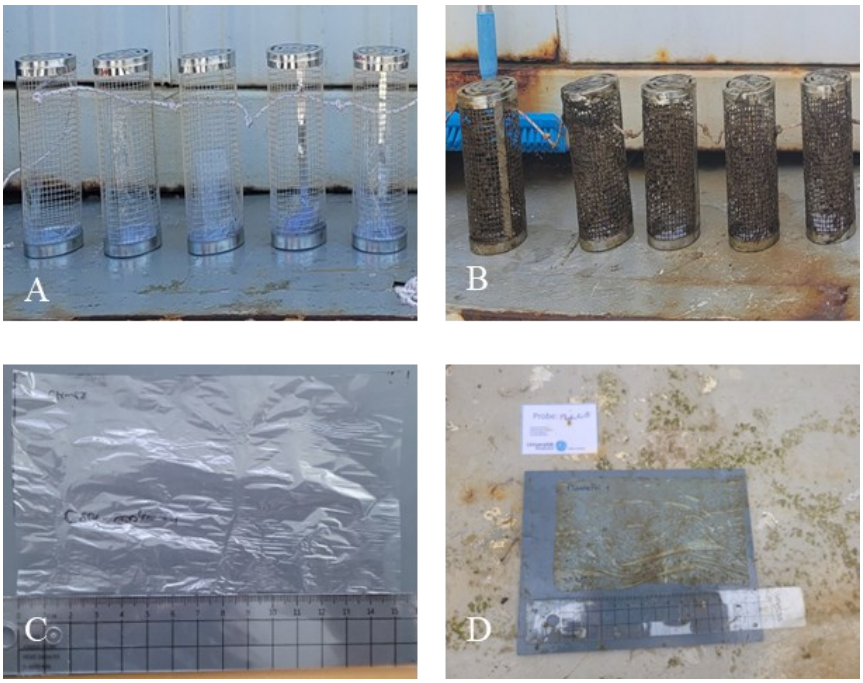

Figure 83. Biodegradation study under Baltic Sea environment: A) cylinder basket before the experiment, B) basket after the experiment, C) prepared sample before the experiment, D) sample observation during the experiment.

IV. References

1. Ncube, A.; Mtetwa, S.; Bukhari, M.; Fiorentino, G.; Passaro, R., Circular Economy and Green Chemistry: The Need for Radical Innovative Approaches in the Design for New Products. *Energies* **2023,** *16* (4), 1752.
2. Perli, G.; Sardon, H.; Vidal, F., Reaction: Is a circular economy for chemicals and materials possible? *Chem* **2024,** *10* (7), 1961-1962.
3. Keijer, T.; Bakker, V.; Slootweg, J. C., Circular chemistry to enable a circular economy. *Nature Chem.* **2019,** *11* (3), 190-195.
4. DESA, U., *The Sustainable Development Goals Report 2024*. New York, USA, 2024.
5. Clark, J. H.; Farmer, T. J.; Herrero-Davila, L.; Sherwood, J., Circular economy design considerations for research and process development in the chemical sciences. *Green Chem.* **2016,** *18* (14), 3914-3934.
6. Anastas, P. T.; Warner, J., Principles of green chemistry. **1998**, 29-56.
7. Sharma, S.; Sharma, V.; Chatterjee, S., Contribution of plastic and microplastic to global climate change and their conjoining impacts on the environment - A review. *Sci. Total. Environ.* **2023,** *875*, 162627.
8. Teixeira, S. C.; Gomes, N. O.; Oliveira, T. V. d.; Fortes-Da-Silva, P.; Soares, N. d. F. F.; Raymundo-Pereira, P. A., Review and Perspectives of sustainable, biodegradable, eco-friendly and flexible electronic devices and (Bio)sensors. *Biosens. Bioelectron. X.* **2023,** *14*, 100371.
9. Li, W. C.; Tse, H. F.; Fok, L., Plastic waste in the marine environment: A review of sources, occurrence and effects. *Sci. Total. Environ.* **2016,** *566-567*, 333-349.
10. Liu, L.; Liang, W.; Zhang, Y.; Fu, Q., Nanoencapsulation in polymeric materials: Weaving magical coats for microorganisms. *Nano Today* **2023,** *52*, 101973.
11. Ibrahim, S.; Riahi, O.; Said, S. M.; Sabri, M. F. M.; Rozali, S., Biopolymers From Crop Plants. In *Reference Module in Materials Science and Materials Engineering*, Elsevier: 2019.
12. Sadasivuni, K. K.; Saha, P.; Adhikari, J.; Deshmukh, K.; Ahamed, B.; Cabibihan, J.-J., Recent advances in mechanical properties of biopolymer composites: a review. *Polym. Compos.* **2019,** *41*, 32-59.
13. Klemm, D.; Heublein, B.; Fink, H.-P.; Bohn, A., Cellulose: Fascinating Biopolymer and Sustainable Raw Material. *Angew. Chem. - Int. Ed.* **2005,** *44* (22), 3358-3393.
14. Seddiqi, H.; Oliaei, E.; Honarkar, H.; Jin, J.; Geonzon, L. C.; Bacabac, R. G.; Klein-Nulend, J., Cellulose and its derivatives: towards biomedical applications. *Cellulose* **2021,** *28* (4), 1893-1931.
15. Zhao, Y.; Moser, C.; Lindström, M. E.; Henriksson, G.; Li, J., Cellulose Nanofibers from Softwood, Hardwood, and Tunicate: Preparation–Structure–Film Performance Interrelation. *ACS Appl. Mater. Interfaces* **2017,** *9* (15), 13508-13519.
16. Rowland, S. P.; Roberts, E. J., The nature of accessible surfaces in the microstructure of cotton cellulose. *J. Polym. Sci. A-1 Polym. Chem.* **1972,** *10* (8), 2447-2461.
17. Lenz, R. W., Cellulose, structure, accessibility and reactivity. *J. Polym. Sci. A Polym. Chem.* **1994,** *32* (12), 2401-2401.

18. Moon, R. J.; Martini, A.; Nairn, J.; Simonsen, J.; Youngblood, J., Cellulose nanomaterials review: structure, properties and nanocomposites. *Chem. Soc. Rev.* **2011,** *40* (7), 3941-3994.
19. Cosgrove, D. J.; Dupree, P.; Gomez, E. D.; Haigler, C. H.; Kubicki, J. D.; Zimmer, J., How Many Glucan Chains Form Plant Cellulose Microfibrils? A Mini Review. *Biomacromolecules* **2024,** *25* (10), 6357-6366.
20. Tai, H.-C.; Chang, C.-H.; Cai, W.; Lin, J.-H.; Huang, S.-J.; Lin, Q.-Y.; Yuan, E. C.-Y.; Li, S.-L.; Lin, Y.-C. J.; Chan, J. C. C.; Tsao, C.-S., Wood cellulose microfibrils have a 24-chain core–shell nanostructure in seed plants. *Nat. Plants* **2023,** *9* (7), 1154-1168.
21. Jonoobi, M.; Oladi, R.; Davoudpour, Y.; Oksman, K.; Dufresne, A.; Hamzeh, Y.; Davoodi, R., Different preparation methods and properties of nanostructured cellulose from various natural resources and residues: a review. *Cellulose* **2015,** *22*.
22. Moigne, N.; Otazaghine, B.; Corn, S.; Angellier-Coussy, H.; Bergeret, A., *Introduction on Natural Fibre Structure: From the Molecular to the Macrostructural Level*. 2018.
23. Reza, M.; Bertinetto, C.; Kesari, K. K.; Engelhardt, P.; Ruokolainen, J.; Vuorinen, T., Cellulose elementary fibril orientation in the spruce S1-2 transition layer. *Sci. Rep.* **2019,** *9* (1), 3869.
24. Dupont, A.-L., Cellulose in lithium chloride/N,N-dimethylacetamide, optimisation of a dissolution method using paper substrates and stability of the solutions. *Polymer* **2003,** *44* (15), 4117-4126.
25. Klemm, D.; Schmauder, H.-P.;Heinze, T., Cellulose. In *Biopolymers Online*, Steinbüchel, A., Ed. 2005.
26. Gupta, P. K.; Uniyal, V.; Naithani, S., Polymorphic transformation of cellulose I to cellulose II by alkali pretreatment and urea as an additive. *Carbohydr. Polym.* **2013,** *94* (2), 843-849.
27. Wada, M.; Nishiyama, Y.; Langan, P., X-ray Structure of Ammonia−Cellulose I: New Insights into the Conversion of Cellulose I to Cellulose III_I. *Macromolecules* **2006,** *39* (8), 2947-2952.
28. Wada, M.; Chanzy, H.; Nishiyama, Y.; Langan, P., Cellulose III_I Crystal Structure and Hydrogen Bonding by Synchrotron X-ray and Neutron Fiber Diffraction. *Macromolecules* **2004,** *37* (23), 8548-8555.
29. Wada, M.; Heux, L.; Sugiyama, J., Polymorphism of Cellulose I Family: Reinvestigation of Cellulose IV_I. *Biomacromolecules* **2004,** *5* (4), 1385-1391.
30. Solhi, L.; Guccini, V.; Heise, K.; Solala, I.; Niinivaara, E.; Xu, W.; Mihhels, K.; Kröger, M.; Meng, Z.; Wohlert, J.; Tao, H.; Cranston, E. D.; Kontturi, E., Understanding Nanocellulose–Water Interactions: Turning a Detriment into an Asset. *Chem. Rev.* **2023,** *123* (5), 1925-2015.
31. Wohlert, M.; Benselfelt, T.; Wågberg, L.; Furó, I.; Berglund, L. A.; Wohlert, J., Cellulose and the role of hydrogen bonds: not in charge of everything. *Cellulose* **2022,** *29* (1), 1-23.
32. Crini, G., Historical review on chitin and chitosan biopolymers. *Environ. Chem. Lett.* **2019,** *17* (4), 1623-1643.

33. Aranaz, I.; Alcántara, A. R.; Civera, M. C.; Arias, C.; Elorza, B.; Heras Caballero, A.; Acosta, N., Chitosan: An Overview of Its Properties and Applications. *Polymers* **2021,** *13* (19), 3256.
34. Knight, B. M.; Edgar, K. J.; De Yoreo, J. J.;Dove, P. M., Chitosan as a Canvas for Studies of Macromolecular Controls on $CaCO_3$ Biological Crystallization. *Biomacromolecules* **2023,** *24* (3), 1078-1102.
35. Krishnan, S.; Chakraborty, K.; Dhara, S., Biomedical potential of β-chitosan from cuttlebone of cephalopods. *Carbohydr. Polym.* **2021,** *273*, 118591.
36. Kameda, T.; Miyazawa, M.; Ono, H.; Yoshida, M., Hydrogen Bonding Structure and Stability of α-Chitin Studied by 13C Solid-State NMR. *Macromol. Biosci.* **2005,** *5* (2), 103-106.
37. Pillai, C. K. S.; Paul, W.; Sharma, C. P., Chitin and chitosan polymers: Chemistry, solubility and fiber formation. *Prog. Polym. Sci.* **2009,** *34* (7), 641-678.
38. Qian, L.; Zhang, K.; Guo, X.; Yu, M., What happens when chitin becomes chitosan? A single-molecule study. *RSC Advances* **2023,** *13* (4), 2294-2300.
39. Ogawa, Y.; Naito, P.-K.; Nishiyama, Y., Hydrogen-bonding network in anhydrous chitosan from neutron crystallography and periodic density functional theory calculations. *Carbohydr. Polym.* **2019,** *207*, 211-217.
40. Mahmoudzadeh, M.; Fassihi, A.; Emami, J.; Davies, N., Physicochemical, pharmaceutical and biological approaches toward designing optimized and efficient hydrophobically modified chitosan-based polymeric micelles as a nanocarrier system for targeted delivery of anticancer drugs. *J. Drug Target.* **2013,** *21*.
41. Alsarra, I. A.; Betigeri, S. S.; Zhang, H.; Evans, B. A.; Neau, S. H., Molecular weight and degree of deacetylation effects on lipase-loaded chitosan bead characteristics. *Biomater.* **2002,** *23* (17), 3637-3644.
42. He, X.; Li, K.; Xing, R.; Liu, S.; Hu, L.; Li, P., The production of fully deacetylated chitosan by compression method. *Egypt. J. Aquat. Res.* **2016,** *42* (1), 75-81.
43. Liu, N.; Chen, X.-G.; Park, H.-J.; Liu, C.-G.; Liu, C.-S.; Meng, X.-H.; Yu, L.-J., Effect of MW and concentration of chitosan on antibacterial activity of Escherichia coli. *Carbohydr. Polym.* **2006,** *64* (1), 60-65.
44. Takahashi, T.; Imai, M.; Suzuki, I.; Sawai, J., Growth inhibitory effect on bacteria of chitosan membranes regulated with deacetylation degree. *Biochem. Eng. J.* **2008,** *40* (3), 485-491.
45. Liu, H.; Wang, C.; Li, C.; Qin, Y.; Wang, Z.; Yang, F.; Li, Z.; Wang, J., A functional chitosan-based hydrogel as a wound dressing and drug delivery system in the treatment of wound healing. *RSC Advances* **2018,** *8* (14), 7533-7549.
46. Padhi, S.; Behera, A.; Hasnain, M. S.; Nayak, A. K., Chapter 6 - Uses of chitosan in drug delivery. In *Chitosan in Biomedical Applications*, Hasnain, M. S.; Beg, S.; Nayak, A. K., Eds. Academic Press: 2022; pp 139-162.
47. Niu, Y.; Hu, W., Preparation, characterization and application in environmental protection of low-molecular-weight chitosan: a review. *Sustain. Environ. Res.* **2024,** *34* (1), 29.
48. De Carli, C.; Aylanc, V.; Mouffok, K. M.; Santamaria-Echart, A.; Barreiro, F.; Tomás, A.; Pereira, C.; Rodrigues, P.; Vilas-Boas, M.; Falcão, S. I., Production of

chitosan-based biodegradable active films using bio-waste enriched with polyphenol propolis extract envisaging food packaging applications. *Int. J. Biol. Macromol.* **2022,** *213*, 486-497.
49. Román-Doval, R.; Torres-Arellanes, S. P.; Tenorio-Barajas, A. Y.; Gómez-Sánchez, A.; Valencia-Lazcano, A. A., Chitosan: Properties and Its Application in Agriculture in Context of Molecular Weight. *Polymers* **2023,** *15* (13).
50. Song, M.-H.; Pham, T. P. T.; Yun, Y.-S., Ionic liquid-assisted cellulose coating of chitosan hydrogel beads and their application as drug carriers. *Sci. Rep.* **2020,** *10* (1), 13905.
51. Fayer, L.; Vasconcellos, R.; Oliveira, E.; Ferreira, C.; Souza, N.; Manhabosco, T.; De Oliveira, L. F.; Martins, M.; Brandao, H.; Munk, M., Cotton cellulose nanofiber/chitosan scaffolds for skin tissue engineering and wound healing applications. *Biomed. Mat.* **2024,** *20*.
52. Qu, T.; Wang, X.; Zhang, F., Antibacterial Food Packaging with Chitosan and Cellulose Blends for Food Preservation. *Polymers* **2025,** *17* (13), 1850.
53. Zhu, K.; Wang, Y.; Lu, A.; Fu, Q.; Hu, J.; Zhang, L., Cellulose/Chitosan Composite Multifilament Fibers with Two-Switch Shape Memory Performance. *ACS Sustain. Chem. Eng.* **2019,** *7* (7), 6981-6990.
54. Liu, X. D.; Nishi, N.; Tokura, S.; Sakairi, N., Chitosan coated cotton fiber: preparation and physical properties. *Carbohydr. Polym.* **2001,** *44* (3), 233-238.
55. Li, M.; Li, X.; Wang, L.; Pei, Y.; An, M.; Liu, J.; Zheng, X.; Tang, K., Highly efficient and selective removal of anionic dyes from water using a cellulose nanofibril/chitosan sponge prepared by dehydrothermal treatment. *J. Environ. Chem. Eng.* **2021,** *9* (5), 105745.
56. Yang, J.; Dahlström, C.; Edlund, H.; Lindman, B.; Norgren, M., pH-responsive cellulose–chitosan nanocomposite films with slow release of chitosan. *Cellulose* **2019,** *26* (6), 3763-3776.
57. Zahra, H.; Sawada, D.; Guizani, C.; Ma, Y.; Kumagai, S.; Yoshioka, T.; Sixta, H.; Hummel, M., Close Packing of Cellulose and Chitosan in Regenerated Cellulose Fibers Improves Carbon Yield and Structural Properties of Respective Carbon Fibers. *Biomacromolecules* **2020,** *21* (10), 4326-4335.
58. Liu, Q.; Yu, H.; Zeng, F.; Li, X.; Sun, J.; Li, C.; Lin, H.;Su, Z., HKUST-1 modified ultrastability cellulose/chitosan composite aerogel for highly efficient removal of methylene blue. *Carbohydr. Polym.* **2021,** *255*, 117402.
59. El Khadem, H. S., Carbohydrates. In *Encyclopedia of Physical Science and Technology (Third Edition)*, Meyers, R. A., Ed. Academic Press: New York, 2003; pp 369-416.
60. Struszczyk, H.; Urbanowski, A., 27 - Some aspects of cellulose carbamate. In *Cellulose and Cellulose Derivatives*, Kennedy, J. F.; Phillips, G. O.; Williams, P. A., Eds. Woodhead Publishing: 1995; pp 207-211.
61. Hytönen, E.; Sorsamäki, L.; Kolehmainen, E.; Sturm, M.; Weymarn, N., Lyocell fibre production using NMMO – A simulation-based techno-economic analysis. *BioResources* **2023,** *18*, 6384-6411.
62. Swatloski, R. P.; Spear, S. K.; Holbrey, J. D.; Rogers, R. D., Dissolution of Cellose with Ionic Liquids. *J. Am. Chem. Soc.* **2002,** *124* (18), 4974-4975.

63. Abe, M.; Fukaya, Y.; Ohno, H., Fast and facile dissolution of cellulose with tetrabutylphosphonium hydroxide containing 40 wt% water. *Chemical Communications* **2012,** *48* (12), 1808-1810.
64. Zhong, C.; Wang, C.; Huang, F.; Jia, H.; Wei, P., Wheat straw cellulose dissolution and isolation by tetra-n-butylammonium hydroxide. *Carbohydr. Polym.* **2013,** *94* (1), 38-45.
65. Westman, G.; Olsson, C., Direct Dissolution of Cellulose: Background, Means and Applications. In *Cellulose - Fundamental Aspects*, Van De Ven, T. G. M.; Godbout, L., Eds. IntechOpen: Rijeka, 2013.
66. Alasalvar, H.; Sürmeli, H. N.; Yildirim, Z., Chitosan films tailored with deep eutectic solvent extracts from Hibiscus sabdariffa: Fabrication and characterization. *J. Mol. Liq.* **2024,** *412*, 125874.
67. Xie, H.; Zhang, S.; Li, S., Chitin and chitosan dissolved in ionic liquids as reversible sorbents of CO2. *Green Chem.* **2006,** *8* (7), 630-633.
68. Tan, X.; Wang, G.; Zhong, L.; Xie, F.; Lan, P.; Chi, B., Regeneration behavior of chitosan from ionic liquid using water and alcohols as anti-solvents. *Int. J. Biol. Macromol.* **2021,** *166*, 940-947.
69. Sikorski, D.; Gzyra-Jagieła, K.;Draczyński, Z., The Kinetics of Chitosan Degradation in Organic Acid Solutions. *Mar. Drugs* **2021,** *19* (5), 236.
70. Rinaudo, M.; Pavlov, G.;Desbrières, J., Influence of acetic acid concentration on the solubilization of chitosan. *Polymer* **1999,** *40* (25), 7029-7032.
71. Zhang, W.; Xia, W., Dissolution and stability of chitosan in a sodium hydroxide/urea aqueous solution. *J. Appl. Polym. Sci.* **2014,** *131* (3).
72. Fan, M.; Hu, Q., Chitosan-LiOH-urea aqueous solution—a novel water-based system for chitosan processing. *Carbohydr. Res.* **2009,** *344* (7), 944-947.
73. Kim, U.-J.; Kimura, S.; Wada, M., Characterization of cellulose–chitosan gels prepared using a LiOH/urea aqueous solution. *Cellulose* **2019,** *26* (10), 6189-6199.
74. Mok, S. Y.; Sivapragasam, M.; Raja Shahrom, M. S.; Bustam @ Khalil, M. A.; Abidin, Z. Z., Screening of ionic liquids for the dissolution of chitosan using COSMO-RS. *Green Chem.* **2024,** *26* (3), 1577-1586.
75. Sun, X.; Tian, Q.; Xue, Z.; Zhang, Y.; Mu, T., The dissolution behaviour of chitosan in acetate-based ionic liquids and their interactions: from experimental evidence to density functional theory analysis. *RSC Advances* **2014,** *4* (57), 30282-30291.
76. Strepikheev, A. A.; Knunyants, I. L.; Nikolaeva, N. S.; Mogilevsky, E. M., The solubility of cellulose in quaternary ammonium bases. *Bull. Acad. Sci. USSR, Div. Chem. Sci.* **1957,** *6* (6), 769-771.
77. Ema, T.; Komiyama, T.; Sunami, S.; Sakai, T., Synergistic effect of quaternary ammonium hydroxide and crown ether on the rapid and clear dissolution of cellulose at room temperature. *RSC Advances* **2014,** *4* (5), 2523-2525.
78. Nguyen, M. N.; Kragl, U.; Barke, I.; Lange, R.; Lund, H.; Frank, M.; Springer, A.; Aladin, V.; Corzilius, B.; Hollmann, D., Coagulation using organic carbonates opens up a sustainable route towards regenerated cellulose films. *Commun. Chem.* **2020,** *3* (1), 116.

79. Shimo, M.; Abe, M.; Ohno, H., Functional Comparison of Polar Ionic Liquids and Onium Hydroxides for Chitin Dissolution and Deacetylation to Chitosan. *ACS Sustain. Chem. Eng.* **2016,** *4* (7), 3722-3727.
80. Ma, Q.; Gao, X.; Bi, X.; Han, Q.; Tu, L.; Yang, Y.; Shen, Y.; Wang, M., Dissolution and deacetylation of chitin in ionic liquid tetrabutylammonium hydroxide and its cascade reaction in enzyme treatment for chitin recycling. *Carbohydr. Polym.* **2020,** *230*, 115605.
81. Dinh, V. M.; Khokarale, S. G.; May, P. O.; Sparrman, T.; Irgum, K.; Mikkola, J.-P., Ionic liquid strategy for chitosan production from chitin and molecular insights. *RSC Sustain.* **2024,** *2* (4), 1154-1164.
82. Abe, M.; Kuroda, K.; Ohno, H., Maintenance-Free Cellulose Solvents Based on Onium Hydroxides. *ACS Sustain. Chem. Eng.* **2015,** *3* (8), 1771-1776.
83. Abe, M.; Yamanaka, S.; Yamada, H.; Yamada, T.; Ohno, H., Almost complete dissolution of woody biomass with tetra-n-butylphosphonium hydroxide aqueous solution at 60 °C. *Green Chem.* **2015,** *17* (8), 4432-4438.
84. Abe, M.; Fukaya, Y.; Ohno, H., Fast and facile dissolution of cellulose with tetrabutylphosphonium hydroxide containing 40 wt% water. *ChemComm* **2012,** *48* (12), 1808-1810.
85. Tasnim, S.; Tipu, M. F. K.; Rana, M. S.; Rahim, M. A.; Haque, M.; Amran, M. S.; Chowdhury, A. A.; Chowdhury, J. A., Modification of Bulk Density, Flow Property and Crystallinity of Microcrystalline Cellulose Prepared from Waste Cotton. *Materials (Basel, Switzerland)* **2023,** *16* (16).
86. Nguyen, M. N.; Kragl, U.; Michalik, D.; Ludwig, R.;Hollmann, D., The Effect of Additives on the Viscosity and Dissolution of Cellulose in Tetrabutylphosphonium Hydroxide. *ChemSusChem* **2019,** *12* (15), 3458-3462.
87. Wei, W.; Meng, F.; Cui, Y.; Jiang, M.; Zhou, Z., Room temperature dissolution of cellulose in tetra-butylammonium hydroxide aqueous solvent through adjustment of solvent amphiphilicity. *Cellulose* **2017,** *24* (1), 49-59.
88. Swensson, B.; Larsson, A.; Hasani, M., Dissolution of cellulose using a combination of hydroxide bases in aqueous solution. *Cellulose* **2020,** *27* (1), 101-112.
89. Kushwaha, P.; Prabhu, N. P., Imidazolium-based ionic liquids with increasing alkyl chain length of cations decrease the stability and fibrillation propensity of lysozyme. *New J. Chem.* **2022,** *46* (23), 11082-11094.
90. Abe, M.; Kuroda, K.; Sato, D.; Kunimura, H.; Ohno, H., Effects of polarity, hydrophobicity, and density of ionic liquids on cellulose solubility. *Phys. Chem. Chem. Phys.* **2015,** *17* (48), 32276-32282.
91. Yang, L.; Yang, X.; Wang, T.; Jiang, G.; Luckham, P. F.; Li, X.; Shi, H.; Luo, J., Effect of Alkyl Chain Length on Shale Hydration Inhibitive Performance of Vinylimidazolium-Based Ionic Liquids. *Ind. Eng. Chem. Res.* **2019,** *58* (20), 8565-8577.
92. Naserifar, S.; Koschella, A.; Heinze, T.; Bernin, D.; Hasani, M., Investigation of cellulose dissolution in morpholinium-based solvents: impact of solvent structural features on cellulose dissolution. *RSC Advances* **2023,** *13* (27), 18639-18650.
93. Zhao, Y.; Liu, X.; Wang, J.; Zhang, S., Effects of Cationic Structure on Cellulose Dissolution in Ionic Liquids: A Molecular Dynamics Study. *ChemPhysChem* **2012,** *13* (13), 3126-3133.

94. Lu, B.; Xu, A.; Wang, J., Cation does matter: how cationic structure affects the dissolution of cellulose in ionic liquids. *Green Chem.* **2014,** *16* (3), 1326-1335.
95. Satria, H.; Kuroda, K.; Tsuge, Y.; Ninomiya, K.; Takahashi, K., Dimethyl sulfoxide enhances both the cellulose dissolution ability and biocompatibility of a carboxylate-type liquid zwitterion. *New J. Chem.* **2018,** *42* (16), 13225-13228.
96. Ren, F.; Wang, J.; Yu, J.; Zhong, C.; Xie, F.; Wang, S., Dissolution of Cellulose in Ionic Liquid–DMSO Mixtures: Roles of DMSO/IL Ratio and the Cation Alkyl Chain Length. *ACS Omega* **2021,** *6* (41), 27225-27232.
97. Dignani, M. T.; Bioni, T. A.; Paixão, T. R. L. C.; El Seoud, O. A., Cellulose Dissolution in Mixtures of Ionic Liquids and Dimethyl Sulfoxide: A Quantitative Assessment of the Relative Importance of Temperature and Composition of the Binary Solvent. *Molecules* **2020,** *25* (24), 5975.
98. Xu, A.; Zhang, Y.; Zhao, Y.; Wang, J., Cellulose dissolution at ambient temperature: Role of preferential solvation of cations of ionic liquids by a cosolvent. *Carbohydr. Polym.* **2013,** *92* (1), 540-544.
99. Ferreira, D. C.; Oliveira, M. L.; Bioni, T. A.; Nawaz, H.; King, A. W. T.; Kilpeläinen, I.; Hummel, M.; Sixta, H.; El Seoud, O. A., Binary mixtures of ionic liquids-DMSO as solvents for the dissolution and derivatization of cellulose: Effects of alkyl and alkoxy side chains. *Carbohydr. Polym.* **2019,** *212*, 206-214.
100. Chen, X.; Chen, X.; Cai, X.-M.; Huang, S.; Wang, F., Cellulose Dissolution in a Mixed Solvent of Tetra(n-butyl)ammonium Hydroxide/Dimethyl Sulfoxide via Radical Reactions. *ACS Appl. Mater. Interfaces* **2018,** *6* (3), 2898-2904.
101. Medronho, B.; Duarte, H.; Magalhães, S.; Alves, L.; Valente, A. J. M.; Romano, A., From a new cellulose solvent to the cyclodextrin induced formation of hydrogels. *Colloids Surf. A: Physicochem. Eng. Asp.* **2017,** *532*, 548-555.
102. Kuzmina, O.; Jankowski, S.; Fabianska, A.; Sashina, E.; Wawro, D., Preswelling of cellulose pulp for dissolution in ionic liquid. *Cellul. Chem. Technol.* **2014,** *48*, 45-51.
103. Qi, H.; Yang, Q.; Na, N.; Liebert, T.; Heinze, T., The dissolution of cellulose in NaOH-based aqueous system by two-step process. *Cellulose* **2011,** *18*, 237-245.
104. De Wever, P.; Janssens, J.; Fardim, P., Fabrication of cellulose cryogel beads via room temperature dissolution in onium hydroxides. *Carbohydr. Polym. Tech. App.* **2022,** *3*, 100206.
105. Kohno, Y.; Ohno, H., Ionic liquid/water mixtures: from hostility to conciliation. *Chem. Commun.* **2012,** *48* (57), 7119-7130.
106. Saita, S.; Kohno, Y.; Ohno, H., Detection of small differences in the hydrophilicity of ions using the LCST-type phase transition of an ionic liquid–water mixture. *ChemComm* **2013,** *49* (1), 93-95.
107. Oki, A.; Tokunaga, Y.; Nonaka, H.; Yamazaki, A.; Iwata, I., Solubility of Cellulose in tetrabutylammonium acetate/dimethylsulfoxide（TBAA/DMSO）Mixed Solvents: ―Effect of Water Content on Cellulose Dissolution at Different TBAA/DMSO Mixing Ratios. *JAPAN TAPPI JOURNAL* **2025,** *79* (3), 256-263.
108. Korhonen, O.; Budtova, T., Gelation of cellulose-NaOH solutions in the presence of cellulose fibers. *Carbohydr. Polym.* **2019,** *224*, 115152.
109. Budtova, T.; Navard, P., Cellulose in NaOH–water based solvents: a review. *Cellulose* **2016,** *23* (1), 5-55.

110. Li, W.; Tan, L.; Fan, Q.; Wei, W.; Zhou, Z., Effect of storage time and temperature on dissolved state of cellulose in TBAH-based solvents and mechanical property of regenerated films. *Rev. Adv. Mater. Sci.* **2021,** *60* (1), 466-478.
111. Lue, A.; Zhang, L., Investigation of the Scaling Law on Cellulose Solution Prepared at Low Temperature. *J. Phys. Chem. B* **2008,** *112* (15), 4488-4495.
112. Moulthrop, J. S.; Swatloski, R. P.; Moyna, G.; Rogers, R. D., High-resolution 13C NMR studies of cellulose and cellulose oligomers in ionic liquid solutions. *Chem. Commun.* **2005,** (12), 1557-1559.
113. Heinze, T.; Liebert, T., 10.05 - Celluloses and Polyoses/Hemicelluloses. In *Polymer Science: A Comprehensive Reference*, Matyjaszewski, K.; Möller, M., Eds. Elsevier: Amsterdam, **2012**; pp 83-152.
114. Kono, H.; Yunoki, S.; Shikano, T.; Fujiwara, M.; Erata, T.; Takai, M., CP/MAS 13C NMR Study of Cellulose and Cellulose Derivatives. 1. Complete Assignment of the CP/MAS 13C NMR Spectrum of the Native Cellulose. *J. Am. Chem. Soc.* **2002,** *124* (25), 7506-7511.
115. Fliri, L.; Heise, K.; Koso, T.; Todorov, A. R.; del Cerro, D. R.; Hietala, S.; Fiskari, J.; Kilpeläinen, I.; Hummel, M.; King, A. W. T., Solution-state nuclear magnetic resonance spectroscopy of crystalline cellulosic materials using a direct dissolution ionic liquid electrolyte. *Nat. Protoc.* **2023,** *18* (7), 2084-2123.
116. Zhong, C.; Cheng, F.; Zhu, Y.; Gao, Z.; Jia, H.; Wei, P., Dissolution mechanism of cellulose in quaternary ammonium hydroxide: Revisiting through molecular interactions. *Carbohydrate Polymers* **2017,** *174*, 400-408.
117. Zheng, Z.; Jin, Z.; Chen, L.; Chen, M.; Liu, J.; Yu, H.; Meng, Q.; Xie, P.;Xu, R., A comparative study of the ageing phenomena in Kraft paper and pressboard used in 500 kV class transformer. *Annu. Rep. - Conf. Electr. Insul.* **2011**, 620-623.
118. Tonoli, G. H. D.; Teixeira, E. M.; Corrêa, A. C.; Marconcini, J. M.; Caixeta, L. A.; Pereira-da-Silva, M. A.; Mattoso, L. H. C., Cellulose micro/nanofibres from Eucalyptus kraft pulp: Preparation and properties. *Carbohydr. Polym.* **2012,** *89* (1), 80-88.
119. Chakraborty, A.; Sain, M.; Kortschot, M., Reinforcing potential of wood pulp-derived microfibres in a PVA matrix. *Holzforschung* **2006,** *60*, 53-58.
120. Koskela, S.; Zha, L.; Wang, S.; Yan, M.; Zhou, Q., Hemicellulose content affects the properties of cellulose nanofibrils produced from softwood pulp fibres by LPMO. *Green Chem.* **2022,** *24* (18), 7137-7147.
121. Röder, T.; Morgenstern, B.; Schelosky, N.; Glatter, O., Solutions of cellulose in N,N-dimethylacetamide/lithium chloride studied by light scattering methods. *Polymer* **2001,** *42* (16), 6765-6773.
122. Zhao, X.; Liu, M.; Zhang, H.; Zhang, L.; Lu, J., Study on the dissolution behavior of different celluloses in quaternary ammonium base/imidazole compound solvent system. *Carbohydr. Res.* **2025,** *553*, 109498.
123. Ma, Y.; You, X.; Nieminen, K.; Sawada, D.; Sixta, H., Influence of DP and MMD of the pulps used in the Ioncell® process on processability and fiber properties. *RSC Sustain.* **2023,** *1* (6), 1497-1510.

124. Kihlman, M.; Aldaeus, F.; Chedid, F.; Germgård, U., Effect of various pulp properties on the solubility of cellulose in sodium hydroxide solutions. *Holzforschung* **2012,** *66* (5), 601-606.
125. Chen, M.; Ren, M.; Zhu, M.; Zhang, H.; Chen, T.; Zhang, Y.; Yang, S., Effect of degree of polymerization on regenerated cellulose ultrafiltration membrane performance through $ZnCl_2/AlCl_3$ aqueous solvent system. *Carbohydr. Polym.* **2024,** *345*, 122557.
126. Ghasemi, M.; Alexandridis, P.; Tsianou, M., Dissolution of Cellulosic Fibers: Impact of Crystallinity and Fiber Diameter. *Biomacromolecules* **2018,** *19*.
127. Qian, X.; Guo, Y.; Zhao, Y.; Hou, L.; Cheng, Y.; Chen, L.; Yang, S.; Zhang, H., Quantitative evaluation of cellulose swelling and dissolution behavior by monitoring the retention of NMMO solvent in cellulose fiber structure. *Int. J. Biol. Macromol.* **2025,** *315*, 144624.
128. Fidale, L. C.; Ruiz, N.; Heinze, T.; Seoud, O. A. E., Cellulose Swelling by Aprotic and Protic Solvents: What are the Similarities and Differences? *Macromol. Chem. Phys.* **2008,** *209* (12), 1240-1254.
129. Navard, P.; Cuissinat, C. *Cellulose swelling and dissolution as a tool to study the fiber structure*; 09/06, 2006.
130. Ren, H.; Xu, Z.; Gao, M.; Xing, X.; Ling, Z.; Pan, L.; Tian, Y.; Zheng, Y.; Fan, W.; Yang, W., Preparation of microcrystalline cellulose from agricultural residues and their application as polylactic acid/microcrystalline cellulose composite films for the preservation of Lanzhou lily. *Int. J. Biol. Macromol.* **2023,** *227*, 827-838.
131. Zhang, L.; Huang, C.; Zhang, C.; Pan, H., Swelling and dissolution of cellulose in binary systems of three ionic liquids and three co-solvents. *Cellulose* **2021,** *28* (8), 4643-4653.
132. Cuissinat, C.; Navard, P., Swelling and dissolution of cellulose, Part III: plant fibres in aqueous systems. *Cellulose* **2008,** *15* (1), 67-74.
133. Zhang, S.; Wang, W. C.; Li, F. X.; Yu, J. Y., Swelling and dissolution of cellulose in NaOH aqueous solvent systems. *Cellul. Chem. Technol.* **2013,** *47*, 671-679.
134. Trache, D.; Hussin, M. H.; Hui Chuin, C. T.; Sabar, S.; Fazita, M. R. N.; Taiwo, O. F. A.; Hassan, T. M.; Haafiz, M. K. M., Microcrystalline cellulose: Isolation, characterization and bio-composites application—A review. *Int. J. Biol. Macromol.* **2016,** *93*, 789-804.
135. Cuissinat, C.; Navard, P., Swelling and Dissolution of Cellulose Part II: Free Floating Cotton and Wood Fibres in NaOH–Water–Additives Systems. *Macromol. Symp* **2006,** *244* (1), 19-30.
136. Medronho, B.; Lindman, B., Competing forces during cellulose dissolution: From solvents to mechanisms. *Curr. Opin. Colloid Interface Sci.* **2014,** *19* (1), 32-40.
137. Peng, H.; Dai, G.; Wang, S.;Xu, H., The evolution behavior and dissolution mechanism of cellulose in aqueous solvent. *J. Mol. Liq.* **2017,** *241*, 959-966.
138. Navard, P.; Cuissinat, C., Cellulose swelling and dissolution as a tool to study the fiber structure. *Alternative Cellulose : Manufacturing, Forming, Properties* **2006**.
139. Antunes, F.; Medronho, B.; Singh, P.; Duarte, H.; Le Moigne, N.; Dormanns, J.; Duchemin, B.; Staiger, M.; Alves, L., From Cellulose Dissolution and Regeneration to Added Value Applications — Synergism Between Molecular Understanding and

Material Development. In *Cellulose - Fundamental Aspects and Current Trends*, Poletto, M., Ed. IntechOpen: Rijeka, 2015.
140. De Assis, T.; Pawlak, J.; Pal, L.; Venditti, R.; Reisinger, L.; Kavalew, D.; Gonzalez, R., Comparison of Wood and Non-Wood Market Pulps for Tissue Paper Application. *Bioresources* **2019,** *14*, 6781-6810.
141. Pang, J.-H.; Liu, X.; Wu, M.; Wu, Y.-Y.; Zhang, X.-M.; Sun, R.-C., Fabrication and Characterization of Regenerated Cellulose Films Using Different Ionic Liquids. *J. spectrosc.* **2014,** *2014* (1), 214057.
142. French, A. D., Idealized powder diffraction patterns for cellulose polymorphs. *Cellulose* **2014,** *21* (2), 885-896.
143. SriBala, G.; Chennuru, R.; Mahapatra, S.; Vinu, R., Effect of alkaline ultrasonic pretreatment on crystalline morphology and enzymatic hydrolysis of cellulose. *Cellulose* **2016,** *23* (3), 1725-1740.
144. Park, S.; Baker, J. O.; Himmel, M. E.; Parilla, P. A.; Johnson, D. K., Cellulose crystallinity index: measurement techniques and their impact on interpreting cellulase performance. *Biotechnol. Biofuels* **2010,** *3* (1), 10.
145. Lee, C. M.; Mittal, A.; Barnette, A. L.; Kafle, K.; Park, Y. B.; Shin, H.; Johnson, D. K.; Park, S.;Kim, S. H., Cellulose polymorphism study with sum-frequency-generation (SFG) vibration spectroscopy: identification of exocyclic CH2OH conformation and chain orientation. *Cellulose* **2013,** *20* (3), 991-1000.
146. Costa, C.; Medronho, B.; Eivazi, A.; Svanedal, I.; Lindman, B.; Edlund, H.;Norgren, M., Lignin enhances cellulose dissolution in cold alkali. *Carbohydr. Polym.* **2021,** *274*, 118661.
147. Segal, L.; Creely, J. J.; Martin, A. E.; Conrad, C. M., An Empirical Method for Estimating the Degree of Crystallinity of Native Cellulose Using the X-Ray Diffractometer. *Text. Res. J.* **1959,** *29* (10), 786-794.
148. Huang, D.; Li, D.; Mo, K.; Xu, R.; Huang, Y.; Cui, Y.; Zhang, Q.; Chang, C., Top-down fabrication of biodegradable multilayer tunicate cellulose films with controlled mechanical properties. *Cellulose* **2021,** *28* (16), 10415-10424.
149. Jang, S.-D.; Kim, J.-H.; Cai, Z.; Kim, J., The effect of chitosan concentration on the electrical property of chitosan-blended cellulose electroactive paper. *Smart Mater. Struct.* **2008,** *18*, 015003.
150. Xia, Q.; Chen, C.; Yao, Y.; Li, J.; He, S.; Zhou, Y.; Li, T.; Pan, X.; Yao, Y.;Hu, L., A strong, biodegradable and recyclable lignocellulosic bioplastic. *Nat. Sustain.* **2021,** *4* (7), 627-635.
151. Voznyak, Y.; Morawiec, J.; Galeski, A., Ductility of polylactide composites reinforced with poly(butylene succinate) nanofibers. *Compos. - A: Appl. Sci. Manuf.* **2016,** *90*, 218-224.
152. Rumi, S. S.; Liyanage, S.; Abidi, N., Soil burial-induced degradation of cellulose films in a moisture-controlled environment. *Sci. Rep.* **2024,** *14* (1), 6921.
153. Emadian, S. M.; Onay, T. T.; Demirel, B., Biodegradation of bioplastics in natural environments. *Waste Management* **2017,** *59*, 526-536.
154. Slezak, R.; Krzystek, L.; Puchalski, M.; Krucińska, I.; Sitarski, A., Degradation of bio-based film plastics in soil under natural conditions. *Sci. Total Environ.* **2023,** *866*, 161401.

155. Ratnayake, R.; Jayasekara, S., Microbial Cellulases: An Overview and Applications. In *Cellulose*, Rodríguez, A.; Eugenio Martin, M. E., Eds. IntechOpen: Rijeka, 2019.
156. Briassoulis, D.; Mistriotis, A., Key parameters in testing biodegradation of bio-based materials in soil. *Chemosphere* **2018,** *207*, 18-26.
157. Royer, S.-J.; Greco, F.; Kogler, M.; Deheyn, D. D., Not so biodegradable: Polylactic acid and cellulose/plastic blend textiles lack fast biodegradation in marine waters. *PLOS ONE* **2023,** *18* (5), e0284681.
158. Zambrano, M. C.; Pawlak, J. J.; Daystar, J.; Ankeny, M.; Goller, C. C.; Venditti, R. A., Aerobic biodegradation in freshwater and marine environments of textile microfibers generated in clothes laundering: Effects of cellulose and polyester-based microfibers on the microbiome. *Mar. Pollut. Bull.* **2020,** *151*, 110826.
159. Xiao, C.; Zhang, Z.; Zhang, J.; Lu, Y.; Zhang, L., Properties of regenerated cellulose films plasticized with α-monoglycerides. *J. Appl. Polym. Sci.* **2003,** *89* (13), 3500-3505.
160. Bonifacio, A.; Bonetti, L.; Piantanida, E.; De Nardo, L., Plasticizer design strategies enabling advanced applications of cellulose acetate. *Eur. Polym. J.* **2023,** *197*, 112360.
161. Teixeira, S. C.; Silva, R. R. A.; de Oliveira, T. V.; Stringheta, P. C.; Pinto, M. R. M. R.; Soares, N. d. F. F., Glycerol and triethyl citrate plasticizer effects on molecular, thermal, mechanical, and barrier properties of cellulose acetate films. *Food Biosci.* **2021,** *42*, 101202.
162. Doosti, M.; Abedini, R., Polyethyleneglycol-Modified Cellulose Acetate Membrane for Efficient Olefin/Paraffin Separation. *Energy Fuels* **2022,** *36* (17), 10082-10095.
163. Cazón, P.; Velazquez, G.; Vázquez, M., Novel composite films from regenerated cellulose-glycerol-polyvinyl alcohol: Mechanical and barrier properties. *Food Hydrocoll.* **2019,** *89*, 481-491.
164. Moreira, R.; Rebelo, R. C.; Coelho, J. F. J.; Serra, A. C., Novel thermally regenerated flexible cellulose-based films. *Eur. j. wood prod* **2024,** *82* (6), 1813-1826.
165. Cerqueira, M. A.; Souza, B. W. S.; Teixeira, J. A.; Vicente, A. A., Effect of glycerol and corn oil on physicochemical properties of polysaccharide films – A comparative study. *Food Hydrocoll.* **2012,** *27* (1), 175-184.
166. Vrandečić, N. S.; Erceg, M.; Jakić, M.; Klarić, I., Kinetic analysis of thermal degradation of poly(ethylene glycol) and poly(ethylene oxide)s of different molecular weight. *Thermochim. Acta* **2010,** *498* (1), 71-80.
167. Pérez, C. D.; Flores, S. K.; Marangoni, A. G.; Gerschenson, L. N.; Rojas, A. M., Development of a High Methoxyl Pectin Edible Film for Retention of l-(+)-Ascorbic Acid. *J. Agric. Food Chem.* **2009,** *57* (15), 6844-6855.
168. Khotsaeng, N.; Simchuer, W.; Imsombut, T.; Srihanam, P., Effect of Glycerol Concentrations on the Characteristics of Cellulose Films from Cattail (Typha angustifolia L.) Flowers. *Polymers* **2023,** *15* (23), 4535.
169. Ahokas, P.; Kunnari, V.; Majoinen, J.; Harlin, A.; Mäkelä, M., Plasticizer Mixing Improved Regenerated Cellulose Films as an Alternative to Plastics. *ACS Sustain. Chem. Eng.* **2025**.

170. Jiang, X.; Li, H.; Luo, Y.; Zhao, Y.; Hou, L., Studies of the plasticizing effect of different hydrophilic inorganic salts on starch/poly (vinyl alcohol) films. *Int. J. Biol. Macromol.* **2016,** *82*, 223-230.
171. Seves, A.; Testa, G.; Bonfatti, A. M.; Dubini Paglia, E.; Selli, E.; Marcandalli, B., Characterization of Native Cellulose/Poly(ethylene glycol) Films. *Macromol. Mater. Eng.* **2001,** *286* (9), 524-528.
172. Jing, B.; Peng, C.; Wang, Y.; Liu, Q.; Tong, S.; Zhang, Y.; Ge, M., Hygroscopic properties of potassium chloride and its internal mixtures with organic compounds relevant to biomass burning aerosol particles. *Sci. Rep.* **2017,** *7* (1), 43572.
173. Ibuki, K.; Bopp, P. A., Molecular dynamics simulations of aqueous LiCl solutions at room temperature through the entire concentration range. *J. Mol. Liq.* **2009,** *147* (1), 56-63.
174. Mastronardo, E.; Piperopoulos, E.; Palamara, D.; Frazzica, A.; Calabrese, L., Morphological Observation of LiCl Deliquescence in PDMS-Based Composite Foams. *Appl. Sci.* **2022,** *12* (3), 1510.
175. Basiak, E.; Lenart, A.; Debeaufort, F., How Glycerol and Water Contents Affect the Structural and Functional Properties of Starch-Based Edible Films. *Polymers* **2018,** *10* (4).
176. Li, K.; Qi, Y.; Zhou, Y.; Sun, X.; Zhang, Z., Microstructure and Properties of Poly(ethylene glycol)-Segmented Polyurethane Antifouling Coatings after Immersion in Seawater. *Polymers* **2021,** *13* (4).
177. Tarique, J.; Sapuan, S. M.; Khalina, A., Effect of glycerol plasticizer loading on the physical, mechanical, thermal, and barrier properties of arrowroot (Maranta arundinacea) starch biopolymers. *Sci. Rep.* **2021,** *11* (1), 13900.
178. Pereira, D.; Santana, I.; Megda, M.; Vieira-Megda, M., Potassium chloride: impacts on soil microbial activity and nitrogen mineralization. *Ciência Rural* **2019,** *49*.
179. Xu, Z.; Zhang, Z.; Peng, S.; Yuan, Y.; Wang, X., Influences of lithium on soil microbial biomass, bacterial community structure, diversity, and function potential. *Environ. Technol. Innov.* **2023,** *32*, 103361.
180. Xu, Z.; Zhang, Z.; Peng, S.; Yuan, Y.;Wang, X., Influences of lithium on soil properties and enzyme activities. *Chemosphere* **2023,** *313*, 137458.
181. Wolfson, A.; Dlugy, C.;Shotland, Y., Glycerol as a green solvent for high product yields and selectivities. *Environ. Chem. Lett.* **2007,** *5* (2), 67-71.
182. Tselana, B. M.; Muniyasamy, S.; Ojijo, V. O.;Mhike, W., Melt Processible Biodegradable Blends of Polyethylene Glycol Plasticized Cellulose Diacetate with Polylactic Acid and Polybutylene Adipate-Co-Terephthalate. *J. Polym. Environ.* **2023,** *31* (11), 4891-4908.
183. Pongchaiphol, S.; Preechakun, T.; Raita, M.; Champreda, V.; Laosiripojana, N., Characterization of Cellulose-Chitosan-Based Materials from Different Lignocellulosic Residues Prepared by the Ethanosolv Process and Bleaching Treatment with Hydrogen Peroxide. *ACS Omega* **2021,** *6* (35), 22791-22802.
184. Kurita, K.; Nishimura, S.-I.; Takeda, T., N-Hydroxyacylation of Chitosan with Lactones. *Polym. J.* **1990,** *22* (5), 429-434.

185. Pang, Z.; Li, N.; Dong, C.; Ji, H.; Liao, Y.; Yang, G.; Pan, X., Insights into the dissolution of cellulose in lithium bromide solution. *Carbohydr. Polym. Technol. Appl.* **2024,** *7*, 100522.
186. Younes, I.; Rinaudo, M., Chitin and Chitosan Preparation from Marine Sources. Structure, Properties and Applications. *Mar. Drugs* **2015,** *13* (3), 1133-1174.
187. Zhao, Y.; Liu, X.; Wang, J.; Zhang, S., Effects of anionic structure on the dissolution of cellulose in ionic liquids revealed by molecular simulation. *Carbohydr. Polym.* **2013,** *94* (2), 723-730.
188. Zhong, C.; Cheng, F.; Zhu, Y.; Gao, Z.; Jia, H.; Wei, P., Dissolution mechanism of cellulose in quaternary ammonium hydroxide: Revisiting through molecular interactions. *Carbohydr. Polym.* **2017,** *174*, 400-408.
189. Podgorbunskikh, E.; Kuskov, T.; Rychkov, D.; Lomovskii, O.; Bychkov, A., Mechanical Amorphization of Chitosan with Different Molecular Weights. *Polymers* **2022,** *14* (20), 4438.
190. Focher, B.; Beltrame, P. L.; Naggi, A.; Torri, G., Alkaline N-deacetylation of chitin enhanced by flash treatments. Reaction kinetics and structure modifications. *Carbohydr. Polym.* **1990,** *12* (4), 405-418.
191. Novikov, V. Y.; Konovalova, I. N.; Dolgopyatova, N. V., The Mechanism of Chitin and Chitosan Deacetylation during Long-Term Alkaline Treatment. *Appl. Biochem. Microbiol.* **2022,** *58* (3), 309-314.
192. Rabideau, B. D.; Agarwal, A.; Ismail, A. E., The Role of the Cation in the Solvation of Cellulose by Imidazolium-Based Ionic Liquids. *J. Phys. Chem. B.* **2014,** *118* (6), 1621-1629.
193. Weißl, M.; Niegelhell, K.; Reishofer, D.; Zankel, A.; Innerlohinger, J.; Spirk, S., Homogeneous cellulose thin films by regeneration of cellulose xanthate: properties and characterization. *Cellulose* **2018,** *25* (1), 711-721.
194. Stefanescu, C.; Daly, W. H.; Negulescu, I. I., Biocomposite films prepared from ionic liquid solutions of chitosan and cellulose. *Carbohydr. Polym.* **2012,** *87* (1), 435-443.
195. Abomosallam, M.; Elalfy, M.; Zheng, Z.; Nagata, K.; Suzuki, M., Adsorption kinetics and thermodynamics of toxic metal ions onto chitosan nanoparticles extracted from shrimp shells. *Nanotechnol. Environ. Eng.* **2022,** *7* (1), 35-47.
196. Hasegawa, M.; Isogai, A.; Onabe, F.; Usuda, M.; Atalla, R. H., Characterization of cellulose–chitosan blend films. *J. Appl. Polym. Sci.* **1992,** *45* (11), 1873-1879.
197. Cheng, Y.; Tian, W.; Mi, Q.; Zheng, X.; Zhang, J., Highly Transparent All-Polysaccharide Composite Films with Tailored Transmission Haze for Light Manipulation. *Adv. Mater. Technol.* **2020,** *5* (9), 2000378.
198. Reis, A. B.; Yoshida, C. M.; Reis, A. P. C.; Franco, T. T., Application of chitosan emulsion as a coating on Kraft paper. *Polym. Int.* **2011,** *60* (6), 963-969.
199. Shapi'i, R. A.; Othman, S. H.; Basha, R. K.; Naim, M. N., Mechanical, thermal, and barrier properties of starch films incorporated with chitosan nanoparticles. *Nanotechnol. Rev.* **2022,** *11* (1), 1464-1477.
200. Yamane, C.; Aoyagi, T.; Ago, M.; Sato, K.; Okajima, K.; Takahashi, T., Two Different Surface Properties of Regenerated Cellulose due to Structural Anisotropy. *Polym. J.* **2006,** *38* (8), 819-826.

201. Almeida, E. V. R.; Frollini, E.; Castellan, A.; Coma, V., Chitosan, sisal cellulose, and biocomposite chitosan/sisal cellulose films prepared from thiourea/NaOH aqueous solution. *Carbohydr. Polym.* **2010,** *80* (3), 655-664.
202. Luo, Y.; Pan, X.; Ling, Y.; Wang, X.;Sun, R., Facile fabrication of chitosan active film with xylan via direct immersion. *Cellulose* **2014,** *21* (3), 1873-1883.
203. Wrońska, N.; Katir, N.; Nowak-Lange, M.; El Kadib, A.; Lisowska, K., Biodegradable Chitosan-Based Films as an Alternative to Plastic Packaging. *Foods* **2023,** *12* (18), 3519.
204. Geyer, R.; Jambeck, J. R.; Law, K. L., Production, use, and fate of all plastics ever made. *Sci. Adv.* **2017,** *3* (7), e1700782.
205. Othman, S. H.; Ronzi, N. D. A.; Shapi'i, R. A.; Dun, M.; Ariffin, S. H.; Mohammed, M. A. P., Biodegradability of Starch Nanocomposite Films Containing Different Concentrations of Chitosan Nanoparticles in Compost and Planting Soils. *Coatings* **2023,** *13* (4), 777.
206. Elieh-Ali-Komi, D.; Hamblin, M. R., Chitin and Chitosan: Production and Application of Versatile Biomedical Nanomaterials. *Int. J. Adv. Res. (Indore)* **2016,** *4* (3), 411-427.
207. Zhang, H.; Neau, S. H., In vitro degradation of chitosan by a commercial enzyme preparation: effect of molecular weight and degree of deacetylation. *Biomater.* **2001,** *22* (12), 1653-1658.
208. Croisier, F.; Jérôme, C., Chitosan-based biomaterials for tissue engineering. *Eur. Polym. J.* **2013,** *49* (4), 780-792.
209. Dropass Cups for Water Vapor Permeability test (ASTM E96). https://www.printables.com/model/215793-cups-for-water-vapor-permeability-test-astm-e96 (accessed September 2024).

V. List of Figures

VI. List of tables

VII. Curriculum Vitae

Name : Nguyen Le Tuan Minh

Gender: Male

Date of birth: August 22nd.1994

Nationality: Vietnamese

Email: nguyenleminh228@gmail.com

Education

2022 - present	PhD student of Chemistry, University of Rostock, Germany
2019-2021	M.Sc. in Natural Water and Environmental Quality, University of Science and Technology of Hanoi, Vietnam
2014-2018	B.Sc. in Chemical Technology, D.Mendeleev University of Chemical Technology of Russia, Moscow, Russia
2012-2013	B.Sc student of Chemistry, Hanoi University of Science and Technology, Hanoi, Vietnam

Scholarship granted

2022	RoHan Scholarship for PhD study in Rostock, Germany
2013	Government Scholarship for Bachelor study in Russia

VIII. List of Publications, Posters, and Presentations

List of publications

- Beyond waste: cellulose-based biodegradable films from bio waste through a cradle-to-cradle approach. M. N. Nguyen, M. T. L. Nguyen, M. Frank, D. Hollmann RSC Sustainability 2024, 2, 4028-4035. https://doi.org/10.1039/D4SU00613E

Patents

- D. Hollmann, N. L. T. Minh, Verfahren zur Herstellung eines regenerierten Celluloseprodukts, DE 10 2025 113 321.2, U. Universität Rostock, D-18055 Rostock, D, 2025.
- D. Hollmann, N. L. T. Minh, Verfahren zur Herstellung eines flexiblen Films aus regeneriertem Polysaccharid, DE10 2025 113 322.0, U. Universität Rostock, D-18055 Rostock, Germany, 2025.

Posters

- "Exploring cellulose transformation: swelling, dissolution, and degradation" 7th RoHan DAAD Summer School 2023, June 12th to 16th 2023 Rostock, Germany
- "In situ observation of the dissolving phenomenon of cellulose by onium hydroxides via optical microscopy", GDCh Science Forum Chemistry, September 4th-6th 2023, Leipzig, Germany

Oral presentations

- "The initial life cycle analysis for the dissolution of cellulose" 6th RoHan DAAD Winter School 2023, November 7th to 11th 2022, Hanoi, Vietnam
- "Exploring cellulose transformation: swelling, dissolution, and degradation", 7th RoHan DAAD Summer School 2023, June 12th to 15th 2023, Rostock, Germany

IX. SELBSTSTÄNDIGKEITSERKLÄRUNG

Ich erkläre, dass ich die eingereichte Promotionsschrift selbstständig und ohne fremde Hilfe verfasst, andere als die von mir angegebenen Quellen und Hilfsmittel nicht benutzt und die den benutzten Werken wörtlich oder inhaltlich entnommenen Stellen als solche kenntlich gemacht habe.

Rostock, 05.09.2025 _____
Nguyen Le Tuan Minh